A New Discontinuous Galerkin Method for Kirchhoff-Love Shells.

L. Noels [a,1,*], R. Radovitzky [b]

[a] *University of Liège, Continuum Mechanics & Thermo-mechanics, Chemin des Chevreuils 1, B-4000 Liège, Belgium*

[b] *Massachusetts Institute of Technology, Department of Aeronautics and Astronautics, 77 Massachusetts Ave, Cambridge, MA 02139-4307*

Abstract

Discontinuous Galerkin methods (DG) have particular appeal in problems involving high order derivatives since they provide a means of weakly enforcing the continuity of the unknown-field derivatives. This paper proposes a new discontinuous Galerkin method for Kirchhoff-Love shells considering only the membrane and bending response. The proposed one-field method utilizes the weak enforcement in such a way that the displacements are the only unknowns, while the rotation continuity is weakly enforced. This work presents the formulation of the new discontinuous Galerkin method for linear elastic shells, demonstrates the consistency and stability of the proposed framework, and establishes the method's convergence rate. After a description of the formulation implementation into a finite-element code, these properties are demonstrated on numerical applications.

Key words: Discontinuous Galerkin method, shells, Kirchhoff-Love, finite-elements

1 Introduction

Spatially-discontinuous Galerkin methods constitute a generalization of weak formulations, which allow for discontinuities of the problem unknowns in its domain interior. This is usually accomplished by integrating by parts the governing equations in sub-domains, leading naturally to boundary integral terms

* Corresponding author
Email addresses: L.Noels@ulg.ac.be (L. Noels), rapa@mit.edu (R. Radovitzky).

[1] Postdoctoral Scholar at the Belgian National Fund for Scientific Research (FNRS)

on the sub-domain interfaces where jump discontinuities are involved. The role of these terms is to weakly enforce the consistency and the continuity of the problem unknowns, where appropriate. In the general context of finite element formulations for elliptic problems, jump-discontinuities are allowed across element boundaries for the solution of linear elasticity [1], non-linear elasticity [2,3], and plasticity [4], resulting in one-field formulations where the displacement field is the unknown.

When considering problems involving high-order derivatives, discontinuous Galerkin methods can also be seen as a means of enforcing higher-order continuity requirements in a weak manner. Recent efforts to exploit this advantage in solid mechanics have included applications to beams and plates [5–7] and for theories of damage [8,9]. In the resulting one-field formulations, the jump discontinuities can be related to the unknown fields and to their derivatives [6], or to the derivatives alone [5,7]. In the context of thin structures, the equations governing the bending of plates, beams and shells involve only higher order derivatives, when shear deformations can be neglected. Moreover, the system of equations can be formulated in terms of the displacement field only. The key concept examined in this paper is the solution of Kirchoff-Love shell mechanics by considering piecewise continuous polynomial approximations of the displacements, with a weak enforcement of the higher-order continuity. In this case, the shape functions do not have to fulfill the high-order continuity requirements, which are hard to enforce in three-dimensional problems, with a few exceptions such as the subdivision method based on NURBS approximation of the surface [10,11].

Another appealing property of discontinuous Galerkin formulations is the reduction of the locking inherent to finite-element discretizations, especially for thin structures like beams, plates or shells. In such structures the locking results in excessive stiffness when the membrane and bending modes are mixed. This is generally solved by considering reduced integration [12,13], or by using a mixed formulation sometimes combined with enhanced assumed strains methods [14–17]). When considering mixed methods, for which the displacement, rotation and stress fields can be both unknown and discontinuous, it has been shown that the discontinuous Galerkin method can reduce the locking effect for Reissner-Mindlin plates [18], for Timoshenko beams [19] and for shells [20,21].

In this paper, a new discontinuous Galerkin formulation for Kirchhoff-Love theory of shells is proposed. In this formulation, the membrane and bending response is considered, while the shearing is neglected. The kinematics of the shell is described within the framework in [16,17] where the surface normal is assumed to remain perpendicular to the shell. This omission of the shearing allows the formulation of the problem as a one-field displacement method [10]. While the displacement field is continuous, discontinuities in the displacement

derivative between two elements are accounted for by considering the variation in their normal direction. Consistency is assured by the addition of the edge integration of the resultant moment; while stability is ensured by a (sufficiently large) quadratic term. Symmetrization of the discontinuous method is also considered. This formulation also exploits the reduced locking inherent to DG methods. In the particular cases when the shells degenerate to beams or plates, the proposed formulation is quite similar to the one proposed by Engel *et al.* [5]. The difference is that in their work the quadratic term is proportional to the scalar product of the jumps, while in the present methodology the quadratic term also involves the Jacobian matrix, the mesh size and the normal to the interelement boundary. The main advantages are to account for 3D effects and to result into a stabilization parameter independent on the problem size and on the material characteristics. Recently Wells and Dung [7] also proposed a DG formulation for Kirchhoff-Love plates, which also leads to a problem-independent stabilization parameter, and which is equivalent to the plate-reduction of our formulation.

This paper is organized as follows: in section 2 the continuum model for a thin body is described. Focus is restricted to the case where the shearing can be neglected, which implies that the shell normal remains perpendicular to the mid-surface during the deformation. The discontinuous Galerkin weak formulation of this problem is presented in section 3. It is shown that a one-field formulation can be used even if high-order derivatives must be considered. The discontinuous method allows the unknown field derivatives to be discontinuous while the consistency is enforced by an interface integral. The method is also stable, provided that a quadratic term is considered and that the stabilization parameter is larger than a constant which depends only on the polynomial approximation. This is demonstrated in section 4. It is also shown that the convergence rate of the method in the energy norm is one order lower than the degree of the polynomial approximation used, which indicates that DG methods are good candidates for the solution of shell problems provided that at least quadratic shape functions are being considered. Optimal-convergence rate in the L^2-norm is also demonstrated under the assumption of at least cubic approximation and of proper ellipticity of the problem. Section 5 describes the implementation of the method. The inter-element boundary terms arising from the discontinuous Galerkin formulation guaranteeing its consistency, symmetry and stability are integrated by recourse to interface elements [3,22]. The potential membrane locking behavior arising from the coupling of membrane and bending modes is addressed either by recourse to reduced integration [12, 13], or by adopting an Enhanced Assumed Strains (EAS) approach [14–17]. However, this is not necessary if the polynomial approximation is higher than two. At last, theoretical properties of the method are verified by means of numerical tests and examples of application. The proposed displacement-based framework enables a simple element formulation for the continuous elements. As a specific example, an 8-node bi-quadratic quadrilateral element integrated on 4

quadrature points and a 16-node bi-cubic quadrilateral element integrated on 16 quadrature points will be presented. The accuracy and robustness of the method is demonstrated in numerical examples in section 6. The numerical tests include a set of conventional patch tests, convergence rate and stability studies verifying the theoretical results. A wide range of applications to beam, membrane, shell, and mixed membrane-shell problems illustrates the versatility of the method.

2 Continuum mechanics of thin bodies

In this section, the formulation of continuum mechanics for thin bodies is summarized. In particular, an explanation on how to describe the deformation of a thin body in terms of its mid-surface is provided. The particular case of Kirchhoff-Love shells is formulated, showing that this problem can be reduced to a set of equations involving displacements of the mid-surface only.

2.1 Kinematics of the shell

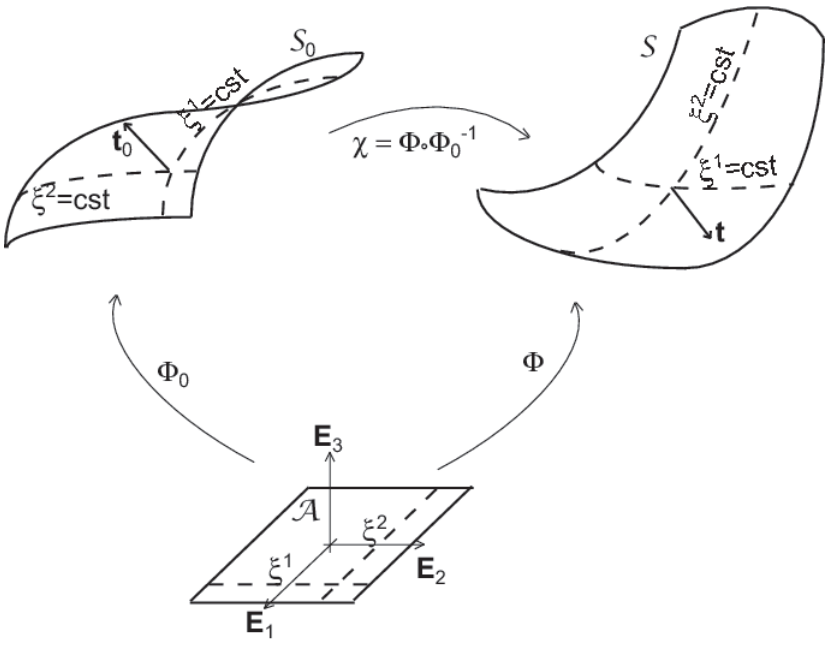

Fig. 1. Description of the different configurations of the shell.

A thin body can be described by considering its mid-surface section as a Cosserat plan $\mathcal{A}$ and a third coordinate, representing the thickness, belonging to the interval $[h_{\min}; h_{\max}]$. In the reference frame $\boldsymbol{E}_I$, this representation is written $\boldsymbol{\xi} = \sum_{I=1}^{3} \xi^I \boldsymbol{E}_I \quad : \quad \mathcal{A} \times [h_{\min}; h_{\max}] \rightarrow \mathbb{R}^3$. Hereinafter, a subscript will be used to refer to values expressed in the considered basis, while

a superscript will be used to refer to values expressed in the conjugate basis. Of course, for the initial frame, $\boldsymbol{E}_I = \boldsymbol{E}^I$. Roman letters as a subscript or superscript substitute for integers between one and three, while Greek letters substitute for integers one or two. The representation of the body in the inertial frame is illustrated in Fig. 1. A configuration of the shell is described by using $\boldsymbol{\varphi}(\xi^1, \xi^2) : \mathcal{A} \to \mathbb{R}^3$ the mapping of the mid-surface and $\boldsymbol{t} : \mathcal{A} \to \mathrm{S}^2 = \left\{ \boldsymbol{t} \in \mathbb{R}^3 |_{\|\boldsymbol{t}\|=1} \right\}$ the director of the mid-surface, with S^2 the unit sphere manifold. A configuration $\mathcal{S}$ of the shell is represented by the manifold of position $\boldsymbol{x}$, which is obtained by the mapping $\boldsymbol{\Phi} : \mathcal{A} \times [h_{\min};\, h_{\max}] \to \mathcal{S}$,

$$\boldsymbol{x} = \boldsymbol{\Phi}\left(\xi^I\right) = \boldsymbol{\varphi}(\xi^\alpha) + \xi^3 \boldsymbol{t}(\xi^\alpha) \,. \tag{1}$$

By convention, $\mathcal{S}$ refers to the current configuration of the shell, while the reference configuration $\mathcal{S}_0$ is obtained by the mapping $\boldsymbol{\Phi}_0$. The two-point deformation mapping

$$\boldsymbol{\chi} = \boldsymbol{\Phi} \circ \boldsymbol{\Phi}_0^{-1} : \mathcal{S}_0 \to \mathcal{S} \tag{2}$$

defines the transformation between the two configurations (see Fig. 1) and is characterized by the two-point deformation gradient

$$\mathbf{F} = \boldsymbol{\nabla}\boldsymbol{\Phi} \circ [\boldsymbol{\nabla}\boldsymbol{\Phi}_0]^{-1} : \mathcal{S}_0 \to \mathrm{GL}_+(3, \mathbb{R}) \,, \tag{3}$$

where $\mathrm{GL}_+(3, \mathbb{R})$ is the invertible Lie group of dimension 3 with a positive Jacobian. In this last relation, the tangent map $\boldsymbol{\nabla}\boldsymbol{\Phi}$ can be evaluated as

$$\boldsymbol{\nabla}\boldsymbol{\Phi} = \boldsymbol{g}_I \otimes \boldsymbol{E}^I \,, \text{ with} \tag{4}$$

$$\boldsymbol{g}_\alpha = \frac{\partial \boldsymbol{\Phi}}{\partial \xi^\alpha} = \boldsymbol{\varphi}_{,\alpha} + \xi^3 \boldsymbol{t}_{,\alpha} \text{ and } \boldsymbol{g}_3 = \frac{\partial \boldsymbol{\Phi}}{\partial \xi^3} = \boldsymbol{t} \,, \tag{5}$$

the convected basis. This convected basis satisfies the relation $\boldsymbol{g}_I = \boldsymbol{\nabla}\boldsymbol{\Phi}\boldsymbol{E}_I$, and its conjugate basis satisfies $\boldsymbol{g}^I = \boldsymbol{\nabla}\boldsymbol{\Phi}^{-T}\boldsymbol{E}^I$. The Jacobian related to the deformation gradient (3) is computed by

$$J = \det(\mathbf{F}) = \frac{j}{j_0}, \text{ with } j = \det(\boldsymbol{\nabla}\boldsymbol{\Phi}) = \boldsymbol{g}_3 \cdot (\boldsymbol{g}_1 \wedge \boldsymbol{g}_2) \,, \tag{6}$$

and the Jacobian related to the deformation of the mid-surface is computed by

$$\bar{J} = \frac{\bar{j}}{\bar{j}_0}, \text{ with } \bar{j} = \|\boldsymbol{\varphi}_{,1} \wedge \boldsymbol{\varphi}_{,2}\| \,. \tag{7}$$

The particular case of Kirchhoff-Love shells involves neglecting shearing deformations. Therefore, the unit vector $\boldsymbol{t}$ is always perpendicular to $\boldsymbol{\varphi}_{,\alpha}$ with

$$\boldsymbol{t} = \frac{\boldsymbol{\varphi}_{,1} \wedge \boldsymbol{\varphi}_{,2}}{\|\boldsymbol{\varphi}_{,1} \wedge \boldsymbol{\varphi}_{,2}\|} \,. \tag{8}$$

Using this assumption, since $\boldsymbol{t}_{,\mu} \cdot \boldsymbol{t} = 0$ the unit vector $\boldsymbol{t}$ is decomposed into its component λ_α^μ such that

$$\boldsymbol{t}_{,\alpha} = \lambda_\alpha^\mu \boldsymbol{\varphi}_{,\mu} \,. \tag{9}$$

Moreover, it is assumed that the mid-surface of the shell is subjected to the small displacement field $\boldsymbol{u}$, with

$$\boldsymbol{\varphi}_{,\alpha} = \boldsymbol{\varphi}_{0,\alpha} + \boldsymbol{u}_{,\alpha} \,. \tag{10}$$

A first order approximation of the unit vector (8) gives the following explicit dependence on $\boldsymbol{u}$

$$\boldsymbol{t}\,(\boldsymbol{u}) = \boldsymbol{t}_0 + \boldsymbol{\Delta t}\,(\boldsymbol{u}) \ , \text{ with} \tag{11}$$

$$\boldsymbol{\Delta t}\,(\boldsymbol{u}) = e_{\alpha\beta 3} \left[\frac{\boldsymbol{\varphi}_{0,\alpha} \wedge \boldsymbol{u}_\beta}{\bar{j}_0} + \boldsymbol{t}_0 \ \ \boldsymbol{u}_{,\alpha} \cdot \frac{\boldsymbol{t}_0 \wedge \boldsymbol{\varphi}_{0,\beta}}{\bar{j}_0} \right] , \tag{12}$$

where the normality relation $\boldsymbol{t}_0 \cdot \boldsymbol{\Delta t} = 0$ also results from $\boldsymbol{t} \cdot \boldsymbol{t} = 1$. In the previous relations e_{ijk} is the permutation tensor. Similarly, the gradient of the unit vector (8) is decomposed into

$$\boldsymbol{t}_{,\gamma} = \boldsymbol{t}_{0,\gamma} + \boldsymbol{\Delta t}_{,\gamma} \,, \tag{13}$$

with

$$\boldsymbol{t}_{0,\gamma} = \frac{e_{\alpha\beta 3}}{\bar{j}_0} \left[\boldsymbol{\varphi}_{0,\alpha\gamma} \wedge \boldsymbol{\varphi}_{0,\beta} - \boldsymbol{t}_0 \ \ \boldsymbol{t}_0 \cdot (\boldsymbol{\varphi}_{0,\alpha\gamma} \wedge \boldsymbol{\varphi}_{0,\beta}) \right] \ , \text{ and} \tag{14}$$

$$\begin{aligned} \boldsymbol{\Delta t}_{,\gamma} = {} & \frac{e_{\alpha\beta 3} \boldsymbol{t}_{0,\gamma}}{\bar{j}_0} \boldsymbol{u}_{,\alpha} \cdot (\boldsymbol{t}_0 \wedge \boldsymbol{\varphi}_{0,\beta}) - \frac{e_{\alpha\beta 3} \boldsymbol{t}_0}{\bar{j}_0} \boldsymbol{u}_{,\alpha\gamma} \cdot (\boldsymbol{t}_0 \wedge \boldsymbol{\varphi}_{0,\beta}) + \\ & \frac{e_{\alpha\beta 3} \boldsymbol{t}_0}{\bar{j}_0} \boldsymbol{u}_{,\alpha} \cdot [\boldsymbol{t}_0 \wedge \boldsymbol{\varphi}_{0,\beta\gamma} + \boldsymbol{t}_{0,\gamma} \wedge \boldsymbol{\varphi}_{0,\beta}] - \\ & \frac{e_{\alpha\beta 3} \boldsymbol{t}_0}{\bar{j}_0} \boldsymbol{u}_{,\alpha} \cdot (\boldsymbol{t}_0 \wedge \boldsymbol{\varphi}_{0,\beta}) \frac{e_{\eta\mu 3}}{\bar{j}_0} \boldsymbol{t}_0 \cdot (\boldsymbol{\varphi}_{0,\eta\gamma} \wedge \boldsymbol{\varphi}_{0,\mu}) + \\ & \frac{e_{\alpha\beta 3}}{\bar{j}_0} [\boldsymbol{\varphi}_{0,\alpha\gamma} \wedge \boldsymbol{u}_{,\beta} + \boldsymbol{\varphi}_{0,\alpha} \wedge \boldsymbol{u}_{,\beta\gamma}] - \\ & \frac{e_{\alpha\beta 3}}{\bar{j}_0} \left[\boldsymbol{\varphi}_{0,\alpha} \wedge \boldsymbol{u}_{,\beta} \frac{e_{\eta\mu 3}}{\bar{j}_0} \boldsymbol{t}_0 \cdot (\boldsymbol{\varphi}_{0,\eta\gamma} \wedge \boldsymbol{\varphi}_{0,\mu}) \right] . \end{aligned} \tag{15}$$

Again using the property $\boldsymbol{t} \cdot \boldsymbol{t} = 1$ leads to other useful relations like $\boldsymbol{t}_0 \cdot \boldsymbol{t}_{0,\gamma} = 0$, $\boldsymbol{t} \cdot \boldsymbol{t}_{,\gamma} = 0$, or again $\boldsymbol{t}_0 \cdot \boldsymbol{\Delta t}_{,\gamma} + \boldsymbol{t}_{0,\gamma} \cdot \boldsymbol{\Delta t} = 0$.

2.2 Governing equations of the shell

The governing equations of a thin body are obtained by integrating on the thickness the equations of force and moment equilibrium, respectively

$$\boldsymbol{\nabla}\cdot\boldsymbol{\sigma} = \quad \boldsymbol{B} \quad \text{in } \mathcal{S} \text{ and} \tag{16}$$
$$\boldsymbol{\Phi}\wedge\boldsymbol{\nabla}\cdot\boldsymbol{\sigma} = \boldsymbol{\Phi}\wedge\boldsymbol{B} \text{ in } \mathcal{S}\,, \tag{17}$$

where $\boldsymbol{\sigma}$ is the Cauchy stress tensor and $\boldsymbol{B}$ are the external applied forces by unit volume. Following [16,17], the integration on the thickness of the Cauchy stress tensor $\boldsymbol{\sigma}$ leads to the definition of

$$\boldsymbol{n}^{\alpha} = \frac{1}{\bar{j}}\int_{h_{\min}}^{h_{\max}} \boldsymbol{\sigma}\boldsymbol{g}^{\alpha}\det\left(\boldsymbol{\nabla}\boldsymbol{\Phi}\right) d\xi^3\,, \tag{18}$$
$$\boldsymbol{m}^{\alpha} = \frac{1}{\bar{j}}\boldsymbol{t}\wedge\int_{h_{\min}}^{h_{\max}} \xi^3\boldsymbol{\sigma}\boldsymbol{g}^{\alpha}\det\left(\boldsymbol{\nabla}\boldsymbol{\Phi}\right) d\xi^3 = \boldsymbol{t}\wedge\tilde{\boldsymbol{m}}^{\alpha}\,, \text{ and} \tag{19}$$
$$\boldsymbol{l} = \frac{1}{\bar{j}}\int_{h_{\min}}^{h_{\max}} \boldsymbol{\sigma}\boldsymbol{g}^{3}\det\left(\boldsymbol{\nabla}\boldsymbol{\Phi}\right) d\xi^3\,, \tag{20}$$

respectively the resultant stress vector, the resultant torque vector and the resultant across-the-thickness stress vector. The balance equations (16) and (17) can be rewritten in term of these resultant quantities, as

$$\frac{1}{\bar{j}}\left(\bar{j}\boldsymbol{n}^{\alpha}\right)_{,\alpha} + \boldsymbol{n}^{\mathcal{A}} = 0 \text{ on } \mathcal{A} \text{ and} \tag{21}$$
$$\frac{1}{\bar{j}}\left(\bar{j}\tilde{\boldsymbol{m}}^{\alpha}\right)_{,\alpha} - \boldsymbol{l} + \lambda\boldsymbol{t} + \tilde{\boldsymbol{m}}^{\mathcal{A}} = 0 \text{ on } \mathcal{A}\,, \tag{22}$$

where λ is an undefined pressure, where $\boldsymbol{n}^{\mathcal{A}}$ is the resultant external surface traction and where $\tilde{\boldsymbol{m}}^{\mathcal{A}}$ is the resultant external torque by unit surface. The latter two terms depend both on the body force $\boldsymbol{B}$ and on the true physical surface tractions applied to the thin body surfaces

$$\boldsymbol{n}^{\mathcal{A}} = \frac{1}{\bar{j}}\left[\left(\boldsymbol{\sigma}\boldsymbol{g}^{3}\det\left(\boldsymbol{\nabla}\boldsymbol{\Phi}\right)\right)_{h_{\min}}^{h_{\max}} + \int_{h_{\min}}^{h_{\max}} \boldsymbol{B}\,\det\left(\boldsymbol{\nabla}\boldsymbol{\Phi}\right) d\xi^3\right]\,, \text{ and} \tag{23}$$
$$\tilde{\boldsymbol{m}}^{\mathcal{A}} = \frac{1}{\bar{j}}\left[\left(\xi^3\boldsymbol{\sigma}\boldsymbol{g}^{3}\det\left(\boldsymbol{\nabla}\boldsymbol{\Phi}\right)\right)_{h_{\min}}^{h_{\max}} + \int_{h_{\min}}^{h_{\max}} \xi^3\rho\boldsymbol{B}\,\det\left(\boldsymbol{\nabla}\boldsymbol{\Phi}\right) d\xi^3\right]\,. \tag{24}$$

At this point, the equations can be expressed in the convected basis related to the mid-surface, *i.e.* $(\boldsymbol{\varphi}_{,1}, \boldsymbol{\varphi}_{,2}, \boldsymbol{t})$. In order to define the stress components, the resultant stress vectors are decomposed in this mid-surface convected basis, as

$$\boldsymbol{n}^{\alpha} = n^{\alpha\beta}\boldsymbol{\varphi}_{,\beta}\,, \text{ and} \tag{25}$$
$$\tilde{\boldsymbol{m}}^{\alpha} = \tilde{m}^{\alpha\beta}\boldsymbol{\varphi}_{,\beta} + \tilde{m}^{3\alpha}\boldsymbol{t}\,, \tag{26}$$

where it has been taken into account that the absence of shearing removes the component of $\boldsymbol{n}^\alpha$ along $\boldsymbol{t}$. In these expressions, $\tilde{m}^{\alpha\beta}$ is the stress couple resultant and $\tilde{m}^{\alpha 3}$ is the out of plane stress couple. At this stage, $n^{\alpha\beta}$ is still coupled with the bending of the shell [16]. However, since $\boldsymbol{\sigma}$ is symmetric, the effective membrane stress resultant $\tilde{n}^{\alpha\beta}$ can be obtained by [16]

$$\tilde{n}^{\alpha\beta} = n^{\alpha\beta} - \lambda^\beta_\mu \tilde{m}^{\alpha\mu} = \tilde{n}^{\beta\alpha} \,. \tag{27}$$
$$\tag{28}$$

Using these definitions, the across-the-thickness stress can be rewritten [16]

$$\boldsymbol{l} = \lambda \boldsymbol{t} + \lambda^\alpha_\mu \tilde{m}^{3\mu} \boldsymbol{\varphi}_{,\alpha} \,. \tag{29}$$

This set of governing equations is accompanied by boundary conditions applied on the boundary $\partial\mathcal{A}$ of the mid-surface $\mathcal{A}$. This boundary $\partial\mathcal{A}$ is decomposed into a part $\partial_T\mathcal{A}$ where the variation of $\boldsymbol{t}$ (corresponding to a variation of angle) is constrained to $\bar{\boldsymbol{\Delta}}\boldsymbol{t}$ and into a part $\partial_M\mathcal{A}$ where the applied torque is $\bar{\tilde{\boldsymbol{m}}}$, such that

$$\boldsymbol{t} = \boldsymbol{t}_0 + \bar{\boldsymbol{\Delta}}\boldsymbol{t} \quad \forall \left(\xi^1, \xi^2\right) \in \partial_T\mathcal{A} \,, \tag{30}$$
$$\tilde{\boldsymbol{m}}^\alpha \nu_\alpha = \quad \bar{\tilde{\boldsymbol{m}}} \quad \forall \left(\xi^1, \xi^2\right) \in \partial_M\mathcal{A} \,, \tag{31}$$

where $\boldsymbol{\nu} = \nu_\alpha \boldsymbol{\varphi}_0^{,\alpha}$ is the external normal of the mid-surface boundary (in this last expression $\boldsymbol{\varphi}_0^{,\alpha}$ denotes, with an abuse of notation, the conjugate basis to $\boldsymbol{\varphi}_{0,\alpha}$). This boundary $\partial\mathcal{A}$ is also decomposed into a part $\partial_U\mathcal{A}$ where the displacement $\bar{\boldsymbol{u}}$ is known and into a part $\partial_N\mathcal{A}$ where the traction is constrained to $\bar{\boldsymbol{n}}$, with

$$\boldsymbol{\varphi} = \boldsymbol{\varphi}_0 + \bar{\boldsymbol{u}} \quad \forall \left(\xi^1, \xi^2\right) \in \partial_U\mathcal{A} \,, \tag{32}$$
$$\boldsymbol{n}^\alpha \nu_\alpha = \quad \bar{\boldsymbol{n}} \quad \forall \left(\xi^1, \xi^2\right) \in \partial_N\mathcal{A} \,. \tag{33}$$

The decomposition of the boundary satisfies

$$\partial_T\mathcal{A} \cap \partial_M\mathcal{A} = 0 \;\text{ and }\; \partial_T\mathcal{A} \cup \partial_M\mathcal{A} = \partial\mathcal{A} \,, \tag{34}$$
$$\partial_U\mathcal{A} \cap \partial_N\mathcal{A} = 0 \;\text{ and }\; \partial_U\mathcal{A} \cup \partial_N\mathcal{A} = \partial\mathcal{A} \,. \tag{35}$$

2.3 Constitutive behavior

The set of governing Eqs. (21-22, 25-29, 30-33) is completed by a constitutive law relating the deformation to the stresses. In this paper a linear elastic response is assumed.

Just as the integrated stresses have been decomposed into membrane, shearing and bending stresses acting on the mid-surface convected basis, the deformations are separated into membrane ε, and torque strain components ρ, respectively defined by the expressions

$$\varepsilon_{\alpha\beta} = \frac{1}{2}\boldsymbol{\varphi}_{,\alpha}\cdot\boldsymbol{\varphi}_{,\beta} - \frac{1}{2}\boldsymbol{\varphi}_{0,\alpha}\cdot\boldsymbol{\varphi}_{0,\beta} = \frac{1}{2}\boldsymbol{\varphi}_{0,\alpha}\cdot\boldsymbol{u}_{,\beta} + \frac{1}{2}\boldsymbol{u}_{,\alpha}\cdot\boldsymbol{\varphi}_{0,\beta}\,, \text{ and} \tag{36}$$

$$\begin{aligned}\rho_{\alpha\beta} &= \boldsymbol{\varphi}_{,\alpha}\cdot\boldsymbol{t}_{,\beta} - \boldsymbol{\varphi}_{0,\alpha}\cdot\boldsymbol{t}_{0,\beta} \\ &= \boldsymbol{\varphi}_{0,\alpha\beta}\cdot\boldsymbol{t}_0\frac{e_{\mu\eta 3}}{\bar{j}_0}\boldsymbol{u}_{,\mu}\cdot(\boldsymbol{\varphi}_{0,\eta}\wedge\boldsymbol{t}_0) + \frac{e_{\mu\eta 3}}{\bar{j}_0}\boldsymbol{u}_{,\mu}\cdot(\boldsymbol{\varphi}_{0,\alpha\beta}\wedge\boldsymbol{\varphi}_{0,\eta}) - \boldsymbol{u}_{,\alpha\beta}\cdot\boldsymbol{t}_0\,.\end{aligned} \tag{37}$$

Note that these strain definitions result from a first order approximation on the displacement $\boldsymbol{u}$.

Following [16], the elastic constitutive relations between the effective stresses and strains are

$$\tilde{n}^{\alpha\beta} = \frac{E\,(h_{\max}-h_{\min})}{1-\nu^2}\mathcal{H}^{\alpha\beta\gamma\delta}\varepsilon_{\gamma\delta} = \mathcal{H}_n^{\alpha\beta\gamma\delta}\varepsilon_{\gamma\delta}\,, \text{ and} \tag{38}$$

$$\tilde{m}^{\alpha\beta} = \frac{E\,(h_{\max}-h_{\min})^3}{12\,(1-\nu^2)}\mathcal{H}^{\alpha\beta\gamma\delta}\rho_{\gamma\delta} = \mathcal{H}_m^{\alpha\beta\gamma\delta}\rho_{\gamma\delta}\,, \tag{39}$$

where E is the Young modulus, ν the Poisson's ration, G is the shear modulus and where

$$\begin{aligned}\mathcal{H}^{\alpha\beta\gamma\delta} = {}& \nu\boldsymbol{\varphi}_0^{,\alpha}\cdot\boldsymbol{\varphi}_0^{,\beta}\ \ \boldsymbol{\varphi}_0^{,\gamma}\cdot\boldsymbol{\varphi}_0^{,\delta} + \frac{1}{2}(1-\nu)\,\boldsymbol{\varphi}_0^{,\alpha}\cdot\boldsymbol{\varphi}_0^{,\gamma}\ \ \boldsymbol{\varphi}_0^{,\delta}\cdot\boldsymbol{\varphi}_0^{,\beta} + \\ & \frac{1}{2}(1-\nu)\,\boldsymbol{\varphi}_0^{,\alpha}\cdot\boldsymbol{\varphi}_0^{,\delta}\ \ \boldsymbol{\varphi}_0^{,\gamma}\cdot\boldsymbol{\varphi}_0^{,\beta}\,.\end{aligned} \tag{40}$$

Once again, in this last expression $\boldsymbol{\varphi}_0^{,\alpha}$ denotes, with an abuse of notation, the conjugate basis to $\boldsymbol{\varphi}_{0,\alpha}$. In relation (39), it has been assumed that the effective torque $\tilde{m}^{\alpha\beta}$ is symmetric. This is a good approximation in the case of small deformations only.

3 Discontinuous Galerkin formulation

In this section, a framework for numerical approximation of the shell equations described above based on a $\mathcal{C}^0$ polynomial approximation of the unknown field $\boldsymbol{u}$ is proposed. In this formulation, the resulting discontinuity in the surface director $\boldsymbol{\Delta t}$ is accounted for using a new discontinuous Galerkin formulation.

The strong form of the problem is defined by the set of Eqs. (21-22, 30-33, 36-39). The corresponding weak form constitutes the stationary point of the

functional $I\left(\boldsymbol{u},\varepsilon_{\alpha\beta},\rho_{\alpha\beta},\tilde{n}^{\alpha\beta},\tilde{m}^{I\beta},\lambda\right)\ :\ \mathbf{H}^4\left(\mathcal{A}\right)\times\mathrm{H}^1\left(\mathcal{A}\right)\times\mathrm{H}^1\left(\mathcal{A}\right)\times\mathrm{H}^1\left(\mathcal{A}\right)\times\mathrm{H}^1\left(\mathcal{A}\right)\times\mathrm{H}^1\left(\mathcal{A}\right)\rightarrow\mathbb{R}$ defined by

$$
\begin{aligned}
I\left(\boldsymbol{u},\varepsilon_{\alpha\beta},\rho_{\alpha\beta},\tilde{n}^{\alpha\beta},\tilde{m}^{I\beta},\lambda\right) &= \int_{\mathcal{A}}\left(\frac{1}{2}\varepsilon_{\alpha\beta}\mathcal{H}_n^{\alpha\beta\gamma\delta}\varepsilon_{\gamma\delta}+\frac{1}{2}\rho_{\alpha\beta}\mathcal{H}_m^{\alpha\beta\gamma\delta}\rho_{\gamma\delta}\right)\bar{j}_0 d\mathcal{A}\\
&+\int_{\mathcal{A}}\tilde{n}^{\alpha\beta}\left(\frac{1}{2}\boldsymbol{\varphi}_{0,\alpha}\cdot\boldsymbol{u}_{,\beta}+\frac{1}{2}\boldsymbol{u}_{,\alpha}\cdot\boldsymbol{\varphi}_{0,\beta}-\varepsilon_{\alpha\beta}\right)\bar{j}_0 d\mathcal{A}+\\
&\int_{\mathcal{A}}\tilde{m}^{\alpha\beta}\left(\boldsymbol{\varphi}_{0,\alpha}\cdot\boldsymbol{\Delta t}\left(\boldsymbol{u}\right)_{,\beta}+\boldsymbol{u}_{,\alpha}\cdot\boldsymbol{t}_{0,\beta}-\rho_{\alpha\beta}\right)\bar{j}_0 d\mathcal{A}-\\
&\int_{\partial_U\mathcal{A}}\left(\boldsymbol{u}-\bar{\boldsymbol{u}}\right)\cdot\left(\tilde{n}^{\beta\alpha}\boldsymbol{\varphi}_{0,\beta}+\lambda_{0\mu}^{\beta}\tilde{m}^{\alpha\mu}\boldsymbol{\varphi}_{0,\beta}+\lambda\boldsymbol{t}_0\right)\nu_\alpha\bar{j}_0 d\partial\mathcal{A}-\\
&\int_{\partial_T\mathcal{A}}\left(\boldsymbol{\Delta t}\left(\boldsymbol{u}\right)-\bar{\boldsymbol{\Delta}}\bar{\boldsymbol{t}}\right)\cdot\left(\tilde{m}^{\beta\alpha}\boldsymbol{\varphi}_{0,\beta}+\tilde{m}^{3\alpha}\boldsymbol{t}_0\right)\nu_\alpha\bar{j}_0 d\partial\mathcal{A}-\int_{\partial_N\mathcal{A}}\bar{\boldsymbol{n}}\cdot\boldsymbol{u}\bar{j}_0 d\partial\mathcal{A}\\
&-\int_{\partial_M\mathcal{A}}\bar{\tilde{\boldsymbol{m}}}\cdot\boldsymbol{\Delta t}\left(\boldsymbol{u}\right)\bar{j}_0 d\partial\mathcal{A}-\int_{\mathcal{A}}\left(\boldsymbol{n}^{\mathcal{A}}\cdot\boldsymbol{u}+\tilde{\boldsymbol{m}}^{\mathcal{A}}\cdot\boldsymbol{\Delta t}\left(\boldsymbol{u}\right)\right)\bar{j}_0 d\mathcal{A}\,, \qquad (41)
\end{aligned}
$$

where H^p is the Sobolev space of degree p in $\mathbb{R}$ and $\mathbf{H}^p$ is the Sobolev space of degree p in $\mathbb{R}^3$. Indeed, the stationary points of (41) with respect to $\varepsilon_{\alpha\beta}$ and to $\rho_{\alpha\beta}$ verify respectively the constitutive relations (38-39), The stationary points with respect to $\tilde{n}^{\alpha\beta}$ and to λ correspond to the weak enforcement of the compatibility equation (36) and the boundary condition (32). Similarly, the stationary point of (41) with respect to $\tilde{m}^{\alpha\beta}$ corresponds to verifying the compatibility equation (37) and the boundary condition (30). Eventually, the balance equations (21-22) are obtained from the stationary point with respect to $\boldsymbol{u}$. This last result is obtained by applying Gauss theorem and by considering

$$
\begin{aligned}
0 &= \int_{\partial\mathcal{A}}\tilde{m}^{3\alpha}\boldsymbol{t}_0\cdot\delta\boldsymbol{\Delta t}\ \bar{j}_0\ \nu_\alpha d\partial\mathcal{A}\\
&= \int_{\mathcal{A}}\left(\tilde{m}^{3\alpha}\boldsymbol{t}_0\ \bar{j}_0\right)_{,\alpha}\cdot\delta\boldsymbol{\Delta t}d\mathcal{A}+\int_{\mathcal{A}}\left(\lambda\boldsymbol{t}_0-\boldsymbol{l}\right)\cdot\delta\boldsymbol{\Delta t}\bar{j}_0 d\mathcal{A}\,, \qquad (42)
\end{aligned}
$$

where $\boldsymbol{\Delta t}\cdot\boldsymbol{t}=0$ has been used, where normality relations, Eqs. (9) and (29) have been used and where λ is the undefined pressure. Demonstration of these points closely follows what is done for the DG discretization and is omitted in this work for conciseness.

At the stationary point of this functional, the pressure λ and the torque component $\tilde{m}^{3\alpha}$ remain undefined. However, these values are not necessary since $\left(\boldsymbol{\Delta t}\left(\boldsymbol{u}\right)-\bar{\boldsymbol{\Delta}}\bar{\boldsymbol{t}}\right)\cdot\boldsymbol{t}_0$ is always equal to zero owing to the normality relation, and since the boundary condition $\boldsymbol{u}=\bar{\boldsymbol{u}}$ will be strongly enforced.

At this point, the mid-surface $\mathcal{A}$ is approximated by a discretization $\mathcal{A}_h$ into finite-elements $\mathcal{A}_e$, with $\mathcal{A}\simeq\mathcal{A}_h=\bigcup_e\bar{\mathcal{A}}_e$. In this last equation, $\bar{\mathcal{A}}_e$ is the union of the open domain $\mathcal{A}_e$ with its boundary $\partial\mathcal{A}_e$. An example of discretization is illustrated in Fig. 2. The boundary $\partial\mathcal{A}_e$ of an element $\mathcal{A}_e$ can be common

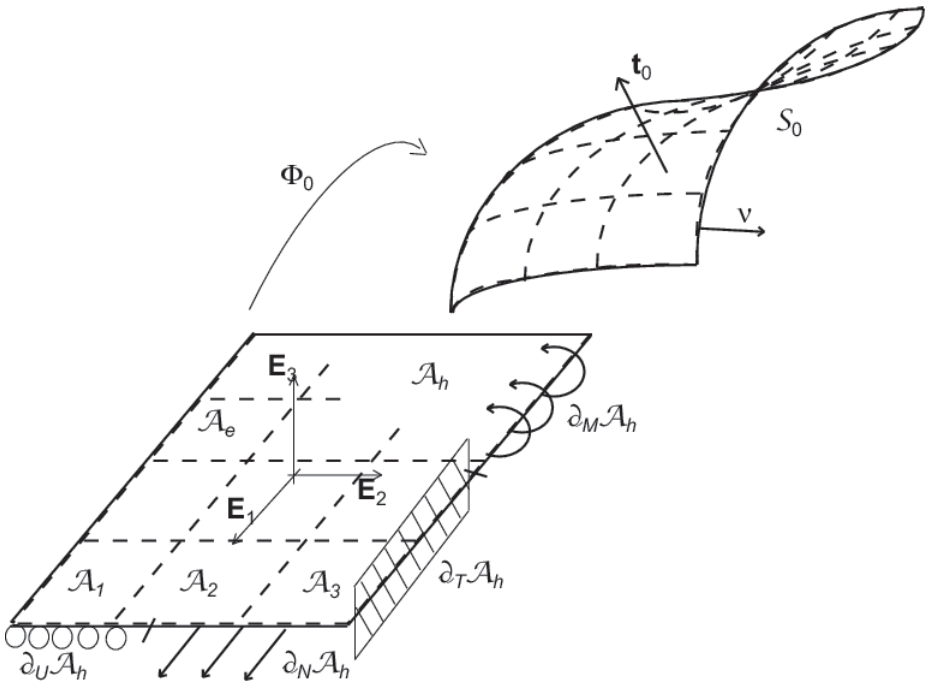

Fig. 2. Description of discretization of the shell.

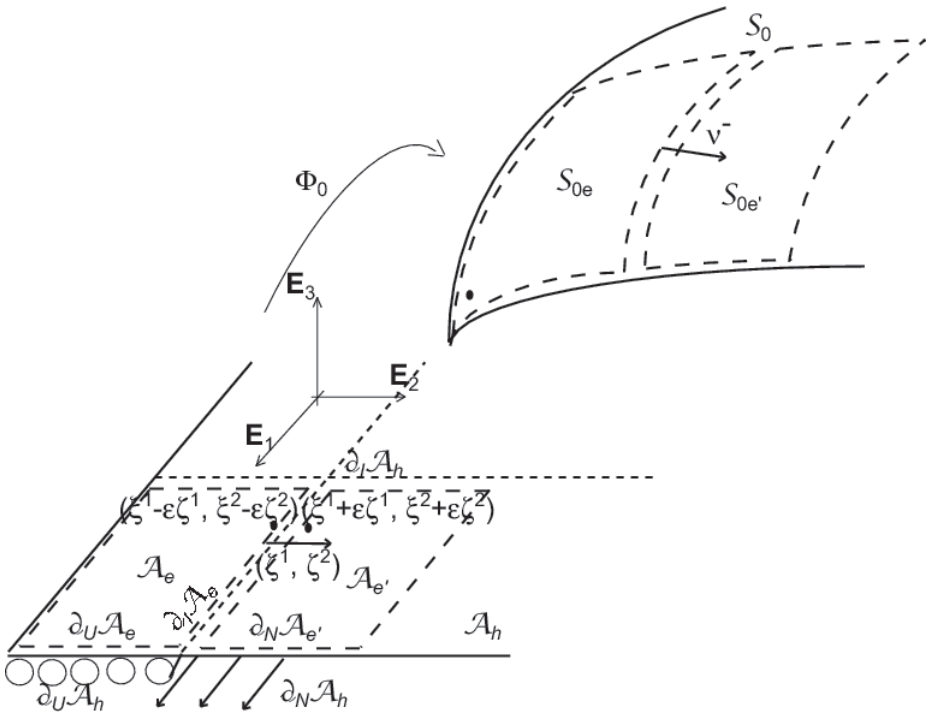

Fig. 3. Details of two elements $\mathcal{A}_e$ and $\mathcal{A}'_e$ of the discretization $\mathcal{A}_h$. Boundaries of the elements, internal boundary $\partial_I \mathcal{A}_h$, and the outward normal between the two elements are represented.

with the boundary of $\mathcal{A}_h$, with

$$\begin{aligned}\partial_U\mathcal{A}_e = \quad \partial\mathcal{A}_e \cap \partial_U\mathcal{A}_h\,, \quad \partial_T\mathcal{A}_e \quad = \partial\mathcal{A}_e \cap \partial_T\mathcal{A}_h\,,\\ \partial_M\mathcal{A}_e = \partial\mathcal{A}_e \cap \partial_M\mathcal{A}_h\,, \text{ and } \partial_N\mathcal{A}_e = \partial\mathcal{A}_e \cap \partial_N\mathcal{A}_h\,.\end{aligned} \tag{43}$$

The remaining part of the boundary $\partial\mathcal{A}_e$ is shared with another finite element (see Fig. 3) and is part of the interior boundary $\partial_I\mathcal{A}_h$, with

$$\partial_I\mathcal{A}_e = \partial\mathcal{A}_e \backslash_{\partial\mathcal{A}_h} = \partial\mathcal{A}_e \cap \partial_I\mathcal{A}_h\,, \text{ with } \partial_I\mathcal{A}_h = \bigcup_e \partial\mathcal{A}_e \backslash_{\partial\mathcal{A}_h}\,. \tag{44}$$

Instead of seeking the exact solution $\boldsymbol{u}$, a polynomial approximation $\boldsymbol{u}_h \in \mathrm{U}_\mathrm{h}^k$ constitutes the solution to the finite element problem. In this work, a continuous polynomial approximation is considered, but the derivatives of the displacement field are allowed to be discontinuous on the element boundaries, leading to the definition of the displacement manifold and of its constrained counterpart

$$\mathrm{U}_\mathrm{h}^k = \left\{\boldsymbol{u}_h \in \mathbf{H}^1\left(\mathcal{A}_h\right) |_{\boldsymbol{u}_h|_{\mathcal{A}_e}\in\mathbb{P}^k \ \forall\mathcal{A}_e\in\mathcal{A}_h}\right\} \subset \mathrm{U}^\mathrm{f}\left(\mathcal{A}_h\right), \tag{45}$$

$$\mathrm{U}_{\mathrm{h}c}^k = \left\{\delta\boldsymbol{u} \in \mathrm{U}_\mathrm{h}^k|_{\delta\boldsymbol{u}|_{\partial_U\mathcal{A}}=0}\right\} \subset \mathrm{U}_c^\mathrm{f}\left(\mathcal{A}_h\right), \tag{46}$$

with $\mathrm{U}^\mathrm{f}\left(\mathcal{A}_h\right) = \mathcal{C}^0\left(\mathcal{A}_h\right) \bigcap \prod_e \mathbf{H}^2\left(\mathcal{A}_e\right)$ for polynomial approximations $k > 1$ and with $\mathrm{U}_c^\mathrm{f}\left(\mathcal{A}_h\right) = \left\{\delta\boldsymbol{u} \in \mathrm{U}^\mathrm{f}\left(\mathcal{A}_h\right)|_{\delta\boldsymbol{u}|_{\partial_U\mathcal{A}}=0}\right\}$. Similarly, the membrane stress field is approximated by $\tilde{n}_h^{\alpha\beta} \in \mathrm{N}_\mathrm{h}^k$ with this manifold and its constrained counterpart defined by

$$\mathrm{N}_\mathrm{h}^k = \left\{\tilde{n}_h^{\alpha\beta} \in \mathrm{L}^2\left(\mathcal{A}_h\right) |_{\tilde{n}_h^{\alpha\beta}|_{\mathcal{A}_e}\in\mathbb{P}^k \ \forall\mathcal{A}_e\in\mathcal{A}_e}\right\} \subset \mathrm{N}^\mathrm{f}\left(\mathcal{A}_h\right), \tag{47}$$

$$\mathrm{N}_{\mathrm{h}c}^k = \left\{\delta\tilde{n}^{\alpha\beta} \in \mathrm{N}_\mathrm{h}^k|_{\delta\tilde{n}^{\alpha\beta}|_{\partial_N\mathcal{A}}=0}\right\} \subset \mathrm{N}_c^\mathrm{f}\left(\mathcal{A}_h\right), \tag{48}$$

where $\mathrm{N}^\mathrm{f}\left(\mathcal{A}_h\right) = \prod_e \mathrm{H}^1\left(\mathcal{A}_e\right)$, and $\mathrm{N}_c^\mathrm{f}\left(\mathcal{A}_h\right) = \left\{\delta\tilde{n}^{\alpha\beta} \in \mathrm{N}^\mathrm{f}\left(\mathcal{A}_h\right)|_{\delta\tilde{n}^{\alpha\beta}|_{\partial_N\mathcal{A}}=0}\right\}$. The moment field is approximated by $\tilde{m}_h^{\alpha I} \in \mathrm{M}_\mathrm{h}^k$, where this manifold and its constrained counterpart are

$$\mathrm{M}_\mathrm{h}^k = \left\{\tilde{m}_h^{\alpha I} \in \mathrm{L}^2\left(\mathcal{A}_h\right) |_{\tilde{m}_h^{\alpha I}|_{\mathcal{A}_e}\in\mathbb{P}^k \ \forall\mathcal{A}_e\in\mathcal{A}_h}\right\} \subset \mathrm{M}^\mathrm{f}\left(\mathcal{A}_h\right), \tag{49}$$

$$\mathrm{M}_{\mathrm{h}c}^k = \left\{\delta\tilde{m}^{\alpha I} \in \mathrm{M}_\mathrm{h}^k|_{\delta\tilde{m}^{\alpha I}|_{\partial_M\mathcal{A}}=0}\right\} \subset \mathrm{M}_c^\mathrm{f}\left(\mathcal{A}_h\right), \tag{50}$$

with $\mathrm{M}^\mathrm{f}\left(\mathcal{A}_h\right) = \prod_e \mathrm{H}^1\left(\mathcal{A}_e\right)$, $\mathrm{M}_c^\mathrm{f}\left(\mathcal{A}_h\right) = \left\{\delta\tilde{m}^{\alpha I} \in \mathrm{M}^\mathrm{f}\left(\mathcal{A}_h\right)|_{\delta\tilde{m}^{\alpha I}|_{\partial_M\mathcal{A}}=0}\right\}$. The strain fields also belong to the manifold of their corresponding stresses, *i.e.* $\varepsilon_{h\alpha\beta} \in \mathrm{N}_\mathrm{h}^k$ and $\rho_{h\alpha\beta} \in \mathrm{M}_\mathrm{h}^k$.

Since only the $\mathcal{C}^0$ continuity is ensured across $\partial_I\mathcal{A}_h$, jump $[\![\bullet]\!]$ and mean $\langle\bullet\rangle$ operators are defined on the space of the trace $\mathbf{TR}\left(\partial_I\mathcal{A}_h\right) = \prod_e \mathbf{L}^2\left(\partial_I\mathcal{A}_e\right)$ of

vectors that can take multiple values on this boundary, with

$$[\![\bullet]\!] = \bullet^+ - \bullet^- \ : \ \mathbf{TR}\left(\partial_I \mathcal{A}_h\right) \rightarrow \mathbf{L}^2\left(\partial_I \mathcal{A}_h\right) \ , \text{ and} \tag{51}$$

$$\langle \bullet \rangle = \frac{1}{2}\left(\bullet^+ + \bullet^-\right) \ : \ \mathbf{TR}\left(\partial_I \mathcal{A}_h\right) \rightarrow \mathbf{L}^2\left(\partial_I \mathcal{A}_h\right) \ . \tag{52}$$

In these relations the bullets represent generic vector fields with

$$\bullet^+ = \lim_{\varepsilon \rightarrow 0^+} \bullet\left(\xi^1 + \varepsilon\zeta^1, \xi^2 + \varepsilon\zeta^2\right) \ \text{ and} \tag{53}$$

$$\bullet^- = \lim_{\varepsilon \rightarrow 0^+} \bullet\left(\xi^1 - \varepsilon\zeta^1, \xi^2 - \varepsilon\zeta^2\right) \ , \tag{54}$$

where ζ^α are the components of the outer unit normal $\boldsymbol{\zeta}$ of $\mathcal{A}_e$ in the basis $\boldsymbol{E}_\alpha$. It is worth noticing that if definition (51) of the jump operator is not independent on the choice of the + and − sides of an element edge, when this jump is used in combination with the outward unit normal of the − element $\boldsymbol{\nu}^-$, the formulation becomes consistent and independent on this choice.

Although jump and mean operators are meaningful on the interior boundary $\partial_I \mathcal{A}$, jump definition can be extended to $\partial_T \mathcal{A}$ with

$$[\![\boldsymbol{\Delta t}]\!] = \bar{\boldsymbol{\Delta}}\boldsymbol{t} - \boldsymbol{\Delta t}, \ [\![\delta\boldsymbol{\Delta t}]\!] = -\delta\boldsymbol{\Delta t} \ \text{ and } \ \langle \tilde{\boldsymbol{m}}^\alpha \rangle = \tilde{\boldsymbol{m}}^\alpha \text{ on } \partial_T \mathcal{A} \, . \tag{55}$$

Based on these definitions, the functional (41) can be redefined on $\mathcal{A}_h$ for a discontinuous Galerkin method by introducing energy contributions resulting from the inter-element jumps. The form of these new terms is similar to the energy contributions resulting from the boundary conditions, leading to the new functional $I_h\left(\boldsymbol{u}_h\right.$,$\varepsilon_{h\alpha\beta}$,$\rho_{h\alpha\beta}$,$\tilde{n}_h^{\alpha\beta}$,$\tilde{m}_h^{I\beta}$, $\left.\lambda\right) : \ \mathrm{U}_\mathrm{h}^k \times \mathrm{N}_\mathrm{h}^k \times \mathrm{M}_\mathrm{h}^k \times \mathrm{N}_\mathrm{h}^k \times \mathrm{M}_\mathrm{h}^k \times \mathrm{N}_\mathrm{h}^k \rightarrow \mathbb{R}$ defined by

$$\begin{aligned}
&I_h\left(\boldsymbol{u}_h, \varepsilon_{h\alpha\beta}, \rho_{h\alpha\beta}, \tilde{n}_h^{\alpha\beta}, \tilde{m}_h^{I\beta}, \lambda\right) = \\
&\int_{\mathcal{A}_h} \left(\frac{1}{2}\varepsilon_{h\alpha\beta}\mathcal{H}_n^{\alpha\beta\gamma\delta}\varepsilon_{h\gamma\delta} + \frac{1}{2}\rho_{h\alpha\beta}\mathcal{H}_m^{\alpha\beta\gamma\delta}\rho_{h\gamma\delta}\right)\bar{j}_0 d\mathcal{A} + \\
&\int_{\mathcal{A}_h} \tilde{n}_h^{\alpha\beta}\left(\frac{1}{2}\boldsymbol{\varphi}_{0,\alpha}\cdot\boldsymbol{u}_{h,\beta} + \frac{1}{2}\boldsymbol{u}_{h,\alpha}\cdot\boldsymbol{\varphi}_{0,\beta} - \varepsilon_{h\alpha\beta}\right)\bar{j}_0 d\mathcal{A} + \\
&\int_{\mathcal{A}_h} \tilde{m}_h^{\alpha\beta}\left(\boldsymbol{\varphi}_{0,\alpha}\cdot\boldsymbol{\Delta t}\left(\boldsymbol{u}_h\right)_{,\beta} + \boldsymbol{u}_{h,\alpha}\cdot\boldsymbol{t}_{0,\beta} - \rho_{h\alpha\beta}\right)\bar{j}_0 d\mathcal{A} - \\
&\int_{\mathcal{A}_h} \left(\boldsymbol{n}^{\mathcal{A}}\cdot\boldsymbol{u}_h + \tilde{\boldsymbol{m}}^{\mathcal{A}}\cdot\boldsymbol{\Delta t}\left(\boldsymbol{u}_h\right)\right)\bar{j}_0 d\mathcal{A} - \\
&\quad\int_{\partial_U\mathcal{A}_h} \left(\boldsymbol{u}_h - \bar{\boldsymbol{u}}\right)\cdot\left(\tilde{n}_h^{\beta\alpha}\boldsymbol{\varphi}_{0,\beta} + \lambda_{0\mu}^{\beta}\tilde{m}_h^{\alpha\mu}\boldsymbol{\varphi}_{0,\beta} + \lambda\boldsymbol{t}_0\right)\nu_\alpha\bar{j}_0 d\partial\mathcal{A} + \\
&\quad\int_{\partial_T\mathcal{A}_h\cup\partial_I\mathcal{A}_h} [\![\boldsymbol{\Delta t}\left(\boldsymbol{u}_h\right)]\!]\cdot\left\langle\bar{j}_0\tilde{m}_h^{\beta\alpha}\boldsymbol{\varphi}_{0,\beta} + \bar{j}_0\tilde{m}_h^{3\alpha}\boldsymbol{t}_0\right\rangle\nu_\alpha^- d\partial\mathcal{A} - \\
&\quad\int_{\partial_N\mathcal{A}_h} \bar{\boldsymbol{n}}\cdot\boldsymbol{u}_h\bar{j}_0 d\partial\mathcal{A} - \int_{\partial_M\mathcal{A}} \bar{\tilde{\boldsymbol{m}}}\cdot\boldsymbol{\Delta t}\left(\boldsymbol{u}_h\right)\bar{j}_0 d\partial\mathcal{A} \, .
\end{aligned} \tag{56}$$

For simplicity, in this work, $\boldsymbol{t}_0$ is assumed to be continuous across element

boundaries [2]. Under these circumstances, the product $[\![\boldsymbol{\Delta t}\,(\boldsymbol{u}_h)]\!]\cdot\langle\bar{j}_0\tilde{m}_h^{3\alpha}\boldsymbol{t}_0\rangle = 0$ and $\tilde{m}_h^{3\alpha}$ need no longer to be determined. Moreover, the boundary condition $\boldsymbol{u}_h = \bar{\boldsymbol{u}}$ on $\partial_U\mathcal{A}$ is enforced strongly, thus removing the dependency on λ.

Reduction to a one-field formulation is achieved by deriving the stationary point of functional (56) and by substituting unknowns with explicit expressions of the displacement field $\boldsymbol{u}_h$. The stationary points with respect to the resultant strains $\varepsilon_{h\alpha\beta} \in \mathrm{N}_{\mathrm{h}}^k$ and $\rho_{\alpha\beta} \in \mathrm{M}_{\mathrm{h}}^k$ are respectively

$$0 = \frac{\partial I_h}{\partial {\varepsilon_h}^{\alpha\beta}}\delta\varepsilon^{\alpha\beta} = \int_{\mathcal{A}_h}\left(\mathcal{H}_n^{\alpha\beta\gamma\delta}\varepsilon_{h\gamma\delta} - \tilde{n}_h^{\alpha\beta}\right)\delta\varepsilon_{\alpha\beta}\bar{j}_0\,d\mathcal{A}\ \ \forall\delta\varepsilon_{\alpha\beta}\in\mathrm{N}_{\mathrm{h}c}^k\,, \tag{57}$$

$$0 = \frac{\partial I_h}{\partial {\rho_h}^{\alpha\beta}}\delta\rho^{\alpha\beta} = \int_{\mathcal{A}_h}\left(\mathcal{H}_m^{\alpha\beta\gamma\delta}\rho_{h\gamma\delta} - \tilde{m}_h^{\alpha\beta}\right)\delta\rho_{\alpha\beta}\bar{j}_0\,d\mathcal{A}\ \ \forall\delta\rho_{\alpha\beta}\in\mathrm{M}_{\mathrm{h}c}^k\,, \tag{58}$$

which enables rewriting the constitutive laws as

$$\tilde{n}_h^{\alpha\beta} = \mathcal{H}_n^{\alpha\beta\gamma\delta}\varepsilon_{h\gamma\delta}\ ,\ \text{and}\ \tilde{m}_h^{\alpha\beta} = \mathcal{H}_m^{\alpha\beta\gamma\delta}\rho_{h\gamma\delta}\ ,\ \text{in}\ \mathcal{A}_e\ . \tag{59}$$

Since $\boldsymbol{u}_h = \bar{\boldsymbol{u}}$ is assumed to be strongly enforced on $\partial_U\mathcal{A}_h$, and since $\boldsymbol{u}_h \in \mathcal{C}^0(\mathcal{A}_h)$, the membrane strain field is directly derived from the stationary point of I_h with respect to $\tilde{n}_h^{\alpha\beta}$, which is

$$0 = \frac{\partial I_h}{\partial \tilde{n}_h^{\alpha\beta}}\delta\tilde{n}^{\alpha\beta} = \int_{\mathcal{A}_h}\delta\tilde{n}^{\alpha\beta}\left(\frac{1}{2}\boldsymbol{\varphi}_{0,\alpha}\cdot\boldsymbol{u}_{h,\beta} + \frac{1}{2}\boldsymbol{u}_{h,\alpha}\cdot\boldsymbol{\varphi}_{0,\beta} - \varepsilon_{h\alpha\beta}\right)\bar{j}_0\,d\mathcal{A}\,,$$
$$\forall\delta\tilde{n}^{\alpha\beta}\in\mathrm{N}_{\mathrm{h}c}^k\,, \tag{60}$$

leading to

$$\varepsilon_{h\alpha\beta} = \frac{1}{2}\boldsymbol{\varphi}_{0,\alpha}\cdot\boldsymbol{u}_{h,\beta} + \frac{1}{2}\boldsymbol{u}_{h,\alpha}\cdot\boldsymbol{\varphi}_{0,\beta}\ ,\ \text{in}\ \mathcal{A}_e\,. \tag{61}$$

When considering the stationary point of I_h with respect to $\tilde{m}_h^{\alpha\beta}$ integrals on the boundary are also involved, since

$$0 = \frac{\partial I_h}{\partial \tilde{m}_h^{\alpha\beta}}\delta\tilde{m}^{\alpha\beta} = \int_{\mathcal{A}_h}\left(\boldsymbol{\varphi}_{0,\alpha}\cdot\boldsymbol{\Delta t}\,(\boldsymbol{u}_h)_{,\beta} + \boldsymbol{u}_{h,\alpha}\cdot\boldsymbol{t}_{0,\beta} - \rho_{h\alpha\beta}\right)\delta\tilde{m}^{\alpha\beta}\bar{j}_0 d\mathcal{A} +$$
$$\int_{\partial_T\mathcal{A}_h\cup\partial_I\mathcal{A}_h}[\![\boldsymbol{\Delta t}\,(\boldsymbol{u}_h)]\!]\cdot\left\langle\delta\tilde{m}^{\alpha\beta}\bar{j}_0\boldsymbol{\varphi}_{0,\beta}\right\rangle\nu_\alpha^- d\partial\mathcal{A}\ \ \forall\delta\tilde{m}^{\beta\alpha}\in\mathrm{M}_{\mathrm{h}c}^k\,, \tag{62}$$

where the relation $[\![\boldsymbol{\Delta t}\,(\boldsymbol{u}_h)]\!]\cdot\langle\bar{j}_0\tilde{m}_h^{3\alpha}\boldsymbol{t}_0\rangle = 0$ has been used. In order to reduce this last expression to a volume boundary, the side lifting operator $r_{\alpha\beta}^s([\![\bullet]\!])$:

[2] Indeed the interface term should consider the jump in the normal ($[\![\boldsymbol{t}]\!]$) between two elements, which would lead to a non-vanishing contribution for $\Delta\boldsymbol{t} = 0$ if $\boldsymbol{t}_0$ is not continuous across the elements interface. Under these circumstances $\boldsymbol{t}_0$ has to be continuous across this interface and $[\![\boldsymbol{t}]\!]$ can be reduced to $[\![\Delta\boldsymbol{t}]\!]$.

$\mathbf{L}^2(s) \to \mathrm{M}_{\mathrm{h}}^k$ is defined for all sides $s \in \partial_I \mathcal{A}_h \cup \partial \mathcal{A}_h$ such that

$$\int_{\mathcal{A}_h} r^s_{\alpha\beta}\left(\llbracket \boldsymbol{\Delta t} \rrbracket\right) \delta\tilde{m}^{\alpha\beta} \bar{j}_0 d\mathcal{A} = \begin{cases} \int_s \llbracket \boldsymbol{\Delta t} \rrbracket \cdot \left\langle \boldsymbol{\varphi}_{0,\beta} \delta\tilde{m}^{\alpha\beta} \bar{j}_0 \right\rangle \nu^-_\alpha d\partial\mathcal{A} & \forall \delta\tilde{m}^{\alpha\beta} \in \mathrm{M}_{\mathrm{h}}^k \text{ if } s \in \partial_I \mathcal{A} \\ \int_s \llbracket \boldsymbol{\Delta t} \rrbracket \cdot \left\langle \boldsymbol{\varphi}_{0,\beta} \delta\tilde{m}^{\alpha\beta} \bar{j}_0 \right\rangle \nu^-_\alpha d\partial\mathcal{A} & \forall \delta\tilde{m}^{\alpha\beta} \in \mathrm{M}_{\mathrm{h}}^k \text{ if } s \in \partial_T \mathcal{A} \\ 0 & \text{if } s \in \partial_M \mathcal{A} \end{cases} . \tag{63}$$

Although relation (62) would formally define $\rho_{h\alpha\beta}$ as

$$\rho_{h\alpha\beta} = \boldsymbol{\varphi}_{0,\alpha} \cdot \boldsymbol{\Delta t}\left(\boldsymbol{u}_h\right)_{,\beta} + \boldsymbol{u}_{h,\alpha} \cdot \boldsymbol{t}_{0,\beta} + \sum_{s \in \partial_I \mathcal{A} \cup \partial_T \mathcal{A}} r^s_{\alpha\beta}\left(\llbracket \boldsymbol{\Delta t} \rrbracket\right) \text{ in } \mathcal{A}_h , \tag{64}$$

a common approximation [1, 3, 23] that reduces the dependency of $\rho_{h\alpha\beta}$ inside an element $\mathcal{A}_e$ to its direct neighbors is

$$\rho_{h\alpha\beta} = \boldsymbol{\varphi}_{0,\alpha} \cdot \boldsymbol{\Delta t}\left(\boldsymbol{u}_h\right)_{,\beta} + \boldsymbol{u}_{h,\alpha} \cdot \boldsymbol{t}_{0,\beta} + \sum_{s \in \partial \mathcal{A}_e} r^s_{\alpha\beta}\left(\llbracket \boldsymbol{\Delta t} \rrbracket\right) \text{ in } \mathcal{A}_e , \tag{65}$$

where $\mathcal{A}_e$ is the open domain. Moreover, as previously proposed for elliptic equations [3], the stabilization can be ensured by introducing a stabilization parameter β when the resultant torque strain is evaluated on an element side s, *i.e.*

$$\rho_h{}^s{}_{\alpha\beta} = \boldsymbol{\varphi}_{0,\alpha} \cdot \boldsymbol{\Delta t}\left(\boldsymbol{u}_h\right)_{,\beta} + \boldsymbol{u}_{h,\alpha} \cdot \boldsymbol{t}_{0,\beta} + \beta r^s_{\alpha\beta}\left(\llbracket \boldsymbol{\Delta t} \rrbracket\right) \text{ on } s \in \partial \mathcal{A}_e . \tag{66}$$

Combining relations (59), (65) and (66) gives expressions for the stress tensors in terms of $\boldsymbol{u}$ only, as follows

$$\tilde{n}^{\alpha\beta}_h = \mathcal{H}^{\alpha\beta\gamma\delta}_n \left(\frac{1}{2} \boldsymbol{\varphi}_{0,\gamma} \cdot \boldsymbol{u}_{h,\delta} + \frac{1}{2} \boldsymbol{u}_{h,\gamma} \cdot \boldsymbol{\varphi}_{0,\delta} \right) \quad \text{in } \mathcal{A}_h , \tag{67}$$

$$\tilde{m}^{\alpha\beta}_h = \mathcal{H}^{\alpha\beta\gamma\delta}_m \left(\boldsymbol{\varphi}_{0,\gamma} \cdot \boldsymbol{\Delta t}\left(\boldsymbol{u}_h\right)_{,\delta} + \boldsymbol{u}_{h,\gamma} \cdot \boldsymbol{t}_{0,\delta} \right) + \sum_{s \in \partial \mathcal{A}_e} \mathcal{H}^{\alpha\beta\gamma\delta}_m r^s_{\gamma\delta}\left(\llbracket \boldsymbol{\Delta t} \rrbracket\right) \quad \text{in } \bar{\mathcal{A}}_e , \text{ and} \tag{68}$$

$$\tilde{m}^{s\ \alpha\beta}_h = \mathcal{H}^{\alpha\beta\gamma\delta}_m \left(\boldsymbol{\varphi}_{0,\gamma} \cdot \boldsymbol{\Delta t}\left(\boldsymbol{u}_h\right)_{,\delta} + \boldsymbol{u}_{h,\gamma} \cdot \boldsymbol{t}_{0,\delta} \right) + \beta \mathcal{H}^{\alpha\beta\gamma\delta}_m r^s_{\gamma\delta}\left(\llbracket \boldsymbol{\Delta t} \rrbracket\right) \quad \text{on } s \in \partial \mathcal{A}_e . \tag{69}$$

The variational statement of the problem then follows from the stationary point of the DG functional (56) with respect to $\boldsymbol{u}_h$. This leads to the moment

equilibrium equations

$$
\begin{aligned}
0 = \frac{\partial I_h}{\partial \boldsymbol{u}_h}\delta\boldsymbol{u} = \int_{\mathcal{A}_h} \tilde{n}_h^{\alpha\beta}\left(\frac{1}{2}\boldsymbol{\varphi}_{0,\alpha}\cdot\delta\boldsymbol{u}_{,\beta} + \frac{1}{2}\boldsymbol{\varphi}_{0,\beta}\cdot\delta\boldsymbol{u}_{,\alpha}\right)\bar{j}_0 d\mathcal{A} + \\
\int_{\mathcal{A}_h} \tilde{m}_h^{\alpha\beta}\left(\boldsymbol{\varphi}_{0,\alpha}\cdot\delta\boldsymbol{\Delta t}\left(\boldsymbol{u}\right)_{,\beta} + \delta\boldsymbol{u}_{,\alpha}\cdot\boldsymbol{t}_{0,\beta}\right)\bar{j}_0 d\mathcal{A} - \\
\int_{\mathcal{A}_h}\left(\boldsymbol{n}^{\mathcal{A}}\cdot\delta\boldsymbol{u} + \tilde{\boldsymbol{m}}^{\mathcal{A}}\cdot\delta\boldsymbol{\Delta t}\left(\boldsymbol{u}\right)\right)\bar{j}_0 d\mathcal{A} + \\
\int_{\partial_I\mathcal{A}_h\cup\partial_T\mathcal{A}_h}[\![\delta\boldsymbol{\Delta t}\left(\boldsymbol{u}\right)]\!]\cdot\left\langle\bar{j}_0\,\tilde{m}_h^{s\ \beta\alpha}\boldsymbol{\varphi}_{0,\beta}\right\rangle\nu_\alpha^- d\partial\mathcal{A} - \\
\int_{\partial_N\mathcal{A}_h}\bar{\boldsymbol{n}}\cdot\delta\boldsymbol{u}\bar{j}_0 d\partial\mathcal{A} - \int_{\partial_M\mathcal{A}}\bar{\tilde{\boldsymbol{m}}}\cdot\delta\boldsymbol{\Delta t}\left(\boldsymbol{u}\right)\bar{j}_0 d\partial\mathcal{A} \quad \forall\delta\boldsymbol{u}\in \mathrm{U}_{\mathrm{hc}}^k\,,
\end{aligned}
\tag{70}
$$

where $\delta\boldsymbol{\Delta t}\left(\boldsymbol{u}\right) = \boldsymbol{\Delta t}\left(\delta\boldsymbol{u}\right)$. Instead of implementing lifting operators, it is a convenient choice to reduce the expressions involving this operator to edge integrals. Indeed, we seek the use of interface elements, which were proved to suit well with DG formulations [3,4]. In particular this leads to high scalability for parallel implementation [4]. The same method can also be applied for non-linear material laws as it has been shown in [3]. In this linear range, the definitions of the "lifting operators" reduces expression (70) in terms of jump on the boundary, since

$$
\begin{aligned}
\int_{\mathcal{A}_h}\sum_{s\in\partial\mathcal{A}_e}\mathcal{H}_m^{\alpha\beta\gamma\delta}r_{\gamma\delta}^s\left([\![\boldsymbol{\Delta t}]\!]\right)\left(\boldsymbol{\varphi}_{0,\alpha}\cdot\delta\boldsymbol{\Delta t}\left(\boldsymbol{u}\right)_{,\beta} + \delta\boldsymbol{u}_{,\alpha}\cdot\boldsymbol{t}_{0,\beta}\right)\bar{j}_0 d\mathcal{A} = \\
\int_{\partial_I\mathcal{A}_h\cup\partial\mathcal{A}_h}[\![\boldsymbol{\Delta t}]\!]\cdot\left\langle\boldsymbol{\varphi}_{0,\gamma}\mathcal{H}_m^{\alpha\beta\gamma\delta}\left(\boldsymbol{\varphi}_{0,\alpha}\cdot\delta\boldsymbol{\Delta t}\left(\boldsymbol{u}\right)_{,\beta} + \delta\boldsymbol{u}_{,\alpha}\cdot\boldsymbol{t}_{0,\beta}\right)\bar{j}_0\right\rangle\nu_\delta^- d\partial\mathcal{A}\,,
\end{aligned}
\tag{71}
$$

and since

$$
\begin{aligned}
\int_{\partial_I\mathcal{A}_h\cup\partial_T\mathcal{A}_h}[\![\delta\boldsymbol{\Delta t}\left(\boldsymbol{u}\right)]\!]\cdot\left\langle\bar{j}_0\,\tilde{m}_h^{s\ \beta\alpha}\boldsymbol{\varphi}_{0,\beta}\right\rangle\nu_\alpha^- d\partial\mathcal{A} = \\
\int_{\partial_I\mathcal{A}_h\cup\partial\mathcal{A}_h}[\![\delta\boldsymbol{\Delta t}]\!]\cdot\left\langle\boldsymbol{\varphi}_{0,\gamma}\mathcal{H}_m^{\alpha\beta\gamma\delta}\left(\boldsymbol{\varphi}_{0,\alpha}\cdot\boldsymbol{\Delta t}\left(\boldsymbol{u}_h\right)_{,\beta} + \boldsymbol{u}_{h,\alpha}\cdot\boldsymbol{t}_{0,\beta}\right)\bar{j}_0\right\rangle\nu_\delta^- d\partial\mathcal{A} \\
+\int_{s\in\partial_I\mathcal{A}_h\cup\partial\mathcal{A}_h}\frac{\beta}{h^s}[\![\delta\boldsymbol{\Delta t}]\!]\cdot\boldsymbol{\varphi}_{0,\gamma}\nu_\delta^-\left\langle\mathcal{H}_m^{\alpha\beta\gamma\delta}\bar{j}_0\right\rangle[\![\boldsymbol{\Delta t}\left(\boldsymbol{u}_h\right)]\!]\cdot\boldsymbol{\varphi}_{0,\alpha}\nu_\beta^- d\partial\mathcal{A}\,,
\end{aligned}
\tag{72}
$$

where h^s is a characteristic size of the side s, *i.e.* $\max_{e\text{ adjacent to }s}\frac{|\mathcal{A}_e|}{|\partial\mathcal{A}_e|}$, see [3] for details.

Therefore, using Eqs. (71-72) the weak formulation defined by the set of Eqs. (67-70) can be stated in the bilinear form, as finding $\boldsymbol{u}_h\in\mathrm{U}_{\mathrm{h}}^k$ such that

$$
a\left(\boldsymbol{u}_h,\,\delta\boldsymbol{u}\right) = b\left(\delta\boldsymbol{u}\right)\quad\forall\delta\boldsymbol{u}\in\mathrm{U}_{\mathrm{hc}}^k\,,
\tag{73}
$$

where

$$a\left(\boldsymbol{u}_h,\,\delta\boldsymbol{u}\right)=\sum_e a_n^e\left(\boldsymbol{u}_h,\,\delta\boldsymbol{u}\right)+\sum_e a_m^e\left(\boldsymbol{u}_h,\,\delta\boldsymbol{u}\right)+\sum_s a_I^s\left(\boldsymbol{u}_h,\,\delta\boldsymbol{u}\right)\,, \tag{74}$$

with, using the original definition of the strain functions Eqs. (36) and (37),

$$a_n^e\left(\boldsymbol{u}_h,\,\delta\boldsymbol{u}\right)=\int_{\mathcal{A}_e}\varepsilon_{\gamma\delta}\left(\boldsymbol{u}_h\right)\mathcal{H}_n^{\alpha\beta\gamma\delta}\delta\varepsilon_{\alpha\beta}\left(\boldsymbol{u}\right)\bar{j}_0 d\mathcal{A}\,, \tag{75}$$

$$a_m^e\left(\boldsymbol{u}_h,\,\delta\boldsymbol{u}\right)=\int_{\mathcal{A}_e}\rho_{\gamma\delta}\left(\boldsymbol{u}_h\right)\mathcal{H}_m^{\alpha\beta\gamma\delta}\delta\rho_{\alpha\beta}\left(\boldsymbol{u}\right)\bar{j}_0 d\mathcal{A}\,,\ \text{and} \tag{76}$$

$$\begin{aligned}a_I^s\left(\boldsymbol{u}_h,\,\delta\boldsymbol{u}\right)=&\underbrace{\int_s[\![\boldsymbol{\Delta t}\left(\boldsymbol{u}_h\right)]\!]\cdot\left\langle\boldsymbol{\varphi}_{0,\gamma}\mathcal{H}_m^{\alpha\beta\gamma\delta}\delta\rho_{\alpha\beta}\left(\boldsymbol{u}\right)\bar{j}_0\right\rangle\nu_\delta^-\,d\partial\mathcal{A}}_{a_{I1}^s(\boldsymbol{u}_h,\,\delta\boldsymbol{u})}+\\&\underbrace{\int_s[\![\delta\boldsymbol{\Delta t}\left(\boldsymbol{u}\right)]\!]\cdot\left\langle\boldsymbol{\varphi}_{0,\gamma}\mathcal{H}_m^{\alpha\beta\gamma\delta}\rho_{\alpha\beta}\left(\boldsymbol{u}_h\right)\bar{j}_0\right\rangle\nu_\delta^-\,d\partial\mathcal{A}}_{a_{I2}^s(\boldsymbol{u}_h,\,\delta\boldsymbol{u})}+\\&\underbrace{\int_s[\![\delta\boldsymbol{\Delta t}\left(\boldsymbol{u}\right)]\!]\cdot\boldsymbol{\varphi}_{0,\gamma}\nu_\delta^-\left\langle\frac{\beta\mathcal{H}_m^{\alpha\beta\gamma\delta}\bar{j}_0}{h^s}\right\rangle[\![\boldsymbol{\Delta t}\left(\boldsymbol{u}_h\right)]\!]\cdot\boldsymbol{\varphi}_{0,\alpha}\nu_\beta^-\,d\partial\mathcal{A}}_{a_{I3}^s(\boldsymbol{u}_h,\,\delta\boldsymbol{u})}\,.\end{aligned} \tag{77}$$

and where

$$\begin{aligned}b\left(\delta\boldsymbol{u}\right)=&\int_{\mathcal{A}_h}\left(\boldsymbol{n}^{\mathcal{A}}\cdot\delta\boldsymbol{u}+\tilde{\boldsymbol{m}}^{\mathcal{A}}\cdot\delta\boldsymbol{\Delta t}\left(\boldsymbol{u}\right)\right)\bar{j}_0 d\mathcal{A}+\\&\int_{\partial_N\mathcal{A}_h}\bar{\boldsymbol{n}}\cdot\delta\boldsymbol{u}\bar{j}_0 d\partial\mathcal{A}+\int_{\partial_M\mathcal{A}}\bar{\tilde{\boldsymbol{m}}}\cdot\delta\boldsymbol{\Delta t}\left(\boldsymbol{u}\right)\bar{j}_0 d\partial\mathcal{A}\,.\end{aligned} \tag{78}$$

In the bilinear form (74), the classical terms of shell theory appear clearly in the first two terms, while the third term is a collection of boundary integrals resulting from the inter-element discontinuities. They enforce respectively (i) the symmetric nature of the Jacobian for $a_{I1}^s\left(\boldsymbol{u}_h,\,\delta\boldsymbol{u}\right)$, (ii) the consistency of the formulation for $a_{I2}^s\left(\boldsymbol{u}_h,\,\delta\boldsymbol{u}\right)$ and (iii) the stability for $a_{I3}^s\left(\boldsymbol{u}_h,\,\delta\boldsymbol{u}\right)$. Those properties are demonstrated in the next section.

4 Numerical properties

This section demonstrates that the weak formulation of the problem defined by Eq. (73) describing the deformation of shells satisfies two essential properties of a numerical method: consistency and stability. The stability is demonstrated if the stability parameter β is sufficiently large. The convergence rate of the method in the energy norm with respect to the mesh-size, in function of the polynomial approximation degree k, is also established as being equal to $k-1$. Eventually, optimal-convergence rate in the L^2-norm is demonstrated for at least cubic elements, under the assumption of proper ellipticity of the problem.

Consider $\boldsymbol{u} \in \mathbf{H}^4\left(\mathcal{A}_h\right)$ the exact solution of the physical problem. This solution belongs to $\mathcal{C}^2\left(\mathcal{A}_h\right)$, which implies that $[\![\boldsymbol{\Delta t}]\!] = \bar{\boldsymbol{\Delta}}\boldsymbol{t} - \boldsymbol{\Delta t} = 0$ on $\partial_I\mathcal{A}$, as opposed to $[\![\delta\boldsymbol{\Delta t}]\!]$, and so for $\boldsymbol{\Delta t}_{,\alpha}$. On the external boundary $\partial_T\mathcal{A}$, $[\![\boldsymbol{\Delta t}]\!] = \bar{\boldsymbol{\Delta}}\boldsymbol{t} - \boldsymbol{\Delta t} = 0$ and $[\![\delta\boldsymbol{\Delta t}]\!] = -\delta\boldsymbol{\Delta t}$. Therefore, Eq. (74) becomes

$$
\begin{aligned}
a\left(\boldsymbol{u},\,\delta\boldsymbol{u}\right) = & \int_{\mathcal{A}_h}\left(\frac{1}{2}\boldsymbol{\varphi}_{0,\gamma}\cdot\boldsymbol{u}_{,\delta} + \frac{1}{2}\boldsymbol{u}_{,\gamma}\cdot\boldsymbol{\varphi}_{0,\delta}\right)\mathcal{H}_n^{\alpha\beta\gamma\delta} \\
& \times\left(\frac{1}{2}\boldsymbol{\varphi}_{0,\alpha}\cdot\delta\boldsymbol{u}_{,\beta} + \frac{1}{2}\boldsymbol{\varphi}_{0,\beta}\cdot\delta\boldsymbol{u}_{,\alpha}\right)\bar{j}_0 d\mathcal{A} + \\
& \int_{\mathcal{A}_h}\left(\boldsymbol{\varphi}_{0,\gamma}\cdot\boldsymbol{\Delta t}\left(\boldsymbol{u}\right)_{,\delta} + \boldsymbol{u}_{,\gamma}\cdot\boldsymbol{t}_{0,\delta}\right)\mathcal{H}_m^{\alpha\beta\gamma\delta} \\
& \times\left(\boldsymbol{\varphi}_{0,\alpha}\cdot\delta\boldsymbol{\Delta t}\left(\boldsymbol{u}\right)_{,\beta} + \delta\boldsymbol{u}_{,\alpha}\cdot\boldsymbol{t}_{0,\beta}\right)\bar{j}_0 d\mathcal{A} - \\
& \int\limits_{\partial_T\mathcal{A}_h}\delta\boldsymbol{\Delta t}\left(\boldsymbol{u}\right)\cdot\boldsymbol{\varphi}_{0,\gamma}\mathcal{H}_m^{\alpha\beta\gamma\delta} \\
& \left(\boldsymbol{\varphi}_{0,\alpha}\cdot\boldsymbol{\Delta t}\left(\boldsymbol{u}_h\right)_{,\beta} + \boldsymbol{u}_{h,\alpha}\cdot\boldsymbol{t}_{0,\beta}\right)\bar{j}_0\nu_\delta d\partial\mathcal{A} - \\
& \sum_e\int_{\partial\mathcal{A}_e\cap\partial_I\mathcal{A}_h}\delta\boldsymbol{\Delta t}^-\left(\boldsymbol{u}\right)\cdot\boldsymbol{\varphi}_{0,\gamma}\mathcal{H}_m^{\alpha\beta\gamma\delta} \\
& \times\left(\boldsymbol{\varphi}_{0,\alpha}\cdot\boldsymbol{\Delta t}\left(\boldsymbol{u}_h\right)_{,\beta} + \boldsymbol{u}_{h,\alpha}\cdot\boldsymbol{t}_{0,\beta}\right)\bar{j}_0\nu_\delta d\partial\mathcal{A}\ \ \forall\delta\boldsymbol{u}\in\mathrm{U}_{\mathrm{hc}}^k\,, \quad (79)
\end{aligned}
$$

where the discontinuous nature of $\delta\boldsymbol{\Delta t}$ across the elements has been taken into account. First, the membrane term is considered. Using Eqs. (36) and (38) in combination with the symmetric nature of $\tilde{n}^{\alpha\beta}$ and Gauss theorem leads to

$$
\begin{aligned}
& \int_{\mathcal{A}_h}\left(\frac{1}{2}\boldsymbol{\varphi}_{0,\gamma}\cdot\boldsymbol{u}_{,\delta} + \frac{1}{2}\boldsymbol{u}_{,\gamma}\cdot\boldsymbol{\varphi}_{0,\delta}\right)\mathcal{H}_n^{\alpha\beta\gamma\delta}\left(\frac{1}{2}\boldsymbol{\varphi}_{0,\alpha}\cdot\delta\boldsymbol{u}_{,\beta} + \frac{1}{2}\boldsymbol{\varphi}_{0,\beta}\cdot\delta\boldsymbol{u}_{,\alpha}\right)\bar{j}_0 d\mathcal{A} \\
& \quad = \int_{\mathcal{A}_h}\tilde{n}^{\alpha\beta}\boldsymbol{\varphi}_{0,\beta}\cdot\delta\boldsymbol{u}_{,\alpha}\bar{j}_0 d\mathcal{A} = \int_{\partial_N\mathcal{A}_h}\tilde{n}^{\alpha\beta}\boldsymbol{\varphi}_{0,\beta}\cdot\delta\boldsymbol{u}\bar{j}_0\nu_\alpha d\partial\mathcal{A} - \\
& \qquad \int_{\mathcal{A}_h}\left(\tilde{n}^{\alpha\beta}\boldsymbol{\varphi}_{0,\beta}\bar{j}_0\right)_{,\alpha}\cdot\delta\boldsymbol{u}d\mathcal{A}\ \ \forall\delta\boldsymbol{u}\in\mathrm{U}_{\mathrm{hc}}^k\,. \qquad (80)
\end{aligned}
$$

Using Eqs. (37) and (39), the torque term becomes

$$
\begin{aligned}
& \int\limits_{\mathcal{A}_h}\left(\boldsymbol{\varphi}_{0,\gamma}\cdot\boldsymbol{\Delta t}\left(\boldsymbol{u}\right)_{,\delta} + \boldsymbol{u}_{,\gamma}\cdot\boldsymbol{t}_{0,\delta}\right)\mathcal{H}_m^{\alpha\beta\gamma\delta}\left(\boldsymbol{\varphi}_{0,\alpha}\cdot\delta\boldsymbol{\Delta t}\left(\boldsymbol{u}\right)_{,\beta} + \delta\boldsymbol{u}_{,\alpha}\cdot\boldsymbol{t}_{0,\beta}\right)\bar{j}_0 d\mathcal{A} \\
& \quad = \int_{\mathcal{A}_h}\tilde{m}^{\alpha\beta}\left(\boldsymbol{\varphi}_{0,\alpha}\cdot\delta\boldsymbol{\Delta t}\left(\boldsymbol{u}\right)_{,\beta} + \delta\boldsymbol{u}_{,\alpha}\cdot\boldsymbol{t}_{0,\beta}\right)\bar{j}_0 d\mathcal{A} = \\
& \qquad \sum_e\int_{\partial\mathcal{A}_e}\tilde{m}^{\alpha\beta}\boldsymbol{\varphi}_{0,\alpha}\cdot\delta\boldsymbol{\Delta t}^-\left(\boldsymbol{u}\right)\bar{j}_0\nu_\beta d\mathcal{A} - \\
& \int_{\mathcal{A}_h}\left(\tilde{m}^{\beta\alpha}\boldsymbol{\varphi}_{0,\beta}\bar{j}_0\right)_{,\alpha}\cdot\delta\boldsymbol{\Delta t}\left(\boldsymbol{u}\right)d\mathcal{A} + \int_{\partial_N\mathcal{A}}\lambda_{0,\beta}^{\mu}\tilde{m}^{\alpha\beta}\delta\boldsymbol{u}\cdot\boldsymbol{\varphi}_{0,\mu}\bar{j}_0\nu_\alpha d\mathcal{A} - \\
& \qquad \int_{\mathcal{A}_h}\left(\lambda_{0,\beta}^{\mu}\tilde{m}^{\beta\alpha}\boldsymbol{\varphi}_{0,\mu}\bar{j}_0\right)_{,\alpha}\cdot\delta\boldsymbol{u}d\mathcal{A}\ \ \forall\delta\boldsymbol{u}\in\mathrm{U}_{\mathrm{hc}}^k\,, \qquad (81)
\end{aligned}
$$

where Eq. (9) has been used in combination with Gauss theorem applied on each elements $\mathcal{A}_e$. Moreover, still using Eqs. (37) and (39), the boundary terms are reduced to

$$\int_{\partial_T \mathcal{A}_h} \delta \boldsymbol{\Delta t}\left(\boldsymbol{u}\right) \cdot \boldsymbol{\varphi}_{0,\gamma} \mathcal{H}_m^{\alpha\beta\gamma\delta} \left(\boldsymbol{\varphi}_{0,\alpha} \cdot \boldsymbol{\Delta t}\left(\boldsymbol{u}\right)_{,\beta} + \boldsymbol{u}_{,\alpha} \cdot \boldsymbol{t}_{0,\beta}\right) \bar{j}_0 \nu_\delta d\partial\mathcal{A} = \int_{\partial_T \mathcal{A}_h} \tilde{m}^{\alpha\beta} \boldsymbol{\varphi}_{0,\alpha} \cdot \delta \boldsymbol{\Delta t}\left(\boldsymbol{u}\right) \bar{j}_0 \nu_\beta d\mathcal{A} \;\; \forall \delta \boldsymbol{u} \in \mathrm{U}_{\mathrm{h}c}^k \,, \tag{82}$$

and

$$\sum_e \int_{\partial\mathcal{A}_e \cap \partial_I \mathcal{A}_h} \delta \boldsymbol{\Delta t}^-\left(\boldsymbol{u}\right) \cdot \boldsymbol{\varphi}_{0,\gamma} \mathcal{H}_m^{\alpha\beta\gamma\delta} \left(\boldsymbol{\varphi}_{0,\alpha} \cdot \boldsymbol{\Delta t}\left(\boldsymbol{u}\right)_{,\beta} + \boldsymbol{u}_{,\alpha} \cdot \boldsymbol{t}_{0,\beta}\right) \bar{j}_0 \nu_\delta d\partial\mathcal{A} = \sum_e \int_{\partial\mathcal{A}_e \cap \partial_I \mathcal{A}_h} \tilde{m}^{\alpha\beta} \boldsymbol{\varphi}_{0,\alpha} \cdot \delta \boldsymbol{\Delta t}^-\left(\boldsymbol{u}\right) \bar{j}_0 \nu_\beta d\mathcal{A} \;\; \forall \delta \boldsymbol{u} \in \mathrm{U}_{\mathrm{h}c}^k \,. \tag{83}$$

The undefined pressure λ is introduced by using Gauss theorem, relations $\boldsymbol{\Delta t} \cdot \boldsymbol{t} = 0$ and $\boldsymbol{t} \cdot \boldsymbol{t}_{,\gamma} = 0$, and Eqs. (9) and (29), which lead to

$$0 = \int_{\partial\mathcal{A}_h} \tilde{m}^{3\alpha} \boldsymbol{t}_0 \cdot \delta \boldsymbol{\Delta t}\; \bar{j}_0\; \nu_\alpha d\partial\mathcal{A} = \int_{\mathcal{A}_h} \left(\tilde{m}^{3\alpha} \boldsymbol{t}_0\; \bar{j}_0\right)_{,\alpha} \cdot \delta \boldsymbol{\Delta t} d\mathcal{A} + \int_{\mathcal{A}_h} \left(\lambda \boldsymbol{t}_0 - \boldsymbol{l}\right) \cdot \delta \boldsymbol{\Delta t} \bar{j}_0 d\mathcal{A} \;\; \forall \delta \boldsymbol{u} \in \mathrm{U}_{\mathrm{h}c}^k \,. \tag{84}$$

The introduction of Eqs. (80-84) into (79) gives the expression

$$\begin{aligned} a\left(\boldsymbol{u},\, \delta\boldsymbol{u}\right) = & \int_{\partial_N \mathcal{A}_h} \left(\tilde{n}^{\alpha\beta} + \lambda_{0,\mu}^\beta \tilde{m}^{\alpha\mu}\right) \boldsymbol{\varphi}_{0,\beta} \cdot \delta \boldsymbol{u} \bar{j}_0 \nu_\alpha d\partial\mathcal{A} + \\ & \int_{\partial_M \mathcal{A}_h} \left(\tilde{m}^{\beta\alpha} \boldsymbol{\varphi}_{0,\beta} + \tilde{m}^{3\alpha} \boldsymbol{t}_0\right) \cdot \delta \boldsymbol{\Delta t}\left(\boldsymbol{u}\right) \bar{j}_0 \nu_\alpha d\mathcal{A} - \\ & \int_{\mathcal{A}_h} \left(\left(\tilde{m}^{\beta\alpha} \boldsymbol{\varphi}_{0,\beta} \bar{j}_0 + \tilde{m}^{3\alpha} \boldsymbol{t}_0 \bar{j}_0\right)_{,\alpha} + \lambda \boldsymbol{t}_0 \bar{j}_0 - \boldsymbol{l} \bar{j}_0\right) \cdot \delta \boldsymbol{\Delta t}\left(\boldsymbol{u}\right) d\mathcal{A} - \\ & \int_{\mathcal{A}_h} \left(\left(\tilde{n}^{\alpha\beta} + \lambda_{0,\mu}^\beta \tilde{m}^{\mu\alpha}\right) \boldsymbol{\varphi}_{0,\beta} \bar{j}_0\right)_{,\alpha} \cdot \delta \boldsymbol{u} d\mathcal{A} \;\; \forall \delta \boldsymbol{u} \in \mathrm{U}_{\mathrm{h}c}^k \,. \end{aligned} \tag{85}$$

Using Eqs. (25-29), this last relation inserted in the governing equation (73) leads to

$$\begin{aligned} & \int_{\partial_N \mathcal{A}_h} \left(\boldsymbol{n}^\alpha - \bar{\boldsymbol{n}}\right) \cdot \delta \boldsymbol{u} \bar{j}_0 \nu_\alpha d\partial\mathcal{A} + \int_{\partial_M \mathcal{A}_h} \left(\tilde{\boldsymbol{m}}^\alpha - \bar{\tilde{\boldsymbol{m}}}\right) \cdot \delta \boldsymbol{\Delta t}\left(\boldsymbol{u}\right) \bar{j}_0 \nu_\alpha d\mathcal{A} = \\ & \int_{\mathcal{A}_h} \left(\left(\tilde{\boldsymbol{m}}^\alpha \bar{j}_0\right)_{,\alpha} + \lambda \boldsymbol{t}_0 \bar{j}_0 - \boldsymbol{l} \bar{j}_0 + \tilde{\boldsymbol{m}}^{\mathcal{A}} \bar{j}_0\right) \cdot \delta \boldsymbol{\Delta t}\left(\boldsymbol{u}\right) d\mathcal{A} + \\ & \int_{\mathcal{A}_h} \left[\left(\boldsymbol{n}^\alpha \bar{j}_0\right)_{,\alpha} + \boldsymbol{n}^{\mathcal{A}} \bar{j}_0\right] \cdot \delta \boldsymbol{u} d\mathcal{A} \;\; \forall \delta \boldsymbol{u} \in \mathrm{U}_{\mathrm{h}c}^k \,. \end{aligned} \tag{86}$$

The arbitrary character of $\delta\boldsymbol{u}$ in Eq. (86) implies that

$$\frac{1}{\bar{\bar{j}}_0}\left(\boldsymbol{n}^\alpha \bar{j}_0\right)_{,\alpha} + \boldsymbol{n}^{\mathcal{A}} = \ 0 \qquad \text{in } \mathcal{A}_h\,, \tag{87}$$

$$\frac{1}{\bar{\bar{j}}_0}\left(\tilde{\boldsymbol{m}}^\alpha \bar{j}_0\right)_{,\alpha} + \lambda\boldsymbol{t}_0 - \boldsymbol{l} + \tilde{\boldsymbol{m}}^{\mathcal{A}} = \lambda_u \boldsymbol{t}_0 \quad \text{in } \mathcal{A}_h\,, \tag{88}$$

$$\boldsymbol{n}^\alpha \nu_\alpha = \ \bar{\boldsymbol{n}} \qquad \text{on } \partial_N \mathcal{A}_h\,, \tag{89}$$

$$\tilde{\boldsymbol{m}}^\alpha \nu_\alpha - \bar{\bar{\boldsymbol{m}}} = \lambda_b \boldsymbol{t}_0 \quad \text{on } \partial_M \mathcal{A}_h\,, \tag{90}$$

Thus the consistency of the method is demonstrated. In these expressions, λ_u and λ_b are undefined and arise because $\delta\boldsymbol{\Delta t}$ is perpendicular to $\boldsymbol{t}_0$. Relation (87) and (88) demonstrate respectively the weak enforcement of the equations of normal force and moment equilibrium(21-22) up to an unknown pressure λ. Equations (89) and (90) correspond to the boundary conditions (31) and (33) up to an undefined value λ_b.

An interesting result provided by the consistency is the orthogonality relation. Since the formulation is consistent, $\boldsymbol{u}$ the exact solution also verifies (73), which implies the orthogonality relation

$$a\left(\boldsymbol{u}_h - \boldsymbol{u},\, \delta\boldsymbol{u}\right) = a\left(\boldsymbol{u}_h,\, \delta\boldsymbol{u}\right) - a\left(\boldsymbol{u},\, \delta\boldsymbol{u}\right) = a\left(\boldsymbol{u}_h,\, \delta\boldsymbol{u}\right) - b\left(\delta\boldsymbol{u}\right) = 0\,. \tag{91}$$

4.2 Energy norm

Both stability and convergence rate studies require the definition of an energy norm $|||\bullet||| : \mathrm{U}_c^{\mathrm{f}}\left(\mathcal{A}_h\right) \to \mathbb{R}_+$. As shown by the use of the manifold $\mathrm{U}_c^{\mathrm{f}}\left(\mathcal{A}_h\right)$, the constrained displacement $\bar{\boldsymbol{u}}$ on $\partial_U\mathcal{A}$ is assumed equal to zero. $\bar{\boldsymbol{\Delta}}\boldsymbol{t} = 0$ on $\partial_T\mathcal{A}$ is also assumed. Therefore, for the discontinuous Galerkin discretization of shells, the following energy norm is proposed:

$$\begin{aligned}
|||\boldsymbol{u}|||^2 = &\sum_e \left\| \sqrt{\mathcal{H}_n \bar{j}_0}^{\alpha\beta} \frac{1}{2}\left(\boldsymbol{\varphi}_{0,\alpha}\cdot\boldsymbol{u}_{,\beta} + \boldsymbol{u}_{,\alpha}\cdot\boldsymbol{\varphi}_{0,\beta}\right)\right\|^2_{\mathrm{L}^2(\mathcal{A}_e)} + \\
&\sum_e \left\| \sqrt{\mathcal{H}_m \bar{j}_0}^{\alpha\beta} \left(\boldsymbol{\varphi}_{0,\alpha}\cdot\boldsymbol{\Delta t}_{,\beta} + \boldsymbol{u}_{,\alpha}\cdot\boldsymbol{t}_{0,\beta}\right)\right\|^2_{\mathrm{L}^2(\mathcal{A}_e)} + \\
&\sum_{s\in\partial_I\mathcal{A}_h} \left\| \sqrt{\frac{\beta\mathcal{H}_m \bar{j}_0}{h_s}}^{\alpha\beta} \boldsymbol{\varphi}_{0,\alpha}\cdot\left[\!\left[\boldsymbol{\Delta t}\right]\!\right]\nu_\beta^-\right\|^2_{\mathrm{L}^2(s)} + \\
&\sum_{s\in\partial_T\mathcal{A}_h} \frac{1}{2}\left\| \sqrt{\frac{\beta\mathcal{H}_m \bar{j}_0}{h_s}}^{\alpha\beta} \boldsymbol{\varphi}_{0,\alpha}\cdot\left[\!\left[\boldsymbol{\Delta t}\right]\!\right]\nu_\beta^-\right\|^2_{\mathrm{L}^2(s)},
\end{aligned} \tag{92}$$

with the abuses of notation

$$\left\| \sqrt{\mathcal{H}}^{\alpha\beta} a_{\alpha\beta} \right\|^2_{\mathrm{L}^2(\mathcal{A}_e)} = \int_{\mathcal{A}_e} a_{\alpha\beta} \mathcal{H}^{\alpha\beta\gamma\delta} a_{\gamma\delta} d\mathcal{A}\,, \text{ and} \tag{93}$$

$$\sum_{s\in\partial_I\mathcal{A}_h} \left\| \sqrt{\frac{\beta\mathcal{H}_m \bar{j}_0}{h_s}}^{\alpha\beta} \boldsymbol{\varphi}_{0,\alpha} \cdot [\![\boldsymbol{\Delta t}]\!]\, \nu^-_\beta \right\|^2_{\mathrm{L}^2(s)} +$$

$$\frac{1}{2} \sum_{s\in\partial_T\mathcal{A}_h} \left\| \sqrt{\frac{\beta\mathcal{H}_m \bar{j}_0}{h_s}}^{\alpha\beta} \boldsymbol{\varphi}_{0,\alpha} \cdot [\![\boldsymbol{\Delta t}]\!]\, \nu^-_\beta \right\|^2_{\mathrm{L}^2(s)} =$$

$$\sum_e \frac{1}{2} \left\| \sqrt{\frac{\beta\mathcal{H}_m \bar{j}_0}{h^s}}^{\alpha\beta} \boldsymbol{\varphi}_{0,\alpha} \cdot [\![\boldsymbol{\Delta t}]\!]\, \nu^-_\beta \right\|^2_{\mathrm{L}^2(\partial\mathcal{A}_e)} =$$

$$\sum_e \frac{1}{2} \int_{\partial\mathcal{A}_e} \boldsymbol{\varphi}_{0,\gamma} \cdot [\![\boldsymbol{\Delta t}]\!]\, \nu^-_\delta \frac{\beta\mathcal{H}^{\alpha\beta\gamma\delta}_m \bar{j}_0}{h^s} \boldsymbol{\varphi}_{0,\alpha} \cdot [\![\boldsymbol{\Delta t}]\!]\, \nu^-_\beta d\partial\mathcal{A}\,, \tag{94}$$

and where the positive semi-definite nature of $\mathcal{H}_m$ has been used. In Eq. (94), integration on all sides s is equivalent to one half of the integration on all the element boundaries. Indeed, the sum on all the element boundaries accounts twice for a side s, except on the domain boundary $\partial_T\mathcal{A}_h$. The parameter β was introduced in the interface energy in order to obtain a more meaningful expression of the interface energy, since the work of these interface forces depends on it.

Expression (92) is a norm, *i.e.* its value is equal to zero only for $\boldsymbol{u} = 0$ on $\mathcal{A}_h$. Indeed, if $|||\boldsymbol{u}|||$ is equal to zero, then all the contributions are also equal to zero but, if this is the case, the only solution is $\boldsymbol{u} = 0$ on $\mathcal{A}_h$, as it is shown in the following lines. If the membrane energy (first term of Eq. (92)) is equal to zero, then the solution of the problem is $\boldsymbol{u}_{,\alpha}$ parallel to $\boldsymbol{t}_0$ on every $\mathcal{A}_e$. If the bending term (second term of Eq. (92)) is equal to zero, it means that $\rho_{\alpha\beta} = 0$ on $\mathcal{A}_e$. Using Eq. (37), and since $\boldsymbol{u}_{,\alpha}$ is parallel to $\boldsymbol{t}_0$, the solution $\rho_{\alpha\beta} = 0$ implies $C = \boldsymbol{u}_{,\alpha} \cdot \boldsymbol{t}_0$ is constant on each $\mathcal{A}_e$. Since the jump in the variation $\boldsymbol{\Delta t}$ is equal to zero between two elements (third term of Eq. (92) equal to zero), this product is constant on the whole domain, by recourse to Eq. (12) - $\boldsymbol{\Delta t}$ cannot be perpendicular to $\boldsymbol{\varphi}_{0,\alpha}$ by definition. So the solution of the problem would be $\boldsymbol{u}_{,\alpha} \cdot \boldsymbol{t}_0 = 0$ on the whole domain since the fourth term of Eq. (92) is equal to zero. Owing $\boldsymbol{u} \in \mathcal{C}^0(\mathcal{A}_h)$ and the constrained displacement $\bar{\boldsymbol{u}} = 0$, the only remaining solution is $\boldsymbol{u} = 0$ on $\mathcal{A}_h$.

Before demonstrating the stability and studying the convergence rate, some intermediate results are established.

4.2.1 Upper bound of the bilinear form

In order to establish the upper bound of $|a(\boldsymbol{u},\,\delta\boldsymbol{u})|^2$, the membrane part of the bilinear form is first considered. Using the Cauchy-Schwartz inequality ($\left|a^{\alpha\beta}b^{\alpha\beta}\right| \leq \sqrt{a^{\alpha\beta}a^{\alpha\beta}}\sqrt{b^{\alpha\beta}b^{\alpha\beta}}$), gives

$$\left|\sum_e a_n^e(\boldsymbol{u},\,\delta\boldsymbol{u})\right| \leq \sum_e \left\|\sqrt{\mathcal{H}_n\bar{j}_0}^{\alpha\beta}\frac{1}{2}\left(\boldsymbol{\varphi}_{0,\alpha}\cdot\boldsymbol{u}_{,\beta}+\boldsymbol{u}_{,\alpha}\cdot\boldsymbol{\varphi}_{0,\beta}\right)\right\|_{\mathrm{L}^2(\mathcal{A}_e)} \times \left\|\sqrt{\mathcal{H}_n\bar{j}_0}^{\gamma\delta}\frac{1}{2}\left(\boldsymbol{\varphi}_{0,\gamma}\cdot\delta\boldsymbol{u}_{,\delta}+\delta\boldsymbol{u}_{,\gamma}\cdot\boldsymbol{\varphi}_{0,\delta}\right)\right\|_{\mathrm{L}^2(\mathcal{A}_e)} . \tag{95}$$

Similarly, the bending term is bounded by

$$\left|\sum_e a_m^e(\boldsymbol{u},\,\delta\boldsymbol{u})\right| \leq \sum_e \left\|\sqrt{\mathcal{H}_m\bar{j}_0}^{\alpha\beta}\left(\boldsymbol{\varphi}_{0,\alpha}\cdot\boldsymbol{\Delta t}_{,\beta}+\boldsymbol{u}_{,\alpha}\cdot\boldsymbol{t}_{0,\beta}\right)\right\|_{\mathrm{L}^2(\mathcal{A}_e)} \times \left\|\sqrt{\mathcal{H}_m\bar{j}_0}^{\gamma\delta}\left(\boldsymbol{\varphi}_{0,\gamma}\cdot\delta\boldsymbol{\Delta t}_{,\delta}+\delta\boldsymbol{u}_{,\gamma}\cdot\boldsymbol{t}_{0,\delta}\right)\right\|_{\mathrm{L}^2(\mathcal{A}_e)} . \tag{96}$$

The bound of the first interface term may be found by using the property $\|\langle\bullet\rangle\|^2_{\mathrm{L}^2(s)} \leq \|\bullet^+\|^2_{\mathrm{L}^2(s)} + \|\bullet^-\|^2_{\mathrm{L}^2(s)}$ which gives

$$\begin{aligned}\left|\sum_s a_{I1}^s(\boldsymbol{u},\,\delta\boldsymbol{u})\right| &\leq \sum_e \left|\int_{\partial\mathcal{A}_e} a_{I1}^s(\boldsymbol{u},\,\delta\boldsymbol{u})\right| \\ &\leq 2\sum_e \left\|\sqrt{h^s\mathcal{H}_m\bar{j}_0}^{\alpha\beta}\left(\boldsymbol{\varphi}_{0,\alpha}\cdot\boldsymbol{\Delta t}_{,\beta}+\boldsymbol{u}_{,\alpha}\cdot\boldsymbol{t}_{0,\beta}\right)\right\|_{\mathrm{L}^2(\partial\mathcal{A}_e)} \\ &\quad\times \left\|\sqrt{\frac{\mathcal{H}_m\bar{j}_0}{h^s}}^{\gamma\delta}\left[\!\left[\boldsymbol{\Delta t}(\delta\boldsymbol{u})\right]\!\right]\cdot\boldsymbol{\varphi}_{0,\delta}\nu_\gamma^-\right\|_{\mathrm{L}^2(\partial\mathcal{A}_e)} ,\end{aligned} \tag{97}$$

or again, with the use of the scaling property [3],

$$\begin{aligned}\left|\sum_s a_{I1}^s(\boldsymbol{u},\,\delta\boldsymbol{u})\right| &\leq \frac{C^k}{\sqrt{\beta}}\sum_e \left\|\sqrt{\mathcal{H}_m\bar{j}_0}^{\alpha\beta}\left(\boldsymbol{\varphi}_{0,\alpha}\cdot\boldsymbol{\Delta t}_{,\beta}+\boldsymbol{u}_{,\alpha}\cdot\boldsymbol{t}_{0,\beta}\right)\right\|_{\mathrm{L}^2(\mathcal{A}_e)} \\ &\quad\times \left\|\sqrt{\frac{\beta\mathcal{H}_m\bar{j}_0}{h^s}}^{\gamma\delta}\left[\!\left[\boldsymbol{\Delta t}(\delta\boldsymbol{u})\right]\!\right]\cdot\boldsymbol{\varphi}_{0,\delta}\nu_\gamma^-\right\|_{\mathrm{L}^2(\partial\mathcal{A}_e)} ,\end{aligned} \tag{98}$$

[3] Hansbo et al have demonstrated [24] that for an element e one has the property $h^s\|a\|^2_{\mathrm{L}^2(\partial\mathcal{A}_e)} \leq C^k\|a\|^2_{\mathrm{L}^2(\mathcal{A}_e)}$ with $C^k > 0$ independent of the element geometry and with $h^s = \frac{|\mathcal{A}_e|}{|\partial\mathcal{A}_e|}$. Constant $C^k = \sup_{a^{\alpha\beta}\in\mathbb{P}^k(\mathcal{A}_e)} \frac{|\mathcal{A}_e|\int_s\left\{a^{\alpha\beta}:a^{\alpha\beta}\right\}d\partial\mathcal{A}}{|s|\int_{\mathcal{A}_e}\left\{a^{\alpha\beta}:a^{\alpha\beta}\right\}d\mathcal{A}}$ depends only on the polynomial degree k.

where C^k depends only on the degree of $\boldsymbol{u}$. Note that for $\boldsymbol{u} \in \mathrm{U}_c^{\mathrm{f}}(\mathcal{A}_h)$ this polynomial degree is *a priori* unknown, but once the bounds are applied to the discretization $\boldsymbol{u}_h \in \mathrm{U}_{\mathrm{hc}}^k$ it will correspond to the degree of the polynomial approximation. Similarly, the second interface term is bounded such that

$$\left|\sum_s a_{I2}^s(\boldsymbol{u},\,\delta\boldsymbol{u})\right| \leq \frac{C^k}{\sqrt{\beta}} \sum_e \left\| \sqrt{\mathcal{H}_m \bar{j}_0}^{\alpha\beta} \left(\boldsymbol{\varphi}_{0,\alpha}\cdot\delta\boldsymbol{\Delta t}_{,\beta} + \delta\boldsymbol{u}_{,\alpha}\cdot\boldsymbol{t}_{0,\beta}\right)\right\|_{\mathrm{L}^2(\mathcal{A}_e)} \times \left\| \sqrt{\frac{\beta\mathcal{H}_m \bar{j}_0}{h^s}}^{\gamma\delta} [\![\boldsymbol{\Delta t}]\!]\cdot\boldsymbol{\varphi}_{0,\delta}\nu_\gamma^- \right\|_{\mathrm{L}^2(\partial\mathcal{A}_e)}, \tag{99}$$

while the quadratic term can straightforwardly be bounded by

$$\left|\sum_s a_{I3}^s(\boldsymbol{u},\,\delta\boldsymbol{u})\right| \leq \sum_e \left\| \sqrt{\frac{\beta\mathcal{H}_m \bar{j}_0}{h^s}}^{\alpha\beta} [\![\delta\boldsymbol{\Delta t}]\!]\cdot\boldsymbol{\varphi}_{0,\beta}\nu_\alpha^- \right\|_{\mathrm{L}^2(\partial\mathcal{A}_e)} \times \left\| \sqrt{\frac{\beta\mathcal{H}_m \bar{j}_0}{h^s}}^{\gamma\delta} [\![\boldsymbol{\Delta t}]\!]\cdot\boldsymbol{\varphi}_{0,\delta}\nu_\gamma^- \right\|_{\mathrm{L}^2(\partial\mathcal{A}_e)} \tag{100}$$

The combination of Eqs. (95-100) completed to obtain the complete binomial terms leads to

$$\begin{aligned}\frac{|a(\boldsymbol{u},\,\delta\boldsymbol{u})|}{C_1^k(\beta)} \leq \sum_e \Bigg[& \left\| \sqrt{\mathcal{H}_n \bar{j}_0}^{\alpha\beta} \frac{1}{2}\left(\boldsymbol{\varphi}_{0,\alpha}\cdot\boldsymbol{u}_{,\beta} + \boldsymbol{u}_{,\alpha}\cdot\boldsymbol{\varphi}_{0,\beta}\right)\right\|_{\mathrm{L}^2(\mathcal{A}_e)} + \\ & \left\| \sqrt{\mathcal{H}_m \bar{j}_0}^{\alpha\beta} \left(\boldsymbol{\varphi}_{0,\alpha}\cdot\boldsymbol{\Delta t}_{,\beta} + \boldsymbol{u}_{,\alpha}\cdot\boldsymbol{t}_{0,\beta}\right)\right\|_{\mathrm{L}^2(\mathcal{A}_e)} + \\ & \left\| \sqrt{\frac{\beta\mathcal{H}_m \bar{j}_0}{2h^s}}^{\alpha\beta} [\![\boldsymbol{\Delta t}]\!]\cdot\boldsymbol{\varphi}_{0,\beta}\nu_\alpha^- \right\|_{\mathrm{L}^2(\partial\mathcal{A}_e)} \Bigg] \times \\ & \Bigg[\left\| \sqrt{\mathcal{H}_n \bar{j}_0}^{\gamma\delta} \frac{1}{2}\left(\boldsymbol{\varphi}_{0,\gamma}\cdot\delta\boldsymbol{u}_{,\delta} + \delta\boldsymbol{u}_{,\gamma}\cdot\boldsymbol{\varphi}_{0,\delta}\right)\right\|_{\mathrm{L}^2(\mathcal{A}_e)} + \\ & \left\| \sqrt{\mathcal{H}_m \bar{j}_0}^{\gamma\delta} \left(\boldsymbol{\varphi}_{0,\gamma}\cdot\delta\boldsymbol{\Delta t}_{,\delta} + \delta\boldsymbol{u}_{,\gamma}\cdot\boldsymbol{t}_{0,\delta}\right)\right\|_{\mathrm{L}^2(\mathcal{A}_e)} + \\ & \left\| \sqrt{\frac{\beta\mathcal{H}_m \bar{j}_0}{2h^s}}^{\gamma\delta} [\![\delta\boldsymbol{\Delta t}]\!]\cdot\boldsymbol{\varphi}_{0,\delta}\nu_\gamma^- \right\|_{\mathrm{L}^2(\partial\mathcal{A}_e)} \Bigg], \end{aligned} \tag{101}$$

with $C_1^k(\beta) = \max\left(2, C^k\sqrt{2/\beta}\right)$. The Cauchy-Schwartz inequality ($\left|\sum_i a_i b_i\right| \leq \sqrt{\sum_i a_i^2 \sum_j b_j^2}$) is now applied to Eq. (101), which becomes after using the prop-

erty $2ab \leq a^2 + b^2$,

$$\frac{|a(\boldsymbol{u},\,\delta\boldsymbol{u})|^2}{9C_2^k(\beta)} \leq \sum_e \left[\left\| \sqrt{\mathcal{H}_n \bar{j}_0}^{\alpha\beta} \frac{1}{2} (\boldsymbol{\varphi}_{0,\alpha} \cdot \boldsymbol{u}_{,\beta} + \boldsymbol{u}_{,\alpha} \cdot \boldsymbol{\varphi}_{0,\beta}) \right\|^2_{\mathrm{L}^2(\mathcal{A}_e)} + \right.$$
$$\left\| \sqrt{\mathcal{H}_m \bar{j}_0}^{\alpha\beta} (\boldsymbol{\varphi}_{0,\alpha} \cdot \boldsymbol{\Delta t}_{,\beta} + \boldsymbol{u}_{,\alpha} \cdot \boldsymbol{t}_{0,\beta}) \right\|^2_{\mathrm{L}^2(\mathcal{A}_e)} +$$
$$\left. \frac{1}{2} \left\| \sqrt{\frac{\beta \mathcal{H}_m \bar{j}_0}{h^s}}^{\alpha\beta} [\![\boldsymbol{\Delta t}]\!] \cdot \boldsymbol{\varphi}_{0,\beta} \nu_\alpha^- \right\|^2_{\mathrm{L}^2(\partial\mathcal{A}_e)} \right] \times$$
$$\sum_{e'} \left[\left\| \sqrt{\mathcal{H}_n \bar{j}_0}^{\gamma\delta} \frac{1}{2} (\boldsymbol{\varphi}_{0,\gamma} \cdot \delta\boldsymbol{u}_{,\delta} + \delta\boldsymbol{u}_{,\gamma} \cdot \boldsymbol{\varphi}_{0,\delta}) \right\|^2_{\mathrm{L}^2(\partial\mathcal{A}_{e'})} + \right.$$
$$\left\| \sqrt{\mathcal{H}_m \bar{j}_0}^{\gamma\delta} (\boldsymbol{\varphi}_{0,\gamma} \cdot \delta\boldsymbol{\Delta t}_{,\delta} + \delta\boldsymbol{u}_{,\gamma} \cdot \boldsymbol{t}_{0,\delta}) \right\|^2_{\mathrm{L}^2(\partial\mathcal{A}_{e'})} +$$
$$\left. \frac{1}{2} \left\| \sqrt{\frac{\beta \mathcal{H}_m \bar{j}_0}{h^s}}^{\gamma\delta} [\![\delta\boldsymbol{\Delta t}]\!] \cdot \boldsymbol{\varphi}_{0,\delta} \nu_\gamma^- \right\|^2_{\mathrm{L}^2(\partial\mathcal{A}_{e'})} \right]. \tag{102}$$

This last relation can be rewritten in the more elegant form

$$|a(\boldsymbol{u},\,\delta\boldsymbol{u})|^2 \leq C^k(\beta) \, |||\boldsymbol{u}|||^2 \, |||\delta\boldsymbol{u}|||^2 \quad \forall \boldsymbol{u},\ \delta\boldsymbol{u} \in \mathrm{U}_c^{\mathrm{f}}(\mathcal{A}_h), \tag{103}$$

where C^k depends only on the degree of $\boldsymbol{u}$. Note that for $\boldsymbol{u} \in \mathrm{U}_c^{\mathrm{f}}(\mathcal{A}_h)$ this polynomial degree is *a priori* unknown, but once the bounds are applied to the discretization $\boldsymbol{u}_h \in \mathrm{U}_{\mathrm{h}c}^k$ it will correspond to the degree of the polynomial approximation.

4.2.2 Lower bound of the energy norm

The lower bound of the bilinear form is obtained from the relation

$$a(\boldsymbol{u},\,\boldsymbol{u}) = \sum_e \left\| \sqrt{\mathcal{H}_n \bar{j}_0}^{\alpha\beta} \frac{1}{2} (\boldsymbol{\varphi}_{0,\alpha} \cdot \boldsymbol{u}_{,\beta} + \boldsymbol{u}_{,\alpha} \cdot \boldsymbol{\varphi}_{0,\beta}) \right\|^2_{\mathrm{L}^2(\mathcal{A}_e)} +$$
$$\sum_e \left\| \sqrt{\mathcal{H}_m \bar{j}_0}^{\alpha\beta} (\boldsymbol{\varphi}_{0,\alpha} \cdot \boldsymbol{\Delta t}_{,\beta} + \boldsymbol{u}_{,\alpha} \cdot \boldsymbol{t}_{0,\beta}) \right\|^2_{\mathrm{L}^2(\mathcal{A}_e)} +$$
$$2 \sum_s \int_s [\![\boldsymbol{\Delta t}]\!] \cdot \boldsymbol{\varphi}_{0,\gamma} \left\langle \left(\boldsymbol{\varphi}_{0,\alpha} \cdot \boldsymbol{\Delta t}(\boldsymbol{u})_{,\beta} + \boldsymbol{u}_{,\alpha} \cdot \boldsymbol{t}_{0,\beta} \right) \mathcal{H}_m^{\alpha\beta\gamma\delta} \bar{j}_0 \right\rangle \nu_\delta^- \, d\partial\mathcal{A}$$
$$+ \sum_s \left\| \sqrt{\frac{\beta \mathcal{H}_m \bar{j}_0}{h^s}}^{\gamma\delta} \boldsymbol{\varphi}_{0,\gamma} \cdot [\![\boldsymbol{\Delta t}(\boldsymbol{u})]\!] \, \nu_\delta^- \right\|^2_{\mathrm{L}^2(s)}. \tag{104}$$

The remaining interface integral can be bounded by the product of $\mathbf{L}^2$-norms with a constant C^k depending on the degree of $\boldsymbol{u}$, see Eq. (99), leading to

$$
\begin{aligned}
a\left(\boldsymbol{u},\,\boldsymbol{u}\right) \geq \quad & \sum_e \left\| \sqrt{\mathcal{H}_n \bar{j}_0}^{\alpha\beta} \frac{1}{2} \left(\boldsymbol{\varphi}_{0,\alpha} \cdot \boldsymbol{u}_{,\beta} + \boldsymbol{u}_{,\alpha} \cdot \boldsymbol{\varphi}_{0,\beta} \right) \right\|^2_{\mathrm{L}^2(\mathcal{A}_e)} + \\
& \sum_e \left\| \sqrt{\mathcal{H}_m \bar{j}_0}^{\alpha\beta} \left(\boldsymbol{\varphi}_{0,\alpha} \cdot \boldsymbol{\Delta t}_{,\beta} + \boldsymbol{u}_{,\alpha} \cdot \boldsymbol{t}_{0,\beta} \right) \right\|^2_{\mathrm{L}^2(\mathcal{A}_e)} - \\
& \frac{2\sqrt{2}C^k}{\sqrt{\beta}} \sum_e \left\| \sqrt{\mathcal{H}_m \bar{j}_0}^{\alpha\beta} \left(\boldsymbol{\varphi}_{0,\alpha} \cdot \boldsymbol{\Delta t}_{,\beta} + \boldsymbol{u}_{,\alpha} \cdot \boldsymbol{t}_{0,\beta} \right) \right\|_{\mathrm{L}^2(\mathcal{A}_e)} \\
& \qquad \times \left\| \sqrt{\frac{\beta \mathcal{H}_m \bar{j}_0}{2h^s}}^{\gamma\delta} \left[\!\left[\boldsymbol{\Delta t} \right]\!\right] \cdot \boldsymbol{\varphi}_{0,\delta} \nu^-_\gamma \right\|_{\mathrm{L}^2(\partial\mathcal{A}_e)} + \\
& \sum_e \left\| \sqrt{\frac{\beta \mathcal{H}_m \bar{j}_0}{2h^s}}^{\gamma\delta} \boldsymbol{\varphi}_{0,\gamma} \cdot \left[\!\left[\boldsymbol{\Delta t}\left(\boldsymbol{u}\right) \right]\!\right] \nu^-_\delta \right\|^2_{\mathrm{L}^2(\partial\mathcal{A}_e)} .
\end{aligned} \tag{105}
$$

The final expression of the lower bound of the bilinear form is obtained by the ε-inequality [4] applied to Eq. (105), leading to

$$
\begin{aligned}
a\left(\boldsymbol{u},\,\boldsymbol{u}\right) \geq & \sum_e \left\| \sqrt{\mathcal{H}_n \bar{j}_0}^{\alpha\beta} \frac{1}{2} \left(\boldsymbol{\varphi}_{0,\alpha} \cdot \boldsymbol{u}_{,\beta} + \boldsymbol{u}_{,\alpha} \cdot \boldsymbol{\varphi}_{0,\beta} \right) \right\|^2_{\mathrm{L}^2(\mathcal{A}_e)} + \\
& (1-\varepsilon) \sum_e \left\| \sqrt{\mathcal{H}_m \bar{j}_0}^{\alpha\beta} \left(\boldsymbol{\varphi}_{0,\alpha} \cdot \boldsymbol{\Delta t}_{,\beta} + \boldsymbol{u}_{,\alpha} \cdot \boldsymbol{t}_{0,\beta} \right) \right\|^2_{\mathrm{L}^2(\mathcal{A}_e)} + \\
& \left(1 - 2\frac{C^{k^2}}{\varepsilon\beta} \right) \sum_e \left\| \sqrt{\frac{\beta \mathcal{H}_m \bar{j}_0}{2h^s}}^{\gamma\delta} \boldsymbol{\varphi}_{0,\gamma} \cdot \left[\!\left[\boldsymbol{\Delta t}\left(\boldsymbol{u}\right) \right]\!\right] \nu^-_\delta \right\|^2_{\mathrm{L}^2(\partial\mathcal{A}_e)} \\
& \qquad \forall \boldsymbol{u} \in \mathrm{U}^{\mathrm{f}}_c\left(\mathcal{A}_h\right) .
\end{aligned} \tag{106}
$$

4.3 Stability

The stability of the proposed discontinuous Galerkin formulation for shells is demonstrated in a straightforward manner from the lower bound (106) of the bilinear form (73). Indeed, for a given $1 > \varepsilon > 0$, there always exists $\beta > 2C^{k^2}/\varepsilon > 0$ such that

$$
a\left(\boldsymbol{u}_h,\,\boldsymbol{u}_h\right) \geq C_2\left(\beta\right) \left|\left|\left| \boldsymbol{u}_h \right|\right|\right|^2 \quad \forall \boldsymbol{u}_h \in \mathrm{U}^k_{\mathrm{hc}} \subset \mathrm{U}^{\mathrm{f}}_c\left(\mathcal{A}_h\right) , \tag{107}
$$

with $C_2\left(\beta\right) > 0$.

[4] $\forall \epsilon > 0 : |ab| \leq \frac{\epsilon}{2}a^2 + \frac{1}{2\epsilon}b^2$ or $\forall \epsilon > 0 : |ab| \leq \epsilon a^2 + \frac{1}{4\epsilon}b^2$.

Therefore, if the stabilization parameter β is larger than a constant which is solely dependent on the degree of the polynomial approximation, then the stability is demonstrated. This follows from the fact that the square of the energy norm $|||\boldsymbol{u}_h|||^2$ is bounded by $a(\boldsymbol{u}_h, \boldsymbol{u}_h) = b(\boldsymbol{u}_h)$, which corresponds to the work of the external forces.

4.4 Convergence rate in the energy norm

Next, the error between the finite element solution and the interpolant of the exact solution in the same space of functions of polynomial degree k is calculated. This establishes the convergence rate of the problem. If $\boldsymbol{u} \in \mathrm{U}_c^{\mathrm{f}}(\mathcal{A}_h)$ is the exact solution of the problem, its interpolant $\boldsymbol{u}^k$ in the manifold $\mathrm{U}_{\mathrm{h}c}^k$ is defined by

$$\int_{\mathcal{A}_h} \left(\boldsymbol{u} - \boldsymbol{u}^k\right) \cdot \delta\boldsymbol{u} \bar{j}_0 d\mathcal{A} = 0 \;\; \forall \delta\boldsymbol{u} \in \mathrm{U}_{\mathrm{h}c}^k \,. \tag{108}$$

The error is defined as

$$\boldsymbol{e} = \boldsymbol{u}_h - \boldsymbol{u} \in \mathrm{U}_c^{\mathrm{f}}(\mathcal{A}_h) \,, \tag{109}$$

where the imposed displacement on $\partial_U \mathcal{A}$ is strictly enforced and equal to zero, whereas the error on the exact solution interpolant is defined as

$$\boldsymbol{e}^k = \boldsymbol{u}_h - \boldsymbol{u}^k \in \mathrm{U}_{\mathrm{h}c}^k \subset \mathrm{U}_c^{\mathrm{f}}(\mathcal{A}_h) \,. \tag{110}$$

Since the terms (74, 78) involved in the bilinear equations (73) are by definition linear, the use of Eqs. (103) and (107) yields

$$\begin{aligned} C_2 \left|\left|\left|\boldsymbol{e}^k\right|\right|\right|^2 &\leq a\left(\boldsymbol{u}_h - \boldsymbol{u}^k,\, \boldsymbol{u}_h - \boldsymbol{u}^k\right) \\ &\leq a\left(\boldsymbol{u}_h - \boldsymbol{u},\, \boldsymbol{u}_h - \boldsymbol{u}^k\right) + a\left(\boldsymbol{u} - \boldsymbol{u}^k,\, \boldsymbol{u}_h - \boldsymbol{u}^k\right) \\ &\leq C_1 \left|\left|\left|\boldsymbol{u} - \boldsymbol{u}^k\right|\right|\right| \left|\left|\left|\boldsymbol{u}_h - \boldsymbol{u}^k\right|\right|\right| = C_1 \left|\left|\left|\boldsymbol{u} - \boldsymbol{u}^k\right|\right|\right| \left|\left|\left|\boldsymbol{e}^k\right|\right|\right| \,, \end{aligned} \tag{111}$$

where the orthogonality relation (91) has been used.

The terms appearing in the norm $\left|\left|\left|\boldsymbol{u} - \boldsymbol{u}^k\right|\right|\right|$ can all be bounded to enable the computation of the error resulting from the discontinuous Galerkin method. Defining $\mathcal{I}^{\alpha\beta\gamma\delta}$ the unit forth order tensor, the membrane energy term can be

bounded by

$$\left\|\sqrt{\mathcal{H}_n\bar{j}_0}^{\alpha\beta}\frac{1}{2}\left(\boldsymbol{\varphi}_{0,\alpha}\cdot\left(\boldsymbol{u}_{,\beta}-\boldsymbol{u}^k_{,\beta}\right)+\left(\boldsymbol{u}_{,\alpha}-\boldsymbol{u}^k_{,\alpha}\right)\cdot\boldsymbol{\varphi}_{0,\beta}\right)\right\|^2_{\mathrm{L}^2(\mathcal{A}_e)}\leq$$
$$C_{n1}\left\|\sqrt{\mathcal{I}}^{\alpha\beta}\boldsymbol{\varphi}_{0,\alpha}\cdot\left(\boldsymbol{u}_{,\beta}-\boldsymbol{u}^k_{,\beta}\right)\right\|^2_{\mathrm{L}^2(\mathcal{A}_e)}\leq$$
$$2C_{n1}\left[\left\|\sqrt{\mathcal{I}}^{\alpha\beta}\left(\boldsymbol{\varphi}_{0,\alpha}\cdot\left(\boldsymbol{u}-\boldsymbol{u}^k\right)\right)_{,\beta}\right\|^2_{\mathrm{L}^2(\mathcal{A}_e)}+\left\|\sqrt{\mathcal{I}}^{\alpha\beta}\boldsymbol{\varphi}_{0,\alpha\beta}\cdot\left(\boldsymbol{u}-\boldsymbol{u}^k\right)\right\|^2_{\mathrm{L}^2(\mathcal{A}_e)}\right]$$
$$\leq 2C_{n2}\left\|\sqrt{\mathrm{I}}^{\alpha}\boldsymbol{\varphi}_{0,\alpha}\cdot\left(\boldsymbol{u}-\boldsymbol{u}^k\right)\right\|^2_{\mathrm{H}^1(\mathcal{A}_e)}+2C_{n1}\left\|\sqrt{\mathcal{I}}^{\alpha\beta}\boldsymbol{\varphi}_{0,\alpha\beta}\cdot\left(\boldsymbol{u}-\boldsymbol{u}^k\right)\right\|^2_{\mathrm{L}^2(\mathcal{A}_e)}$$
$$\leq C_{n3}\left(\left\|\boldsymbol{u}-\boldsymbol{u}^k\right\|^2_{\mathbf{H}^1(\mathcal{A}_e)}+\left\|\boldsymbol{u}-\boldsymbol{u}^k\right\|^2_{\mathbf{L}^2(\mathcal{A}_e)}\right)\leq$$
$$C_{n4}h^{s2k}\left|\boldsymbol{u}\right|^2_{\mathbf{H}^{k+1}(\mathcal{A}_e)}+C_{n5}h^{s2k+2}\left|\boldsymbol{u}\right|^2_{\mathbf{H}^{k+1}(\mathcal{A}_e)}\leq C_n h^{s2k}\left|\boldsymbol{u}\right|^2_{\mathbf{H}^{k+1}(\mathcal{A}_e)}\qquad(112)$$

using the positive and symmetric nature of $\mathcal{H}_n$, the derivation by part, the property $(a+b)^2<2a^2+2b^2$, the definition of the Sobolev space ($\|a_{,\alpha}\|_{\mathrm{H}^0(\mathcal{A}_e)}\leq\|a\|_{\mathrm{H}^1(\mathcal{A}_e)}$), the property $\|\boldsymbol{a}\cdot\boldsymbol{b}\|\leq\|\boldsymbol{a}\|\,\|\boldsymbol{b}\|$, the basic error estimates of interpolation theory [5] and the assumption $h^s<1$. Thus it is assumed that the description of the surface is continuous and regular (no singular point).

By using the definition (15) of $\boldsymbol{\Delta t}_{,\gamma}$, and doing the same analysis here as above for all the terms involved in the products $\boldsymbol{\Delta t}_{,\beta}\cdot\boldsymbol{\varphi}_{0,\alpha}$ and $\boldsymbol{u}_{,\alpha}\cdot\boldsymbol{t}_{0,\beta}$. It is clear that terms up to the second derivative will appear, leading to

$$\left\|\sqrt{\mathcal{H}_m\bar{j}_0}^{\alpha\beta}\left(\boldsymbol{\varphi}_{0,\alpha}\cdot\boldsymbol{\Delta t}_{,\beta}\left(\boldsymbol{u}-\boldsymbol{u}^k\right)+\left(\boldsymbol{u}_{,\alpha}-\boldsymbol{u}^k_{,\alpha}\right)\cdot\boldsymbol{t}_{0,\beta}\right)\right\|^2_{\mathrm{L}^2(\mathcal{A}_e)}\leq$$
$$C_{m1}\left\|\boldsymbol{u}-\boldsymbol{u}^k\right\|^2_{\mathrm{H}^2(\mathcal{A}_e)}+C_{m2}\left\|\boldsymbol{u}-\boldsymbol{u}^k\right\|^2_{\mathrm{H}^1(\mathcal{A}_e)}+C_{m3}\left\|\boldsymbol{u}-\boldsymbol{u}^k\right\|^2_{\mathrm{L}^2(\mathcal{A}_e)}\qquad(113)$$

Using the error estimates from interpolation theory and the fact that $h^s<1$, this relation becomes

$$\left\|\sqrt{\mathcal{H}_m\bar{j}_0}^{\alpha\beta}\left(\boldsymbol{\varphi}_{0,\alpha}\cdot\boldsymbol{\Delta t}_{,\beta}\left(\boldsymbol{u}-\boldsymbol{u}^k\right)+\left(\boldsymbol{u}_{,\alpha}-\boldsymbol{u}^k_{,\alpha}\right)\cdot\boldsymbol{t}_{0,\beta}\right)\right\|^2_{\mathrm{L}^2(\mathcal{A}_e)}\leq$$
$$C_m h^{s2k-2}\left|\boldsymbol{u}\right|^2_{\mathbf{H}^{k+1}(\mathcal{A}_e)}\ .\qquad(114)$$

Now the interface terms are considered. Using Eqs. (7) and (12), leads to the

[5] Given a mapping $\boldsymbol{u}\in\mathbf{H}^{k+1}(\mathcal{A}_e)$, then $\forall\boldsymbol{u}^k\in\mathbb{P}^k$ interpolating $\boldsymbol{u}$ in $\mathcal{A}_e$: $\left\|\boldsymbol{u}-\boldsymbol{u}^k\right\|_{\mathbf{H}^q(\mathcal{A}_e)}\leq C_i h^{sk+1-q}\left|\boldsymbol{u}\right|_{\mathbf{H}^{k+1}(\mathcal{A}_e)}\ \forall 0\leq q\leq k+1$, with C_i independent of h^s, the size of $\mathcal{A}_e$ [1].

property $[\![\boldsymbol{\Delta t}]\!] \cdot \boldsymbol{\varphi}_{0,\alpha} = -[\![\boldsymbol{u}_{,\alpha}]\!] \cdot \boldsymbol{t}_0$, which enables writing

$$\frac{1}{2}\sum_e \left\| \sqrt{\frac{\beta \mathcal{H}_m \bar{j}_0}{h^s}}^{\alpha\beta} \boldsymbol{\varphi}_{0,\alpha} \cdot \left[\!\!\left[\boldsymbol{\Delta t} \left(\boldsymbol{u} - \boldsymbol{u}^k \right) \right]\!\!\right] \nu_\beta^- \right\|^2_{\mathrm{L}^2(\partial\mathcal{A}_e)} \leq$$

$$\sum_e \left\| \sqrt{\frac{\beta \mathcal{H}_m \bar{j}_0}{h^s}}^{\alpha\beta} \boldsymbol{t}_0 \cdot \left(\boldsymbol{u}_{,\alpha} - \boldsymbol{u}^k_{,\alpha} \right) \nu_\beta^- \right\|^2_{\mathrm{L}^2(\partial\mathcal{A}_e)} \leq$$

$$\sum_e \frac{C_{I1}\beta}{h^s} \left\| \sqrt{\mathrm{I}}^\alpha \left(\boldsymbol{u}_{,\alpha} - \boldsymbol{u}^k_{,\alpha} \right) \right\|^2_{\mathbf{L}^2(\partial\mathcal{A}_e)} \leq$$

$$\sum_e \frac{C_{I2}\beta}{h^{s^2}} \| \sqrt{\mathrm{I}}^\alpha \left(\boldsymbol{u}_{,\alpha} - \boldsymbol{u}^k_{,\alpha} \right) \|^2_{\mathbf{L}^2(\mathcal{A}_e)} + \sum_e C_{I3}\beta \left\| \sqrt{\mathcal{I}}^{\alpha\beta} \left(\boldsymbol{u}_{,\alpha\beta} - \boldsymbol{u}^k_{,\alpha\beta} \right) \right\|^2_{\mathbf{L}^2(\mathcal{A}_e)} \leq$$

$$\sum_e \frac{C_{I2}\beta}{h^{s^2}} \left\| \boldsymbol{u} - \boldsymbol{u}^k \right\|^2_{\mathbf{H}^1(\mathcal{A}_e)} + \sum_e C_{I3}\beta \left\| \boldsymbol{u} - \boldsymbol{u}^k \right\|^2_{\mathbf{H}^2(\mathcal{A}_e)} \leq$$

$$\sum_e \frac{C_{I4}\beta}{h^{s^4}} \left\| \boldsymbol{u} - \boldsymbol{u}^k \right\|^2_{\mathbf{L}^2(\mathcal{A}_e)} \leq$$

$$\sum_e C_I \beta h^{s2k-2} \left| \boldsymbol{u} \right|^2_{\mathbf{H}^{k+1}(\mathcal{A}_e)} , \tag{115}$$

using the positive and symmetric natures of $\mathcal{H}_m$, the property $\|\boldsymbol{a}\cdot\boldsymbol{b}\| \leq \|\boldsymbol{a}\|\|\boldsymbol{b}\|$, the trace inequality [6], the definition of Sobolev spaces (*i.e.* $\|\boldsymbol{\nabla x}\|_{\mathbf{H}^0(\mathcal{A}_e)} \leq \|\boldsymbol{x}\|_{\mathbf{H}^1(\mathcal{A}_e)}$), the inverse inequality [7] and the the interpolation theory. In this development, h^s is assumed to be constant.

Combining these last three results, Eq. (111) may be rewritten as

$$\left|\!\left|\!\left| \boldsymbol{e}^k \right|\!\right|\!\right| \leq \sum_e C h^{sk-1} \left| \boldsymbol{u} \right|_{\mathbf{H}^{k+1}(\mathcal{A}_e)} . \tag{116}$$

As expected, the presence of high-order derivatives in the governing equation implies an order of convergence lower than the degree of the polynomial approximation. For this reason, the use of at least quadratic interpolation is required. In fact, for linear shell elements only the stabilization terms remain non-zero in the interface terms of Eq. (74). In that case, the method corresponds to a penalty method and the converged solution depends on the value of the stabilization parameter with no possibility of ascertaining the convergence toward the exact solution.

Note that in membrane problems, only term (112) is different from zero and the error becomes

$$\left|\!\left|\!\left| \boldsymbol{e}^k \right|\!\right|\!\right|_{\text{membrane}} \leq \sum_e C h^{sk} \left| \boldsymbol{u} \right|_{\mathbf{H}^{k+1}(\mathcal{A}_e)} , \tag{117}$$

[6] $\forall \boldsymbol{v} \in \mathrm{H}^1(\mathcal{A}_e) \quad \exists C_T > 0 : \|\boldsymbol{v}\|^2_{\mathbf{L}^2(\partial\mathcal{A}_e)} \leq \frac{C_T}{h^s} \|\boldsymbol{v}\|^2_{\mathbf{L}^2(\mathcal{A}_e)} + C_T h^s \|\boldsymbol{v}_{,\alpha}\|^2_{\mathbf{L}^2(\mathcal{A}_e)}$.

[7] $\forall m \geq l \quad \exists C_I > 0 : \quad \|\boldsymbol{v}\|_{\mathbf{H}^m(\mathcal{A}_e)} \leq C_I h^{sl-m} \|\boldsymbol{v}\|_{\mathbf{H}^l(\mathcal{A}_e)}$.

which is consistent with the $\mathcal{C}^0$ properties of the shape functions, implying that no DG method is applied to the membrane mode.

4.5 Convergence in the $\mathbf{L}^2$ *norm*

Optimal-convergence rate in the $\mathbf{L}^2$-norm is also demonstrated under the assumption of cubic approximation and of proper elliptic regularity of the problem.

In order to simplify the notation, the linear dependence of vector $\boldsymbol{\Delta t}$ with $\boldsymbol{u}_{,\alpha}$ can be exposed from Eq. (12), leading to

$$\boldsymbol{\Delta t} = \tilde{\boldsymbol{\Delta}}\mathbf{t}_\alpha \boldsymbol{u}_{,\alpha} \text{ with} \tag{118}$$

$$\tilde{\boldsymbol{\Delta}}\mathbf{t}_\alpha = \frac{e_{\beta\alpha 3}}{\bar{j}_0}\left[\tilde{\boldsymbol{\varphi}}_{0,\beta} - \boldsymbol{t}_0 \otimes (\boldsymbol{t}_0 \wedge \boldsymbol{\varphi}_{0,\beta})\right] , \tag{119}$$

where $\tilde{\boldsymbol{\Delta}}\mathbf{t}_\alpha$ is a second order tensor and $\tilde{\boldsymbol{\varphi}}_{0,\beta}$ is the skew rotation matrix associated to $\boldsymbol{\varphi}_{0,\beta}$. For simplicity, pure Dirichlet boundary conditions are assumed, with

$$\partial_U \mathcal{A}_h = \partial_T \mathcal{A}_h = \partial \mathcal{A}_h \text{ and } \partial_N \mathcal{A}_h = \partial_M \mathcal{A}_h = \emptyset , \tag{120}$$

$$\boldsymbol{u} = \boldsymbol{\Delta t} = \mathbf{0} \text{ on } \partial \mathcal{A}_h . \tag{121}$$

As the consistency of the method has been established, the exact deformation fields $\boldsymbol{u} \in \mathrm{U}_c^{\mathrm{f}}(\mathcal{A}_h)$ satisfy the bilinear form (73), with $a(\boldsymbol{u}, \delta\boldsymbol{u})$ defined by Eq. (74) and $b(\delta\boldsymbol{u})$ defined by Eq. (78), $\forall \ \delta\boldsymbol{u} \in \mathrm{U}_c^{\mathrm{f}}(\mathcal{A}_h)$. For pure Dirichlet boundary conditions, using Eqs. (118) and (121), this last term can be rewritten as

$$b^{\boldsymbol{n}^{\mathcal{A}}, \tilde{\boldsymbol{m}}^{\mathcal{A}}}(\delta\boldsymbol{u}) = \int_{\mathcal{A}_h} \left[\bar{j}_0 \boldsymbol{n}^{\mathcal{A}} - \left(\bar{j}_0 \tilde{\boldsymbol{\Delta}}\mathbf{t}_\mu^T \tilde{\boldsymbol{m}}^{\mathcal{A}}\right)_{,\mu}\right] \cdot \delta\boldsymbol{u} d\mathcal{A} . \tag{122}$$

Let $\boldsymbol{u}_d \in \mathrm{U}_c^{\mathrm{f}}(\mathcal{A}_h)$ be the exact solution of a problem governed by the system (73) for a given pair $\left(\boldsymbol{n}_d^{\mathcal{A}}, \ \tilde{\boldsymbol{m}}^{\mathcal{A}} d\right)$. Therefore, considering the error $\boldsymbol{e} \in \mathrm{U}_c^{\mathrm{f}}(\mathcal{A}_h)$ (109) as the virtual displacements yields

$$\begin{aligned} b^{\boldsymbol{n}^{\mathcal{A}}, \tilde{\boldsymbol{m}}^{\mathcal{A}}}(\boldsymbol{e}) &= a(\boldsymbol{u}_d, \boldsymbol{e}) = a\left(\boldsymbol{u}_d - \boldsymbol{u}_d^k, \boldsymbol{e}\right) + a\left(\boldsymbol{u}_d^k, \boldsymbol{e}\right) \\ &= a\left(\boldsymbol{u}_d - \boldsymbol{u}_d^k, \boldsymbol{e}\right) + a\left(\boldsymbol{e}, \boldsymbol{u}_d^k\right) \\ &= a\left(\boldsymbol{u}_d - \boldsymbol{u}_d^k, \boldsymbol{e}\right) + a\left(\boldsymbol{u}_h - \boldsymbol{u}, \boldsymbol{u}_d^k\right) = a\left(\boldsymbol{u}_d - \boldsymbol{u}_d^k, \boldsymbol{e}\right) \\ &= a\left(\boldsymbol{u}_d - \boldsymbol{u}_d^k, \boldsymbol{u}_h - \boldsymbol{u}^k\right) + a\left(\boldsymbol{u}_d - \boldsymbol{u}_d^k, \boldsymbol{u}^k - \boldsymbol{u}\right) \end{aligned} \tag{123}$$

where the $\boldsymbol{u}_d^k$ is the interpolation of $\boldsymbol{u}_d$ in the manifold $\mathrm{U}_{\mathrm{hc}}^k$ (108), and where the symmetric nature of $a(,)$ as well as the orthogonality relation (91) have

been used. Since all the terms involved belong to the manifold $\mathrm{U}_c^{\mathrm{f}}(\mathcal{A}_h)$, Eq. (103) can be used, and the particular choice of the adjoint problem

$$\bar{j}_0 \boldsymbol{n}^{\mathcal{A}} - \left(\bar{j}_0 \tilde{\boldsymbol{\Delta}} \mathbf{t}_\mu^T \tilde{\boldsymbol{m}}^{\mathcal{A}} \right)_{,\mu} = \boldsymbol{e}\,, \tag{124}$$

enables rewriting (123) as

$$\|\boldsymbol{e}\|^2_{\mathbf{L}^2(\mathcal{A}_h)} \leq C^k(\beta) \left|\!\left|\!\left| \boldsymbol{u}_d - \boldsymbol{u}_d^k \right|\!\right|\!\right| \left[\ \left|\!\left|\!\left| \boldsymbol{e}^k \right|\!\right|\!\right| + \left|\!\left|\!\left| \boldsymbol{u}^k - \boldsymbol{u} \right|\!\right|\!\right| \ \right]. \tag{125}$$

The key to establishing the convergence rate is to bound the term $\left|\!\left|\!\left| \boldsymbol{u}_d - \boldsymbol{u}_d^k \right|\!\right|\!\right|$ using theorems 5.1 and 5.4 in [25] adapted to the Dirichlet problem under consideration. These theorems are summarized by the following:

Theorem 1 *Consider the problem*

$$\mathbf{A} \cdot \boldsymbol{u} = \boldsymbol{f} \in \mathcal{A}\,, \tag{126}$$
$$\mathbf{B}_i \cdot \boldsymbol{u} = \boldsymbol{g}_i \text{ on } \partial\mathcal{A} \qquad \text{for } i = 0,\, 1\,, ...,\, m-1\,, \tag{127}$$

with the proper elliptic operator $\mathbf{A} \ : \ \mathcal{C}^\infty(\mathcal{A}) \to \mathbf{H}^{s-2m}(\mathcal{A})$ *and the operator* $\mathbf{B}_i \ : \ \mathcal{C}^\infty(\partial\mathcal{A}) \to \mathbf{H}^{s-i-1/2}(\partial\mathcal{A})$ *which respectively take the expression*

$$\mathbf{A} \cdot \boldsymbol{u} = \sum_{0 \leq p,q \leq m} (-1)^p D^p \left(\mathbf{a}_{pq}(\xi^\alpha) D^q \boldsymbol{u} \right), \tag{128}$$
$$\mathbf{B}_i \cdot \boldsymbol{u} = \frac{\partial^i}{\partial \boldsymbol{\zeta}^i} \boldsymbol{u}\,, \tag{129}$$

with $\boldsymbol{\zeta}$ *the outer normal of* $\partial\mathcal{A}$*, and with*

$$D^p = \frac{\partial^{p_1+p_2}}{\partial \xi^{1 p_1} \partial \xi^{2 p_2}}\,, \quad p_1 + p_2 = p\,. \tag{130}$$

Therefore, if $\boldsymbol{u} \in \mathbf{H}^{2m}(\mathcal{A})$ *and if* $\mathbf{A} \cdot \boldsymbol{u} \in \mathbf{H}^{p-2m}(\mathcal{A})$, $\mathbf{B}_i \cdot \boldsymbol{u} \in \mathbf{H}^{p-i-1/2}(\partial\mathcal{A})$, *one has* $\forall p \geq 2m$

$$\|\boldsymbol{u}\|_{\mathbf{H}^p(\mathcal{A})} \leq C^p \left\{ \|\mathbf{A} \cdot \boldsymbol{u}\|_{\mathbf{H}^{p-2m}(\mathcal{A})} + \sum_i \|\mathbf{B}_i \cdot \boldsymbol{u}\|_{\mathbf{H}^{p-i-1/2}(\partial\mathcal{A})} \right\}. \tag{131}$$

The use of this theorem requires the proper elliptic regularity of the problem. This proper elliptic regularity can easily be demonstrated for particular cases like pure bending, but is not obvious for complex problems. Nevertheless we will assume it in the following.

Eq. (116) allows to write

$$\left|\left|\left|\boldsymbol{u}_d - \boldsymbol{u}_d^k\right|\right|\right| \leq \begin{cases} Ch^{s2} \left|\boldsymbol{u}_d\right|_{\mathbf{H}^4(\mathcal{A}_h)} & \text{if } k > 2 \\ Ch^{s} \left|\boldsymbol{u}_d\right|_{\mathbf{H}^4(\mathcal{A}_h)} & \text{if } k = 2 \end{cases}, \tag{132}$$

this last result for $k = 2$ being obtained following the argumentation of Wells and Dung [7]. Therefore, theorem 1 can be applied to Eq. (132) with $m = 2$, $p = 4 \geq 2m$, $\boldsymbol{f} = \boldsymbol{e}$ and $\boldsymbol{g}_i = 0$, which leads to

$$\left|\left|\left|\boldsymbol{u}_d - \boldsymbol{u}_d^k\right|\right|\right| \leq \begin{cases} C^r h^{s2} \left\|\boldsymbol{e}\right\|_{\mathbf{L}^2(\mathcal{A}_h)} & \text{if } k > 2 \\ C^r h^{s} \left\|\boldsymbol{e}\right\|_{\mathbf{L}^2(\mathcal{A}_h)} & \text{if } k = 2 \end{cases}. \tag{133}$$

This last results in combination with (116) enables rewriting (125) as

$$\left\|\boldsymbol{e}\right\|_{\mathbf{L}^2(\mathcal{A}_h)} \leq \begin{cases} \sum\limits_e Ch^{sk+1} \left|\boldsymbol{u}\right|_{\mathbf{H}^{k+1}(\mathcal{A}_e)} & \text{if } k > 2 \\ \sum\limits_e Ch^{s2} \left|\boldsymbol{u}\right|_{\mathbf{H}^3(\mathcal{A}_e)} & \text{if } k = 2 \end{cases} \tag{134}$$

The DG shell formulation exhibits an optimal-convergence in the $\mathbf{L}^2$ norm when provided that at least cubic elements are used. In fact, it will be shown in the numerical examples that the optimal convergence rate can be observed even for quadratic elements.

For pure membrane problem, Eq. (117) allows to write

$$\left|\left|\left|\boldsymbol{u}_d - \boldsymbol{u}_d^k\right|\right|\right| \leq Ch^{s} \left|\boldsymbol{u}_d\right|_{\mathbf{H}^2(\mathcal{A}_h)}. \tag{135}$$

Theorem 1 can be applied to Eq. (135) with $m = 1$, $p = 2 \geq 2m$, $\boldsymbol{f} = \boldsymbol{e}$ and $\boldsymbol{g}_0 = 0$, which leads to

$$\left|\left|\left|\boldsymbol{u}_d - \boldsymbol{u}_d^k\right|\right|\right| \leq Ch^{sp-1} \left|\boldsymbol{u}_d\right|_{\mathbf{H}^p(\mathcal{A}_h)} \leq C^r h^{s} \left\|\boldsymbol{e}\right\|_{\mathbf{L}^2(\mathcal{A}_h)}. \tag{136}$$

Combining this last result with (112) and (117), Eq. (125) can be expressed as

$$\left\|\boldsymbol{e}\right\|_{\mathbf{L}^2(\mathcal{A}_h)} \leq \sum_e Ch^{sk+1} \left|\boldsymbol{u}\right|_{\mathbf{H}^{k+1}(\mathcal{A}_e)}, \tag{137}$$

if $k \geq 1$. This demonstrates that the membrane formulation exhibits an optimal-convergence in the $\mathbf{L}^2$ norm when only the membrane modes are present. This behavior is consistent with the fact that the presented membrane formulation is a continuous Galerkin method.

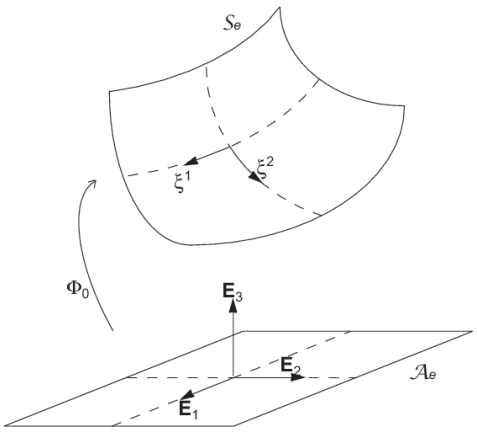

Fig. 4. Definition of the iso-parametric elements.

5 Implementation

The preceding discontinuous Galerkin formulation is taken as a basis for computational finite-element implementation.

5.1 Integration of the membrane contributions

Conventional iso-parametric elements defined in the reference frame $\boldsymbol{E}_\alpha$ by $(\xi^1,\, \xi^2) \in [-1,\, 1] \times [-1,\, 1]$, with associated shape functions N^a, Fig. 4, are used for discretizing (75). The corresponding displacement field $\boldsymbol{u}_h$ follows in terms of the element nodal displacements $\boldsymbol{u}^a$ as

$$\boldsymbol{u}_h = N^a \boldsymbol{u}^a \,, \tag{138}$$

and similarly for the virtual displacement field $\delta\boldsymbol{u}$.

From the nodal coordinates in the reference configuration $\boldsymbol{X}^a$, the convected basis and its derivative are computed as

$$\boldsymbol{\varphi}_{0,\alpha} = \frac{\partial N^a}{\partial \xi^\alpha} \boldsymbol{X}^a \,, \text{ and } \boldsymbol{\varphi}_{0,\alpha\beta} = \frac{\partial^2 N^a}{\partial \xi^\alpha \partial \xi^\beta} \boldsymbol{X}^a \,. \tag{139}$$

From these, the director unit vector $\boldsymbol{t}_0$ and the Jacobian $\bar{j}_0$ follow directly from Eqs. (7) and (8), while $\boldsymbol{\varphi}_0^{,\alpha}$ follows directly from the usual duality relations.

Based on this convected basis, the resultant membrane strain tensor (36), as well as its virtual variation, can be determined respectively as

$$\varepsilon_{\alpha\beta}\left(\boldsymbol{u}_h\right) = \boldsymbol{B}_{n\alpha\beta}^{\;a} \cdot \boldsymbol{u}^a \,, \text{ and by } \delta\varepsilon_{\alpha\beta}\left(\boldsymbol{u}\right) = \boldsymbol{B}_{n\alpha\beta}^{\;a} \cdot \delta\boldsymbol{u}^a \,, \tag{140}$$

where $\boldsymbol{B}_{n\alpha\beta}^{\ a} = \left(\frac{1}{2}\boldsymbol{\varphi}_{0,\alpha}\frac{\partial N^a}{\partial \beta} + \frac{1}{2}\boldsymbol{\varphi}_{0,\beta}\frac{\partial N^a}{\partial \alpha}\right)$ is the linearized first order tensor of the membrane strains.

The corresponding bilinear term (75) can therefore be computed by

$$a_n^e\left(\boldsymbol{u}_h,\, \delta\boldsymbol{u}\right) = \boldsymbol{F}_n^{e\,a} \cdot \delta\boldsymbol{u}^a\,, \tag{141}$$

where

$$\boldsymbol{F}_n^{e\,a} = \int_{\mathcal{A}_e} \boldsymbol{B}_{n\gamma\delta}^{\ a} \otimes \boldsymbol{B}_{n\alpha\beta}^{\ b} \mathcal{H}_n^{\alpha\beta\gamma\delta} \bar{j}_0 d\mathcal{A}\ \ \boldsymbol{u}^b\,, \tag{142}$$

is the element internal membrane force. The element membrane Jacobian matrix can be deduced directly from the previous equation, yielding

$$\mathbf{K}_n^{e\,a\,b} = \int_{\mathcal{A}_e} \boldsymbol{B}_{n\gamma\delta}^{\ a} \otimes \boldsymbol{B}_{n\alpha\beta}^{\ b} \mathcal{H}_n^{\alpha\beta\gamma\delta} \bar{j}_0 d\mathcal{A}\,. \tag{143}$$

The computation of the integrals (142) and (143) is done by Gauss quadrature, see sections 5.5 and 5.6.

5.2 Integration of the bending contributions

For the purpose of integrating the bending term (76), the same finite element approximation (138-139) is used.

The resultant bending strain tensor (37), as well as its virtual variation, can be determined respectively by the expressions

$$\rho_{\alpha\beta}\left(\boldsymbol{u}_h\right) = \boldsymbol{B}_{m\alpha\beta}^{\ a} \cdot \boldsymbol{u}^a\,, \text{ and by } \delta\rho_{\alpha\beta}\left(\boldsymbol{u}\right) = \boldsymbol{B}_{m\alpha\beta}^{\ a} \cdot \delta\boldsymbol{u}^a\,, \tag{144}$$

where

$$\boldsymbol{B}_{m\alpha\beta}^{\ a} = \frac{e_{\mu\eta 3}}{\bar{j}_0}\left[\boldsymbol{\varphi}_{0,\alpha\beta} \cdot \boldsymbol{t}_0\left(\boldsymbol{\varphi}_{0,\eta} \wedge \boldsymbol{t}_0\right) + \left(\boldsymbol{\varphi}_{0,\alpha\beta} \wedge \boldsymbol{\varphi}_{0,\eta}\right)\right]\frac{\partial N^a}{\partial \xi^\mu} - \boldsymbol{t}_0 \frac{\partial^2 N^a}{\partial \xi^\alpha \partial \xi^\beta}\,. \tag{145}$$

Proceeding as with the membrane equations, the bending bilinear term (76) becomes

$$a_m^e\left(\boldsymbol{u}_h,\, \delta\boldsymbol{u}\right) = \boldsymbol{F}_m^{e\,a} \cdot \delta\boldsymbol{u}^a\,, \tag{146}$$

where

$$\boldsymbol{F}_m^{e\,a} = \int_{\mathcal{A}_e} \boldsymbol{B}_{m\gamma\delta}^{\ a} \otimes \boldsymbol{B}_{m\alpha\beta}^{\ b} \mathcal{H}_m^{\alpha\beta\gamma\delta} \bar{j}_0 d\mathcal{A}\ \ \boldsymbol{u}^b\,, \tag{147}$$

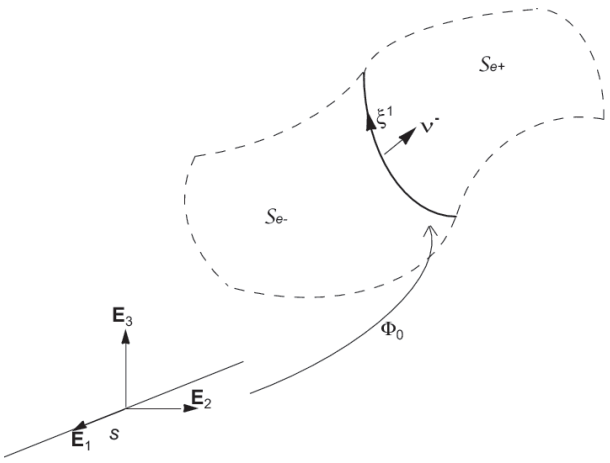

Fig. 5. Integration of the interface term on the side s common to element $\mathcal{A}_{e^-}$ and to $\mathcal{A}_{e^+}$.

is the element internal bending force, while

$$\mathbf{K}_m^{e\ a\,b} = \int_{\mathcal{A}_e} \boldsymbol{B}_{m\,\gamma\delta}^{\ a} \otimes \boldsymbol{B}_{m\,\alpha\beta}^{\ b} \mathcal{H}_m^{\alpha\beta\gamma\delta} \bar{j}_0 d\mathcal{A}\,, \tag{148}$$

is the element bending Jacobian matrix.

In addition to these contributions, in order to compute the interface terms (77) (see section 5.3), the shell element must also provide the variation of the unit vector (12) in terms of nodal displacements:

$$\boldsymbol{\Delta t}\,(\boldsymbol{u}_h) = \tilde{\boldsymbol{\Delta}}\mathbf{t}^{\,a}\,\boldsymbol{u}^a\,,\ \text{and}\ \delta\boldsymbol{\Delta t}\,(\boldsymbol{u}) = \tilde{\boldsymbol{\Delta}}\mathbf{t}^{\,a}\,\delta\boldsymbol{u}^a\,, \tag{149}$$

where

$$\tilde{\boldsymbol{\Delta}}\mathbf{t} = \frac{e_{\alpha\beta 3}}{\bar{j}_0}\left[\tilde{\boldsymbol{\varphi}}_{0,\alpha} - \boldsymbol{t}_0 \otimes (\boldsymbol{t}_0 \wedge \boldsymbol{\varphi}_{0,\alpha})\right] \frac{\partial N}{\partial \xi^\beta}\,, \tag{150}$$

is the linearized unit vector variation tensor, and where $\tilde{\boldsymbol{\varphi}}_{0,\alpha}$ is the equivalent skew rotation matrix associated with $\boldsymbol{\varphi}_{0,\alpha}$.

5.3 Integration of the interface contributions

The interface term (77) is integrated on a curve defined in the reference frame $\boldsymbol{E}_1$ by $\xi^1 \in [-1,\,1]$ see Fig. 5. For the purpose of computing the integrals, the curve is parametrized using a finite element interpolation defined with shape functions N_s^a and supported on the edge nodes. The integration is accomplished via Gauss quadrature. The various quantities involving neighboring elements information, the basis vectors $\boldsymbol{\varphi}_{0,\alpha}^{\pm}$, the resultant bending strains $\rho_{\alpha\beta}^{\pm}(\boldsymbol{u}_h)$, the virtual bending strains $\delta\rho_{\alpha\beta}^{\pm}(\boldsymbol{u})$, the unit vector variations $\boldsymbol{\Delta t}^{\pm}$,

the virtual unit vector variations $\delta\boldsymbol{\Delta t}^{\pm}$, and the Hooke tensors $\mathcal{H}_m^{\pm}$, are evaluated at the quadrature points on the edge element. This evaluation is performed as described in sections 5.1-5.2. A superscript $+(-)$ refers to values coming from the neighboring element $\mathcal{A}_{e^+}(\mathcal{A}_{e^-})$.

It should be noted that the basis vectors of the neighboring elements $\boldsymbol{\varphi}_{0,\alpha}^{+}$ and $\boldsymbol{\varphi}_{0,\alpha}^{+}$ differ in general. We define the basis vectors on the edge s as

$$\boldsymbol{t}_0 = \frac{\boldsymbol{t}_0^+ + \boldsymbol{t}_0^-}{\left\|\boldsymbol{t}_0^+ + \boldsymbol{t}_0^-\right\|}\,, \tag{151}$$

$$\boldsymbol{\varphi}_{0,1} = \sum_{a=1,2,7} \frac{\partial N_s^a}{\partial \xi^1} \boldsymbol{X}^a\,, \text{ and } \boldsymbol{\varphi}_{0,2} = \frac{\boldsymbol{t}_0 \wedge \boldsymbol{\varphi}_{0,1}}{\|\boldsymbol{t}_0 \wedge \boldsymbol{\varphi}_{0,1}\|}\,. \tag{152}$$

With this definition, the Jacobian $\bar{j}_0$ associated with the curve length is still equal to $\|\boldsymbol{\varphi}_{0,1} \wedge \boldsymbol{\varphi}_{0,2}\|$, and the outer unit normal $\boldsymbol{\nu}^-$ is equal to $\boldsymbol{\varphi}_{0,2}$. The push-forward tensors $T^{\pm}$ corresponding to the change of metric, are defined by

$$T_{\beta^+}^{\alpha} = \boldsymbol{\varphi}_0^{,\alpha} \cdot \boldsymbol{\varphi}_{0,\beta}^{+}\,, \text{ and } T_{\beta^-}^{\alpha} = \boldsymbol{\varphi}_0^{,\alpha} \cdot \boldsymbol{\varphi}_{0,\beta}^{-}\,, \tag{153}$$

while the corresponding inverse transformation tensors $t^{\pm}$ are defined by

$$t_{\beta}^{\alpha^+} = \boldsymbol{\varphi}_0^{+,\alpha} \cdot \boldsymbol{\varphi}_{0,\beta}\,, \text{ and } t_{\beta}^{\alpha^-} = \boldsymbol{\varphi}_0^{-,\alpha} \cdot \boldsymbol{\varphi}_{0,\beta}\,. \tag{154}$$

From these definitions, the push-forward mapping $\varphi_*()$ of the resultant bending strains ρ coming from the neighbors leads to the expression of the bending strains in the new metric:

$$\hat{\rho}_{\alpha\beta}^{\pm}(\boldsymbol{u}_h) = \varphi_*\left(\rho^{\pm}\right)_{\alpha\beta} = t_{\alpha}^{\gamma^{\pm}}\ \rho_{\gamma\delta}^{\pm}\ t_{\beta}^{\delta^{\pm}}\ . \tag{155}$$

This last relation is easily obtained by considering the frame invariance of the resultant bending strain tensor $\boldsymbol{\rho}^{\pm} = \hat{\rho}_{\alpha\beta}^{\pm}\boldsymbol{\varphi}_0^{,\alpha} \otimes \boldsymbol{\varphi}_0^{,\beta} = \rho_{\alpha\beta}^{\pm}\boldsymbol{\varphi}_0^{\pm,\alpha} \otimes \boldsymbol{\varphi}_0^{\pm,\beta}$. Using Eq. (144), (155) can be rewritten as

$$\hat{\rho}_{\alpha\beta}^{\pm}(\boldsymbol{u}_h) = \hat{\boldsymbol{B}}_{m\,\alpha\beta}^{\pm\,a}\,\boldsymbol{u}^a\,, \tag{156}$$

where

$$\hat{\boldsymbol{B}}_{m\,\alpha\beta}^{\pm\,a} = \varphi_*\left(\boldsymbol{B}_m^{\pm a}\right)_{\alpha\beta} = t_{\alpha}^{\gamma^{\pm}}\ \boldsymbol{B}_{m\gamma\delta}^{\pm a}\ t_{\beta}^{\delta^{\pm}}\ , \tag{157}$$

corresponds to the nodal value of the linearized resultant bending strains tensor. In addition to the nodes defining the curve, the nodes of the adjacent elements $\mathcal{A}_{e^-}$ and $\mathcal{A}_{e^+}$ also contribute to these terms. But vector $\boldsymbol{B}_m^{+\,a}$ resulting from neighbor $\mathcal{A}_{e^+}$ is different from zero only for nodes common with element $\mathcal{A}_{e^+}$, and similarly for vector $\boldsymbol{B}_m^{-\,a}$. Similarly, the virtual bending strain

variations are obtained by

$$\hat{\delta\rho}^{\pm}_{\alpha\beta}(\boldsymbol{u}) = \hat{\boldsymbol{B}}^{\pm\,a}_{m\,\alpha\beta}\,\delta\boldsymbol{u}^a\,. \tag{158}$$

Although the bending Hooke tensors $\hat{\mathcal{H}}^{\pm}_m$ can be computed directly from the local basis vectors, by virtue of Eq. (40), the same technique can also be used, yielding

$$\hat{\mathcal{H}}^{\pm\,\alpha\beta\gamma\delta}_m = \varphi_*\left(\mathcal{H}^{\pm}_m\right)^{\alpha\beta\gamma\delta} = T^{\alpha}_{\mu^\pm}\,T^{\beta}_{\nu^\pm}\,\mathcal{H}^{\pm\,\mu\nu\xi o}_m\,T^{\gamma}_{\xi^\pm}\,T^{\delta}_{o^\pm}\,. \tag{159}$$

The remaining terms that must be evaluated from the neighboring elements are the variations of the unit vector $\boldsymbol{\Delta t}^{\pm}$ and of the virtual unit vector $\delta\boldsymbol{\Delta t}^{\pm}$. Since these are vectors, no push-forward operations are needed, and the direct result from Eqs. (149) is

$$\boldsymbol{\Delta t}^{\pm}(\boldsymbol{u}_h) = \tilde{\boldsymbol{\Delta}}\mathbf{t}^{\pm\,a}\boldsymbol{u}^a\,,\ \text{and}\ \delta\boldsymbol{\Delta t}^{\pm}(\boldsymbol{u}) = \tilde{\boldsymbol{\Delta}}\mathbf{t}^{\pm\,a}\delta\boldsymbol{u}^a\,. \tag{160}$$

Using Eqs. (156, 158 - 160), the interface bilinear term (77) becomes

$$\begin{aligned} a^s_I(\boldsymbol{u}_h,\,\delta\boldsymbol{u}) = &\int_s \left\langle \hat{\mathcal{H}}^{\alpha\beta\gamma\delta}_m\ \hat{\boldsymbol{B}}^{a}_{m\,\gamma\delta}\right\rangle \otimes \left(\left[\!\left[\tilde{\boldsymbol{\Delta}}\mathbf{t}^{b}\right]\!\right]^T\boldsymbol{\varphi}_{0,\alpha}\right)\boldsymbol{u}^b\bar{j}_0\nu^-_\beta\,d\partial\mathcal{A}\cdot\delta\boldsymbol{u}^a + \\ &\int_s \left(\left[\!\left[\tilde{\boldsymbol{\Delta}}\mathbf{t}^{a}\right]\!\right]^T\boldsymbol{\varphi}_{0,\alpha}\right)\otimes\left\langle \hat{\mathcal{H}}^{\alpha\beta\gamma\delta}_m\ \hat{\boldsymbol{B}}^{b}_{m\,\gamma\delta}\right\rangle\boldsymbol{u}^b\bar{j}_0\nu^-_\beta\,d\partial\mathcal{A}\cdot\delta\boldsymbol{u}^a + \\ &\int_s \left(\left[\!\left[\tilde{\boldsymbol{\Delta}}\mathbf{t}^{a}\right]\!\right]^T\boldsymbol{\varphi}_{0,\gamma}\right)\otimes\left(\left[\!\left[\tilde{\boldsymbol{\Delta}}\mathbf{t}^{b}\right]\!\right]^T\boldsymbol{\varphi}_{0,\alpha}\right)\boldsymbol{u}^b\left\langle\frac{\beta\hat{\mathcal{H}}^{\alpha\beta\gamma\delta}_m}{h^s}\right\rangle\nu^-_\delta\nu^-_\beta\bar{j}_0 d\partial\mathcal{A}\cdot\delta\boldsymbol{u}^a\,. \end{aligned} \tag{161}$$

This last expression can be rewritten as

$$a^s_I(\boldsymbol{u}_h,\,\delta\boldsymbol{u}) = \boldsymbol{F}^{ea}_I\cdot\delta\boldsymbol{u}^a\,, \tag{162}$$

where

$$\begin{aligned} \boldsymbol{F}^{ea}_I = &\int_s \left\langle \hat{\mathcal{H}}^{\alpha\beta\gamma\delta}_m\ \hat{\boldsymbol{B}}^{a}_{m\,\gamma\delta}\right\rangle \otimes \left(\left[\!\left[\tilde{\boldsymbol{\Delta}}\mathbf{t}^{b}\right]\!\right]^T\boldsymbol{\varphi}_{0,\alpha}\right)\boldsymbol{u}^b\bar{j}_0\nu^-_\beta\,d\partial\mathcal{A} + \\ &\int_s \left(\left[\!\left[\tilde{\boldsymbol{\Delta}}\mathbf{t}^{a}\right]\!\right]^T\boldsymbol{\varphi}_{0,\alpha}\right)\otimes\left\langle \hat{\mathcal{H}}^{\alpha\beta\gamma\delta}_m\ \hat{\boldsymbol{B}}^{b}_{m\,\gamma\delta}\right\rangle\boldsymbol{u}^b\bar{j}_0\nu^-_\beta\,d\partial\mathcal{A} + \\ &\int_s \left(\left[\!\left[\tilde{\boldsymbol{\Delta}}\mathbf{t}^{a}\right]\!\right]^T\boldsymbol{\varphi}_{0,\gamma}\right)\otimes\left(\left[\!\left[\tilde{\boldsymbol{\Delta}}\mathbf{t}^{b}\right]\!\right]^T\boldsymbol{\varphi}_{0,\alpha}\right)\boldsymbol{u}^b\left\langle\frac{\beta\hat{\mathcal{H}}^{\alpha\beta\gamma\delta}_m}{h^s}\right\rangle\nu^-_\delta\nu^-_\beta\bar{j}_0 d\partial\mathcal{A}\,, \end{aligned} \tag{163}$$

is the element internal interface force. The corresponding Jacobian matrix is

easily obtained as

$$\begin{aligned}\mathbf{K}_I^{e\,a\,b} = &\int_s \left\langle \hat{\mathcal{H}}_m^{\alpha\beta\gamma\delta}\ \hat{\boldsymbol{B}}^a_{m\,\gamma\delta} \right\rangle \otimes \left(\left[\!\left[\tilde{\boldsymbol{\Delta}}\mathbf{t}^{\,b} \right]\!\right]^T \boldsymbol{\varphi}_{0,\alpha} \right) \bar{j}_0 \nu_\beta^- \, d\partial\mathcal{A} + \\ &\int_s \left(\left[\!\left[\tilde{\boldsymbol{\Delta}}\mathbf{t}^{\,a} \right]\!\right]^T \boldsymbol{\varphi}_{0,\alpha} \right) \otimes \left\langle \hat{\mathcal{H}}_m^{\alpha\beta\gamma\delta}\ \hat{\boldsymbol{B}}^b_{m\,\gamma\delta} \right\rangle \bar{j}_0 \nu_\beta^- \, d\partial\mathcal{A} + \\ &\int_s \left(\left[\!\left[\tilde{\boldsymbol{\Delta}}\mathbf{t}^{\,a} \right]\!\right]^T \boldsymbol{\varphi}_{0,\gamma} \right) \otimes \left(\left[\!\left[\tilde{\boldsymbol{\Delta}}\mathbf{t}^{\,b} \right]\!\right]^T \boldsymbol{\varphi}_{0,\alpha} \right) \left\langle \frac{\beta \hat{\mathcal{H}}_m^{\alpha\beta\gamma\delta}}{h^s} \right\rangle \nu_\delta^- \nu_\beta^- \bar{j}_0 \, d\partial\mathcal{A} \end{aligned} \tag{164}$$

5.4 Assembly

Combining Eqs. (141, 146, and 162) leads to the formulation of the problem (73) in the assembled form

$$\sum_e \left(\boldsymbol{F}_n^{e\,a} + \boldsymbol{F}_m^{e\,a} + \boldsymbol{F}_I^{e\,a} \right) = \boldsymbol{F}_{\text{ext}}{}^a \,, \tag{165}$$

where the internal forces are given by Eqs. (142, 147, and 163), while the external forces result from (78). Upon application of appropriate boundary conditions, this linear system can be solved directly for the nodal displacements from the alternative expression

$$\sum_e \left(\mathbf{K}_n^e + \mathbf{K}_m^e + \mathbf{K}_I^e \right)^{a\,b} \boldsymbol{u}^b = \boldsymbol{F}_{\text{ext}}{}^a \,. \tag{166}$$

5.5 Particular case of 8-node bi-quadratic quadrangular elements

For a 8-node bi-quadratic element, the membrane terms (142) and (143) lead to locking if a full Gauss integration using 3×3 Gauss points is used. In order to address this well-known issue, two commonly adopted approaches are used. The first approach preserves the full integration and is based on an Enhanced Assumed (membrane) Strains (EAS) method, see appendix A. The second approach is based simply on a reduced integration of the membrane strain terms using 2×2 Gauss points. In this paper the two methods are compared, but since no advantage to using the EAS method was discerned, most of the numerical examples are performed with a reduced integration for the membrane equations.

Locking due to the bending terms (147) and (148) is taken care of by the DG formulation, and full integration of these terms can be performed. However, substantial computational savings can be achieved if the same quadrature as for the membrane terms is used, without affecting the results ostensibly.

The interface term is integrated on the quadratic edge element defined in the referential frame $\boldsymbol{E}_1$ by $\xi^1 \in [-1, 1]$. In addition to the 3 nodes defining the curve, the nodes of the adjacent elements $\mathcal{A}_{e^-}$ and $\mathcal{A}_{e^+}$ also contribute to the forces related to the bilinear term (77), which leads to an interface element defined on 13 nodes. Both internal forces (163) and Jacobian matrix (164) are obtained by using 3 Gauss. Once again, the DG formulation prevents locking that would otherwise arise for curved surfaces. When reduced integration of the membrane is performed, only 2 Gauss points are used for the interface element.

5.6 Particular case of 16-node bi-cubic quadrangular elements

For this high order of polynomial interpolation, full 4×4 Gauss quadrature is used both for the membrane terms (142, 143), and the bending terms (147, 148), without appearance of locking.

The interface term is integrated on a cubic edge element defined in the referential frame $\boldsymbol{E}_1$ by $\xi^1 \in [-1, 1]$. In addition to the 4 nodes defining the curve, the nodes of the adjacent elements $\mathcal{A}_{e^-}$ and $\mathcal{A}_{e^+}$ also contribute to the forces related to the bilinear term (77), which leads to an interface element defined on 28 nodes. Both internal forces (163) and Jacobian matrix (164) are obtained by using 4 Gauss points. Once again, the DG formulation prevents locking that would otherwise arise for curved surfaces.

6 Numerical examples

In this section, the DG formulation for Kirchhoff-Love shells developed in the foregoing is subjected to a series of standard numerical tests and examples of application for the purpose of verifying its numerical properties, including convergence rate and influence of the stabilization parameter. The results are compared with other shell formulations from the literature. Three different implementations of the DG formulation are considered: 8-node bi-quadratic quadrangular elements with EAS method (Q8EAS), 8-node bi-quadratic quadrangular elements with reduced integration (Q8RI) and 16-node bi-cubic quadrangular elements with full integration (Q16).

6.1 Beam bending examples exercising membrane and shell response

The first test considers the bending of a beam of length L and uniform square cross-section of thickness t. The beam is subject to a uniformly distributed

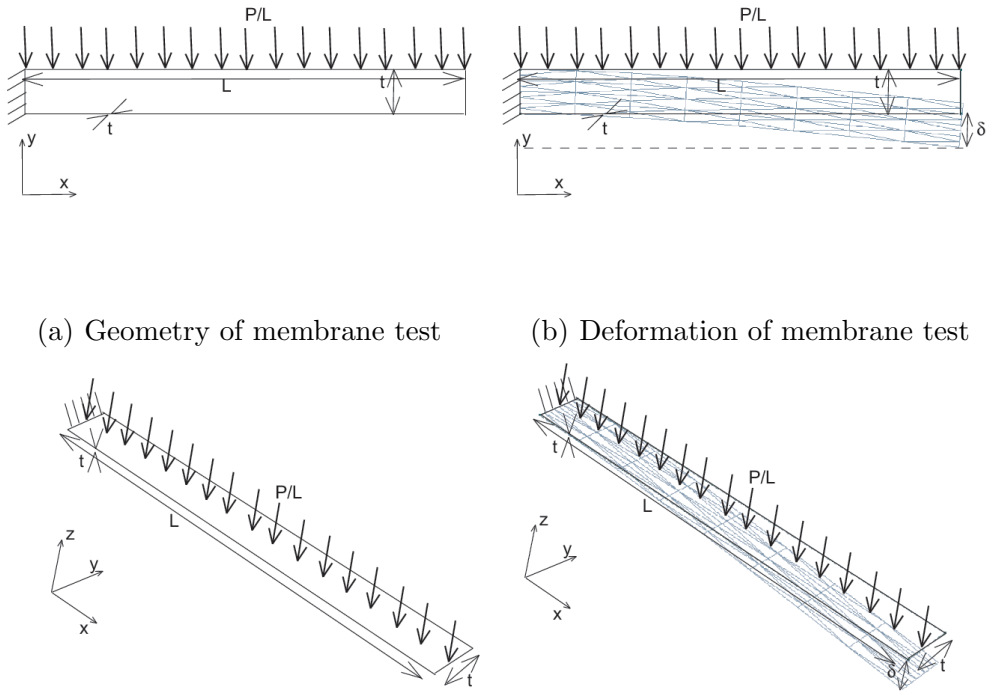

(a) Geometry of membrane test (b) Deformation of membrane test

(c) Geometry of shell test (d) Deformation of shell test

Fig. 6. Application to beam bending. Problem dimensions: length L and square cross-section of thickness t, loading P uniformly distributed. a) Geometry of the membrane test. b) Deformation of the membrane test for a regular mesh of 4 quadratic quadrangular elements on each side. c) Geometry of the shell test. d) Deformation of the shell test for a regular mesh of 4 quadratic quadrangular elements on each side.

Table 1
Material and geometrical properties for the beam bending tests.

Property	Value
Length	$L = 2$ m
Thickness	$t = 0.2$ m
Young modulus	$E = 10^5$ N·m^{-2}
Poisson's ratio	$\nu = 0.3$
Applied force	$P/L = 1$ N·m^{-1}

line load P/L. This problem has a closed-form analytical solution, which gives the deflection of the beam axis $\delta(x)$ as

$$\delta(x) = \frac{P}{24EIL}\left(x^4 - 4x^3L + 6x^2L^2\right) \text{ and } , \tag{167}$$

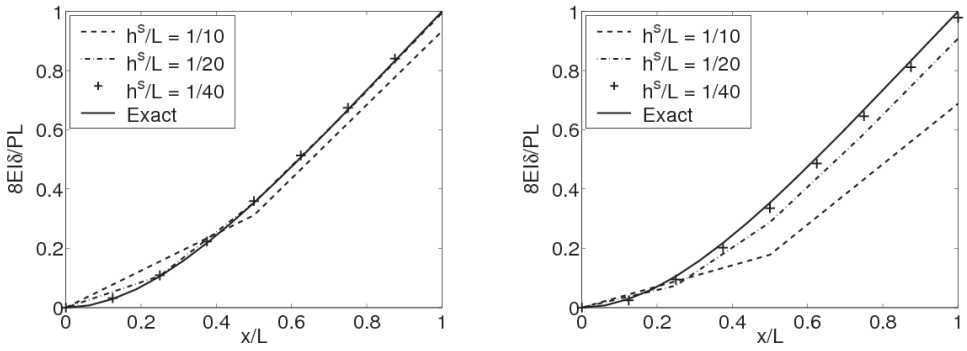

(a) Membrane (b) Shell, $\beta = 10^2$

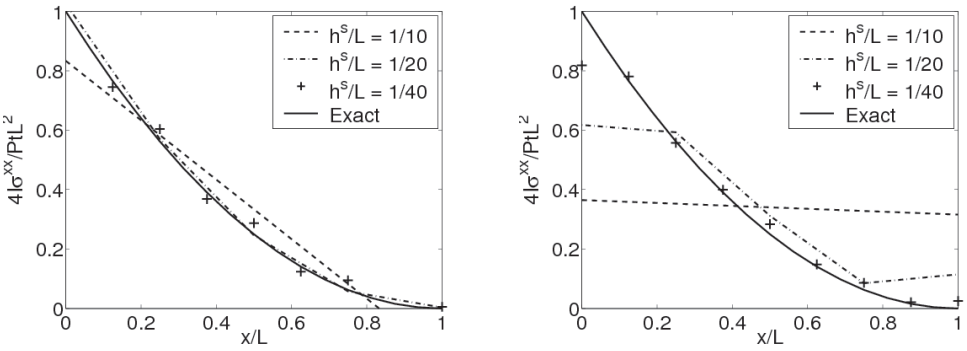

(c) Membrane (d) Shell, $\beta = 10^2$

Fig. 7. Influence of mesh-size on the solution evolution for the beam bending test a) $\delta(x)$ for the membrane test with reduced integration. b) $\delta(x)$ for the shell test with $\beta = 10^2$. c) $\sigma^{xx}_{\max}(x)$ for the membrane test with reduced integration. b) $\sigma^{xx}_{\max}(x)$ for the shell test with $\beta = 10^2$.

from which the maximum stress at each section along the axis of the beam $\sigma^{xx}_{\max}(x)$ is obtained as

$$\sigma^{xx}_{\max}(x) = \frac{Pt}{48IL}\left(12x^2 - 24xL + 12L^2\right). \tag{168}$$

In these relations, $I = t^4/12$ is the moment of inertia of the cross section. In particular, the tip deflection of the beam is $\delta(L) = \frac{PL^3}{8EI}$. The values of the geometric, material and bending parameters used in simulations are given in Table 1.

This example is used to evaluate both the bending and the membrane behavior of the formulation. Toward this end, the simulations are conducted for two loading conditions in which the line load is applied:

- in the plane of the shell, which subjects the shell mesh to membrane deformations, Fig. 6a-b;
- in the plane perpendicular to the shell, which subjects the shell mesh to bending deformations, Fig. 6c-d.

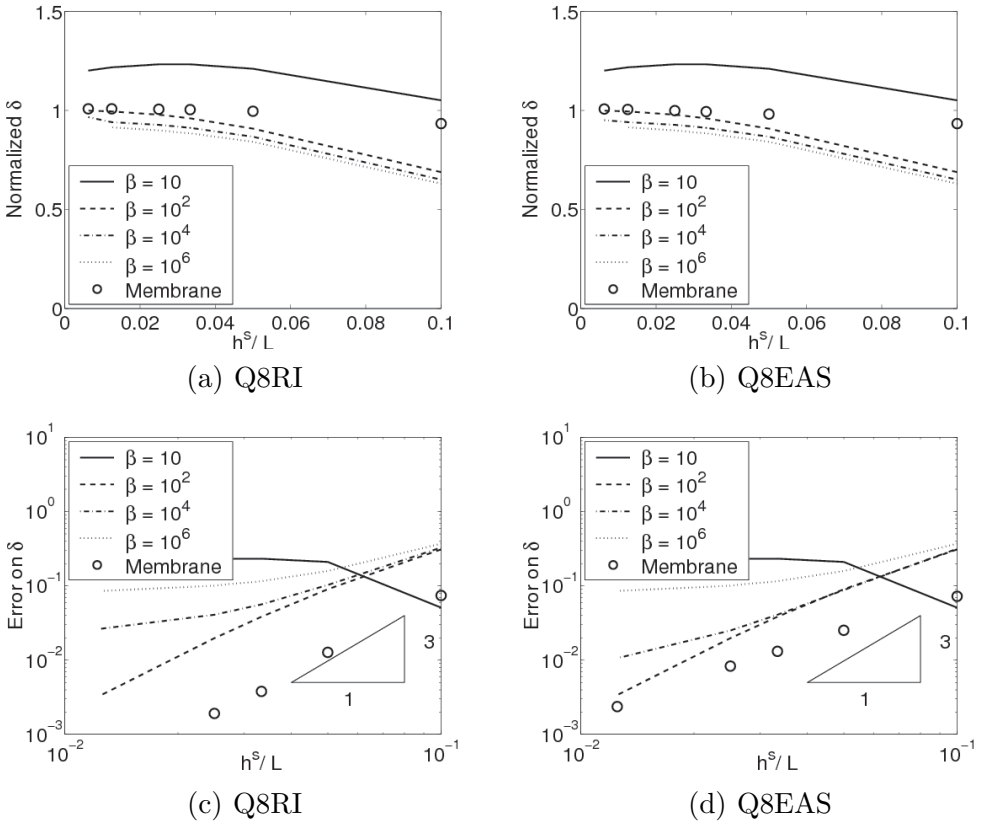

(a) Q8RI (b) Q8EAS

(c) Q8RI (d) Q8EAS

Fig. 8. Influence of mesh-size and stabilization parameter on the deflection for the beam bending test. Curves for a given β are related to the shell tests, and curves denoted "Membrane" are related to the membrane test. a) Maximal deflection with reduced integration of the membrane equations. b) Maximal deflection with EAS method for the membrane equations. c) Error on the maximal deflection with reduced integration of the membrane equations. d) Error on the Maximal deflection with EAS method for the membrane equations.

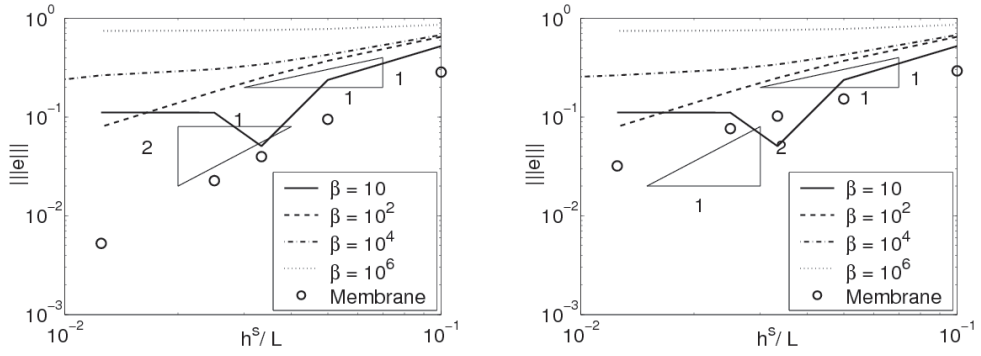

(a) Q8RI (b) Q8EAS

Fig. 9. Influence of mesh-size and stabilization parameter on the error in the energy deflection for the beam bending test. a) Q8RI elements. b) Q8EAS elements.

In this example, the behavior of the 8-node bi-quadratic quadrangular elements with two approaches (EAS and RI) for avoiding membrane locking is studied. In order to assess the convergence of the method with the mesh size, simulations are conducted with a series of meshes of decreasing mesh size, consisting of 1×1, 2×2, ..., 32×32 elements, which corresponds to elements sizes $h^s = 1$, $\frac{1}{2}$, ..., $\frac{1}{32}$ of the beam width t. For the shell bending tests, the influence of the stabilization parameter β is studied by repeating the simulations with varying values of β =10, 10^2, ..., 10^6.

Figure 7 shows plots of the normalized deflection $8EI\delta/PL$ and of the normalized maximum stress $4I\sigma^{xx}/PtL^2$ of the beam versus the normalized location x/L along the axis of the beam. The simulations results shown in this figure correspond to the reduced integration in the case of membrane loading and $\beta = 10^2$, in the case of shell loading. It may be observed in these plots that the numerical solutions converge to the exact solution when the mesh size is reduced. A more detailed convergence rate study is presented in Fig. 8, in which the tip displacement is compared to the exact value and the error is computed for different mesh sizes, stabilization parameters, membrane or shell behavior and membrane locking control methods. The membrane formulation is found to converge for both locking control methods with the theoretical rate in the case of reduced integration and a lower rate for the EAS method. When the problem is solved using shell bending, a low stability parameter β leads to instability, while $\beta > 10$ ensures convergences toward the analytical solution. However, if β increases, a stiffer behavior is observed, as the method evolves toward the locking behavior of the continuous Galerkin method. The convergence rate in the L^2-norm is equal to 3 (Fig. 8c-d), although theory predicts only 2 for quadratic elements, providing that the stability parameter is not too high, which leads to locking, or too low ($\beta \leq 10$), in which case the method is unstable. Figure 9 shows the corresponding convergence plots for the energy norm. It is found that the results exhibit the expected theoretical convergence rates, with similar observations on the influence of the stabilization parameters as in the L^2-norm.

The absence of a clear advantage of the EAS method justifies the use of reduced integration in the following applications.

6.2 Plate bending examples

The bending behavior resulting from the proposed shell formulation of the element is now studied with plate ending examples. A square plate of length L and thickness t is subject to a concentrated load P applied at its center (Fig. 10). Only one quarter of the plate is considered by exploiting the symmetry of the problem. The zero-slope boundary condition on clamped edges and at

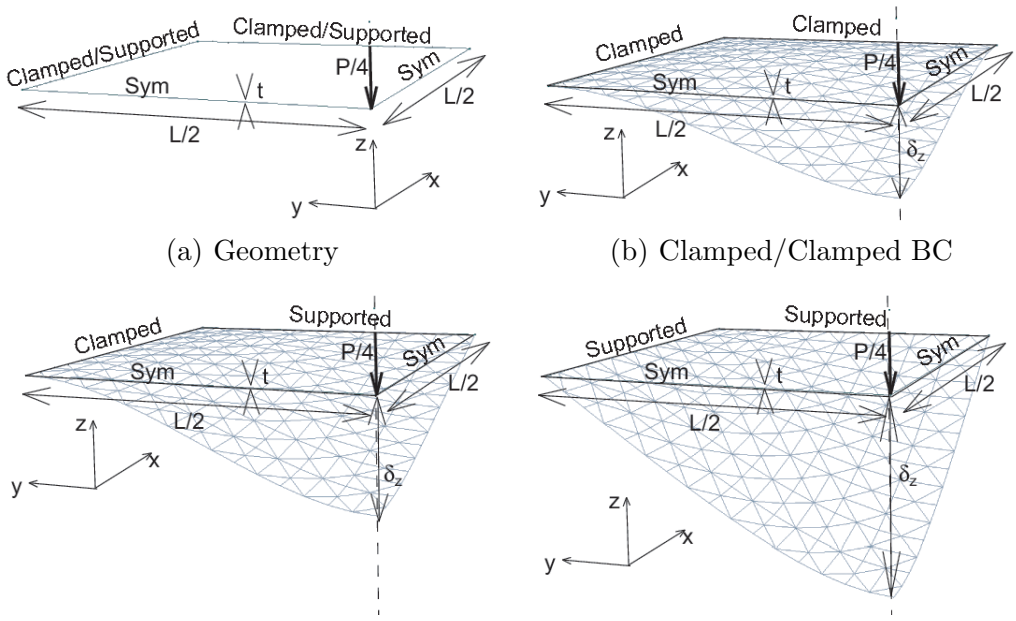

(a) Geometry (b) Clamped/Clamped BC

(c) Supported/Clamped BC (d) Supported/Supported BC

Fig. 10. Study of square plate. Problem dimensions: length L and thickness t, concentrated loading P. a) Geometry of the plate. One fourth of the plate is considered. The boundary conditions considered are b) all edges clamped, c) edges simply supported and clamped, d) edges simply supported. Magnified deflections computed are shown for each case, for a regular mesh of 8×8 quadratic quadrangular elements.

Table 2
Material and geometrical properties for the plate bending tests.

Property	Value
Length	$L = 10$ m
Thickness	$t = 0.1$ m
Young modulus	$E = 10^6$ N·m^{-2}
Poisson's ratio	$\nu = 0.3$
Applied force	$P = 200$ N

the symmetry edges is weakly enforced with DG interface elements. Three types of boundary conditions, for which analytical solution of the plate center deflection δ_z exists [26], are considered:

- All edges clamped, see Fig. 10b ($\delta_z = 0.00561 \frac{P L^2}{D}$);
- Two opposing edges clamped, two simply supported, see Fig. 10c ($\delta_z = 0.007071 \frac{P L^2}{D}$);
- All edges simply supported, see Fig. 10d ($\delta_z = 0.01160 \frac{P L^2}{D}$).

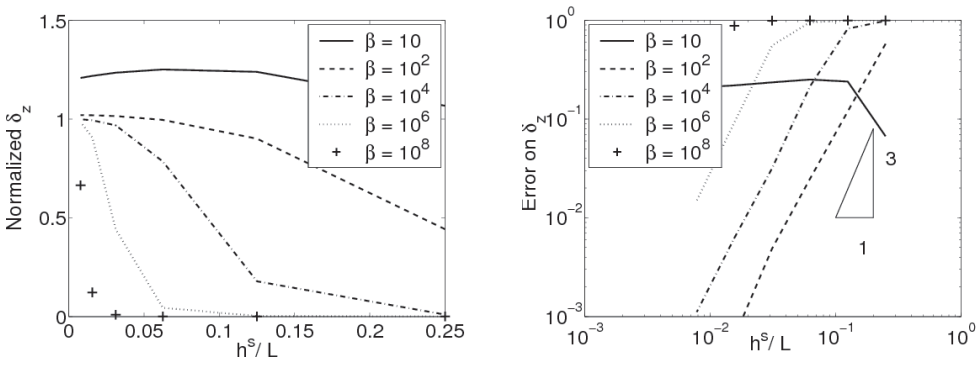

(a) Deflection (b) Error on deflection

Fig. 11. Influence of mesh-size and stabilization parameter on the deflection for the bending of the plate (all edges clamped case) with Q8RI elements. a) Normalized deflection, b) Error on the deflection.

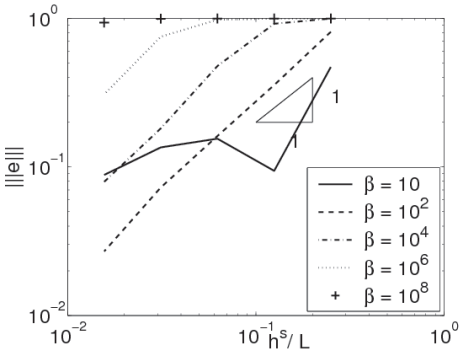

Fig. 12. Influence of mesh-size and stabilization parameter on the error in the energy norm for the bending of the plate with Q8RI elements.

In these results, $D = \frac{E\,t^3}{12(1-\nu^2)}$ is the rigidity of the plate. The values of the geometric, material and bending parameters used in simulations is given in Table 2.

In this series of tests, the 8-node bi-quadratic elements with reduced integration are used. In order to study the stability and convergence, the set of stabilization parameters β =10, 10^2, ..., 10^8 is used, whereas, the meshes for the quarter-plate are uniform with 2×2, 4×4, ..., and 64×64 elements. First, the discontinuous Galerkin formalism is studied in the all edges-clamped case. Figure 11a shows plots of the normalized center-plate deflection δ_z versus the normalized mesh-size h^s/L for different values of β. Figure 11b shows the corresponding absolute values of the error. It is observed that for a small value of $\beta = 10$, the method is not stable, as expected, and the computed deflection is overestimated, Fig. 11a. For increasing values of $\beta > 10$, the error is larger as the behavior is stiffer. However, the convergence rate is not affected if the method is stable and the mesh size is sufficiently small. The method is also shown to converge in the energy norm with the expected rate, see Fig. 12.

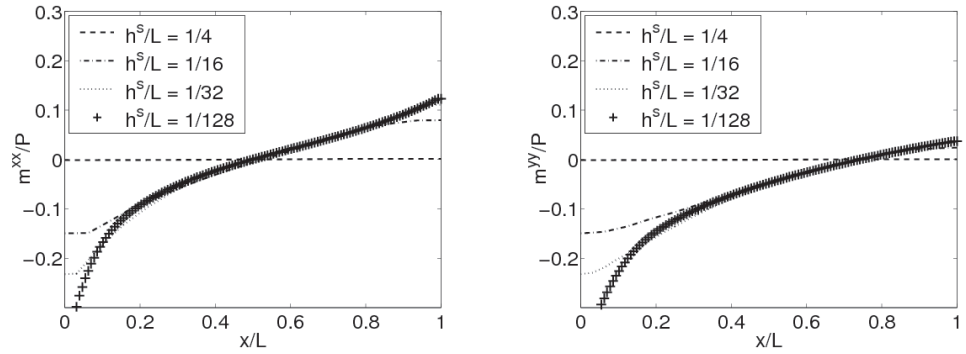

(a) Along XX axis (b) Along YY axis

Fig. 13. Influence of mesh-size on the moment of evolution at $y = 0$ for the bending of a plate with $\beta = 10^4$ with Q8RI elements. a) Evolution along the XX axis. b) Evolution along YY axis.

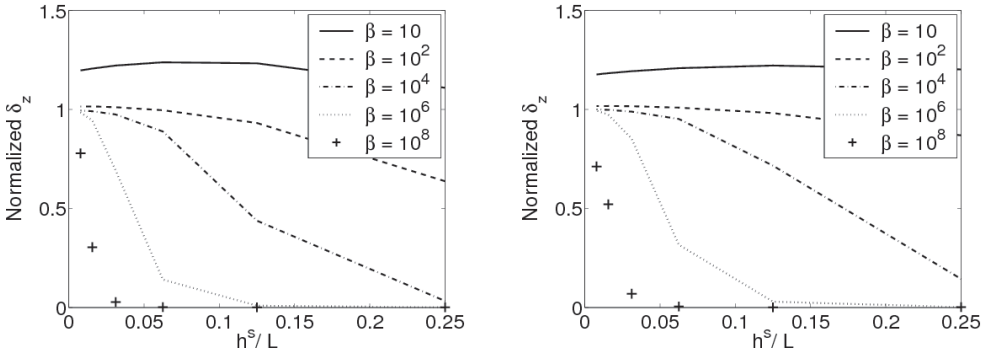

(a) Supported/clamped case (b) Supported/supported case

Fig. 14. Influence of mesh-size and stabilization parameter on the deflection for the bending of the plate with Q8RI elements. a) clamped/simply supported case b) all edges simply supported case.

Figure 13 shows the point-wise convergence of the bending moments along the symmetry planes, illustrating how the method attempts to capture the singularity at the center of the plate due to the concentrated load, when the mesh is refined. Figure 14 shows the convergence analysis corresponding to the other two types of boundary conditions considered.

6.3 Arch bending example

This series of tests is intended to show the model's ability to describe combined bending and membrane situations for curved surfaces. An arch of radius R, width L and thickness t, is subject to a line load P/L applied at its middle section in the radial direction, see Fig. 15. Only one half of the arch is studied, by taking advantage of the symmetry of the problem. The bending moment distribution along the arch $M^{zz}(\theta)$ and the traction force $N(\theta)$, can be ob-

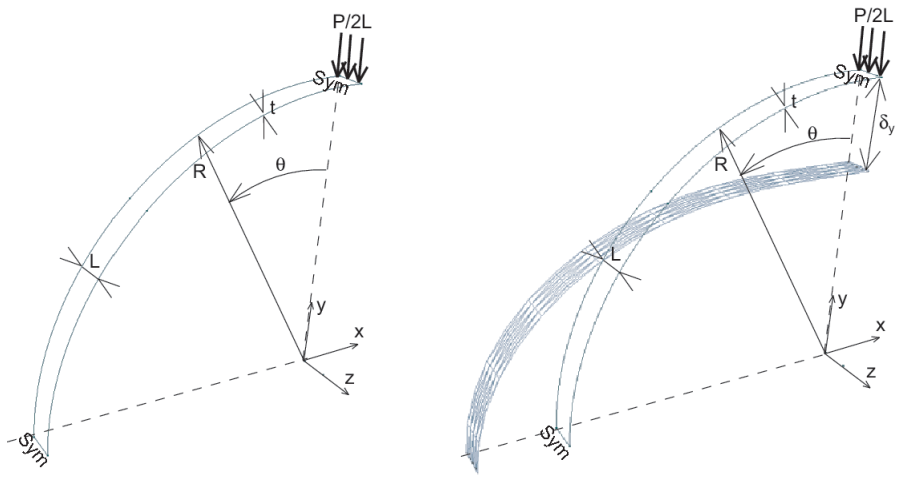

(a) Geometry (b) Deformation

Fig. 15. Study of the arch. Problem dimensions: radius R, width L, thickness t, and line loading P/L. a) Geometry of the arch. One half of the arch is considered, b) Magnified deformation for a regular mesh of 8 quadratic quadrangular elements on the radius and 4 on the width.

Table 3
Material and geometrical properties for the arch test.

Property	Value
Radius	$R = 10$ m
Width	$L = 1$ m
Thickness	$t = 1$ m
Young modulus	$E = 3 \times 10^7$ N·m^{-2}
Poisson's ratio	$\nu = 0.3$
Applied line force	$P/L = 10^5$ N·m^{-1}

tained exactly using Castigliano's theorem, which leads to the expressions

$$M^{zz}(\theta) = \frac{P\,L\,R}{2}\left[\sin\theta - \frac{2}{\pi}\right], \text{ and} \tag{169}$$

$$N(\theta) = \frac{P\,L}{2}\sin\theta\,, \tag{170}$$

where $I = L\,t^3/12$ is the moment of inertia of the cross-section. From Eq. (169), it is clear that the maximum momentum, maximum vertical deflection

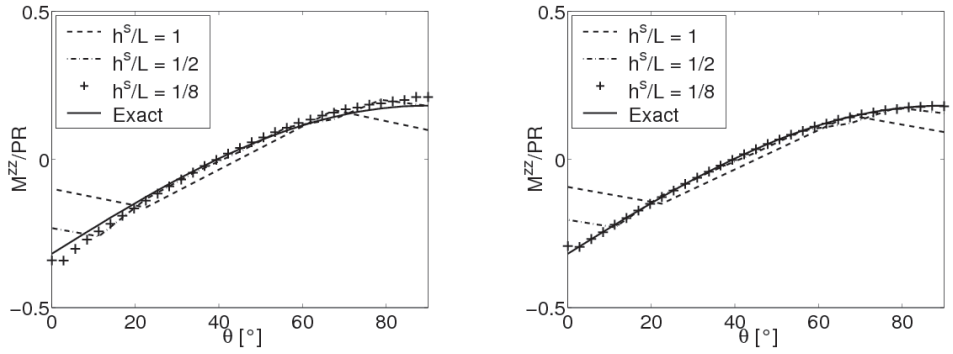

(a) $\beta = 10$ (b) $\beta = 10^6$

Fig. 16. Influence of mesh-size on the momentum for the arch test, with Q8RI elements. a) For $\beta = 10$ the method is unstable. b) For $\beta = 10^6$ the method is stable.

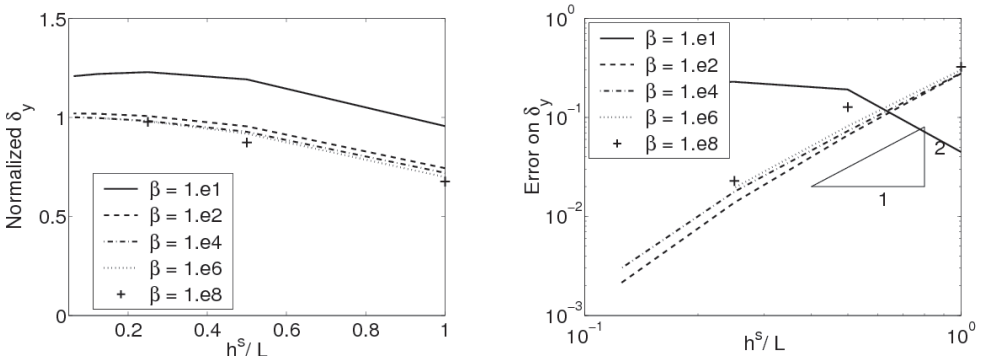

(a) Deflection (b) Error on deflection

Fig. 17. Influence of mesh-size and stabilization parameter on the deflection for the arch test, with Q8RI elements. a) Normalized deflection. b) Error on the normalized deflection.

δ_y and maximum stress are obtained for $\theta = 0$, and their respective values are

$$M^{zz} = -\frac{P\,L\,R}{\pi}\,, \tag{171}$$

$$\delta_y = \frac{P\,L\,R^3}{2EI}\left(\frac{\pi}{4} - \frac{2}{\pi}\right) + \frac{P\,L\,R\,\pi}{8EA}\,, \text{ and} \tag{172}$$

$$\sigma^{\max} = \frac{P\,L\,R\,t}{2\,\pi\,I}\,. \tag{173}$$

These exact values are taken as a basis for verification of the numerical method. The numerical simulations conducted toward this end use the property values shown in Table 3 and consist of uniform computational meshes with 1×2, 2×4, ..., 16×32 8-node bi-quadratic elements with reduced integration. As before the influence of the stabilization parameter β is studied by repeating the simulations for different values of β =10, 10^2, ..., 10^8.

Figures 16-18 respectively show comparison of the moment distribution along

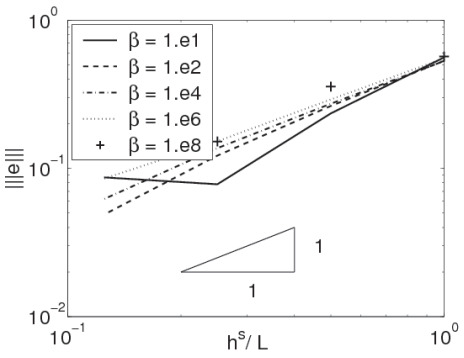

Fig. 18. Influence of mesh-size and stabilization parameter on the energy norm for the arch test, with Q8RI elements.

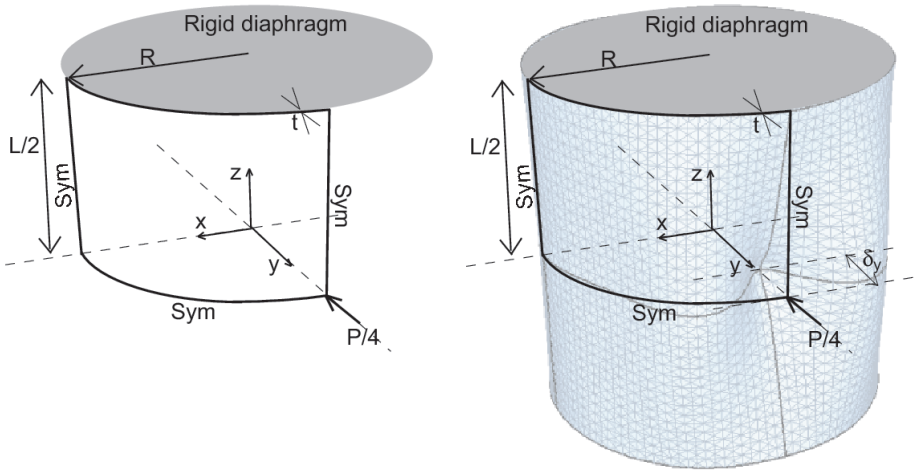

(a) Geometry (b) Deformation

Fig. 19. Study of the pinched cylinder. Problem dimensions: radius R, thickness t, length L, concentrated loading P. a) Geometry of the cylinder. One eighth is considered. b) Magnified deformation of the completed cylinder regular mesh of 16 quadratic quadrangular elements on each side.

the arch, normalized tip displacement and its error, and error in the energy norm, as the mesh is refined for different values of β. Similar conclusions are obtained with regard to the convergence and stability properties of the method with the exception that the convergence rate for the tip displacement is two, see Fig 17b, which is consistent to the theory for $k = 2$, in which case optimal convergence rate is not ensured.

6.4 Pinched cylinder example

This example is intended to further test the proposed method under a more complex membrane state of deformation. Toward this end, a cylinder with

Table 4
Material and geometrical properties for the pinched cylinder test.

Property	Value
Radius	$R = 0.3$ m
Length	$L = 0.6$ m
Thickness	$t = 3$ mm
Young modulus	$E = 3$ N·m^{-2}
Poisson's ratio	$\nu = 0.3$
Applied force	$P = 2 \times 10^6$ N

radius R, length L, thickness t, closed at its extremities by rigid diaphragms and subjected to compressive normal loads P applied on one diameter, is considered, see Fig. 19a. One eight of the structure is modeled exploiting the symmetries of the problem. Analytical deflection under the loads can be computed analytically for the geometry reported in Table 5, [17], leading to

$$|\delta_y| = 0.0182488 \, [\mathrm{m} \cdot \mathrm{N}^{-1}] \, P \, . \tag{174}$$

This exact value is taken as a basis for verification of the numerical method. The numerical simulations conducted consist of uniform computational meshes with 2×2, 4×4, ..., 32×32 elements. Results obtained with 8-node bi-quadratic elements with reduced integration and 16-node bi-cubic elements are compared. As before the influence of the stabilization parameter β is studied by repeating the simulations for different values of β =10, 10^2, ..., 10^6.

Figures 20 and 21 show the convergence of the maximum displacement, its error and the error of the energy norm for the different polynomial approximations, mesh sizes and stabilization parameters. In this example, the convergence in the L^2-norm is only of the order of 2 for quadratic elements and of 4 for cubic ones, accordingly to the theory when proper elliptic regularity is assumed.

6.5 Pinched open hemisphere example

This example is intended to further test the proposed method under more complex shell bending conditions involving curvature in two directions. To this end, the problem of an open hemisphere, proposed in [27], with radius R, thickness t, and an opening of a spherical sector angle θ, subjected to radial loads P applied on two diametral directions, is considered, Fig. 22a. The load is compressive in the y-direction and tensile in x-direction. One quarter of the structure is modeled exploiting the symmetries of the problem. Analytical

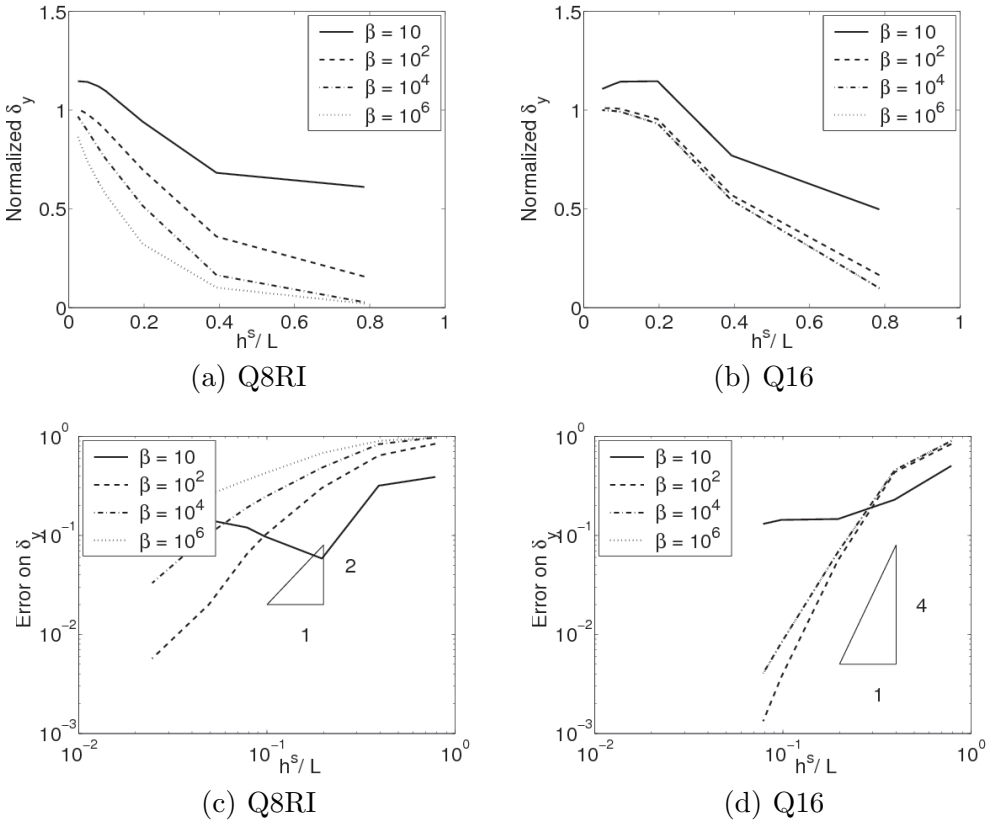

(a) Q8RI (b) Q16

(c) Q8RI (d) Q16

Fig. 20. Influence of mesh-size and stabilization parameter on the deflection for the pinched cylinder. a) Normalized deflection for Q8RI. b) Normalized deflection for Q16. c) Error on the deflection for Q8RI. d) Error on the deflection for Q16.

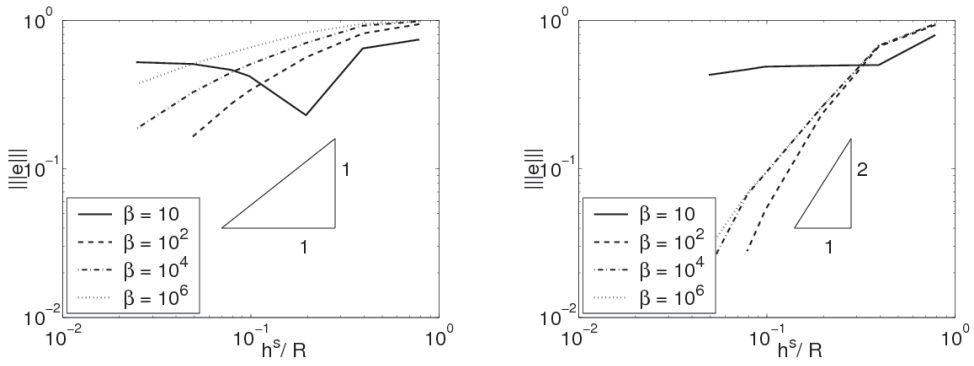

(a) Q8RI (b) Q16

Fig. 21. Influence of mesh-size and stabilization parameter on the error in the energy norm for the pinched cylinder. a) For Q8RI elements. b) For Q16 elements.

deflection under the loads can be computed analytically for the geometry reported in Table 5, [17], leading to

$$|\delta_x| = |\delta_y| = 0.093\ [\mathrm{m} \cdot \mathrm{N}^{-1}]\ \frac{P}{2}\,. \tag{175}$$

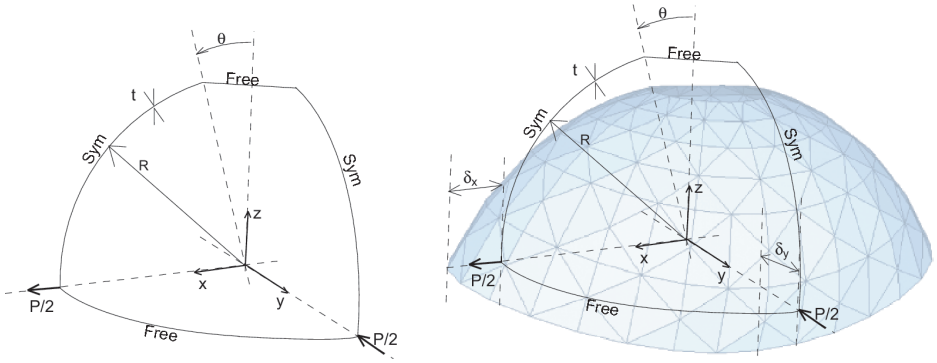

(a) Geometry (b) Deformation

Fig. 22. Study of the pinched open hemisphere. Problem dimensions: radius R, thickness t, opening θ, concentrated loading P. a) Geometry of the open hemisphere. One fourth is considered. b) Magnified deformation of the completed hemisphere for a regular mesh of 4 quadratic quadrangular elements on each side.

Table 5
Material and geometrical properties for the pinched open hemisphere test.

Property	Value
Radius	$R = 10$ m
Thickness	$t = 0.04$ m
Opening	$\theta = 18^{o}$
Young modulus	$E = 6.825{\times}10^{7}$ N·m^{-2}
Poisson's ratio	$\nu = 0.3$
Applied force	$P = 40$ N

This exact value is taken as a basis for verification of the numerical method. The numerical simulations conducted toward this end consist of uniform computational meshes with 2×2, 4×4, ..., 32×32 elements. Results obtained with two different degrees of polynomial approximations are compared by using 8-node bi-quadratic elements with reduced integration and 16-node bi-cubic elements. As before the influence of the stabilization parameter β is studied by repeating the simulations for different values of β =10, 10^2, ..., 10^8.

Figures 23, 24 show the convergence of the maximum displacement, its error and the error of the energy norm for the different polynomial approximations, mesh sizes and stabilization parameters. As for previous tests, a small value $\beta = 10$ leads to instability while higher valuesr lead to the expected convergence rate, *i.e.* $k+1$ for the L^2-norm and $k-1$ for the energy norm. It can also be observed that the stiffness of the structure is less important for cubic than for quadratic interpolations when the stabilization parameter is high.

In this example, we compare the results of our presented formulation, which

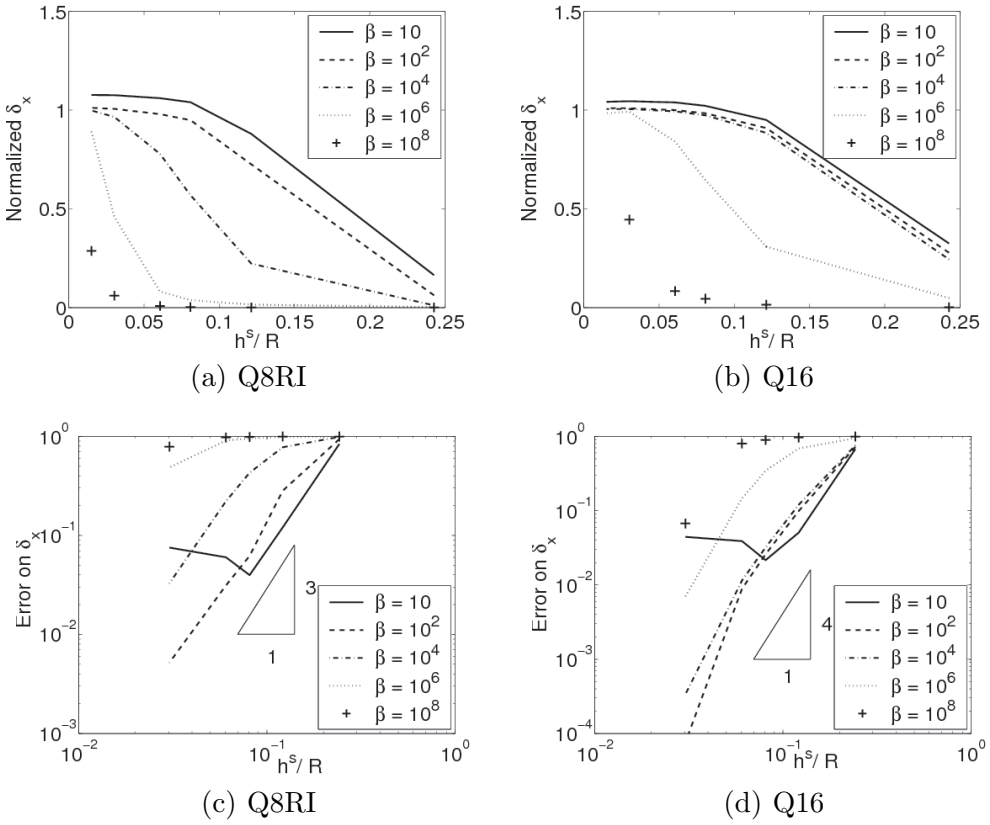

(a) Q8RI (b) Q16

(c) Q8RI (d) Q16

Fig. 23. Influence of mesh-size and stabilization parameter on the deflection for the pinched open hemisphere. a) Normalized deflection for Q8RI. b) Normalized deflection for Q16. c) Error on the deflection for Q8RI. d) Error on the deflection for Q16.

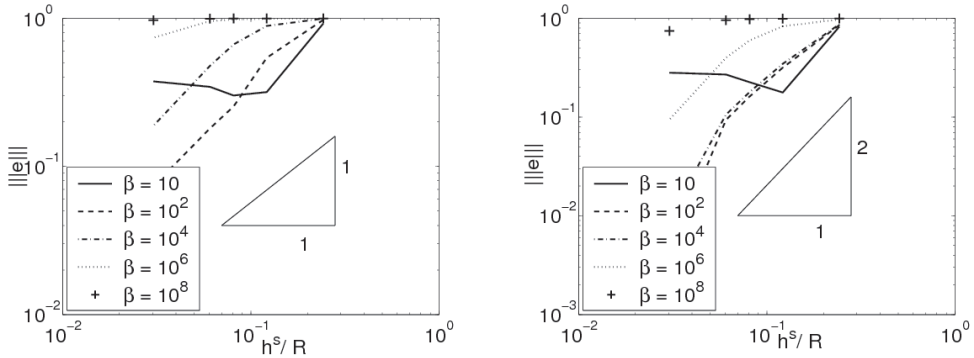

(a) Q8RI (b) Q16

Fig. 24. Influence of mesh-size and stabilization parameter on the error in the energy norm for the pinched open hemisphere. a) For Q8RI elements. b) For Q16 elements.

uses only 3 displacement degrees of freedom per node to:

- The bi-quadratic 8-node quadrangular element formulation proposed by MacNeal and Harder [27], which requires 6 degrees of freedom per node

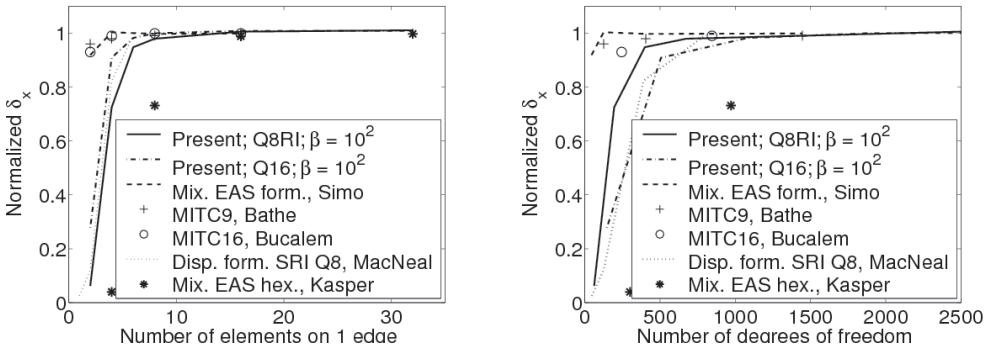

(a) In terms of elements (b) In terms of dofs

Fig. 25. Comparison of the convergence with other elements for the pinched open hemisphere. a) In terms of number of elements. b) In terms of degrees of freedom.

(3 displacements $\boldsymbol{u}$ and 3 rotations) and uses a Selective Reduced Integration;

- The mixed Enhanced Assumed Strains formulation proposed by Simo *et al.* [17] using bilinear quadrangular elements and requiring 5 global degrees of freedom per node (3 displacements $\boldsymbol{u}$, 2 rotations). This model has in addition internal degrees of freedom resulting from the Enhanced Assumed Strains (EAS) formulation;
- The Mixed Interpolation of Tensorial Components (MITC) shell element with either 9 or 16 nodes [28], which require 5 global degrees of freedom per node (3 displacements $\boldsymbol{u}$ and 2 rotations) and internal degrees of freedom;
- The mixed EAS formulation applied to tri-linear hexahedra, proposed by Kasper and Taylor, requiring 3 degrees of freedom on the global level, and internal degrees of freedom resulting from the EAS formulation.

Figures 25a and Fig. 25b compare, respectively, the convergence in terms of the number of elements per edge and the total number of degrees of freedom. It can be observed in these figures that the proposed method is comparable to those references in terms of number of degrees of freedom required to capture the deformation state.

7 Conclusions

In this paper, the numerical approximation of the theory of shells neglecting shear deformations is considered. In such case, the section of the shell remains perpendicular to its mid-surface, even after deformation, thus enabling the discrete finite-elements formulation to be written as a one-field method. Usually this formulation requires the shape functions to be $\mathcal{C}^1$ continuous on the whole domain, which in 3D simulations is not easily achieved. The discontinuous Galerkin formulation proposed in this paper addresses this issue by

enforcing the higher-order continuity at the inter-element boundaries in a weak manner. The proposed method is shown to be consistent and stable, and to have a convergence rate in the energy norm one order lower than the degree of the polynomial approximation used. Assuming proper elliptic regularity, the convergence rate in the $\mathbf{L}^2$-norm is optimal for at least cubic elements and equal to 2 for quadratic elements.

The formulation is numerically tested for the case of bi-quadratic and bi-cubic interpolations on quadrilateral meshes. Since the high-order continuity requirement is built-in naturally into the formulation, the integration of the bending and membrane terms in the weak form can be performed on the reduced coordinate basis inside each element in a straightforward manner. In the case of 8-node bi-quadratic elements, membrane locking is avoided by reduced 2×2 Gauss integration. Cubic elements do not suffer from locking, thus allowing for a full integration.

Interface elements are introduced at the interelement boundaries, in order to integrate the DG interface terms. This integration is performed by extracting required information from the adjacent shell elements on Gauss points located on the shared edge.

Various tests involving beams, plates and double-curved surfaces are used to demonstrate the theoretical properties of the method, including extensive convergence analysis. In particular, it is found that a stabilization parameter between 10 and 100 is large enough to guarantee stability of the method and is low enough to annihilate the locking of the bending modes.

Appendix

A Enhanced Assumed Strains (EAS) method

The Enhanced Assumed Strains (EAS) method consists of the addition of n_{EAS} linearly independent internal modes $\tilde{\phi}^i_{\alpha\beta} \subset \mathbb{P}^k(\mathcal{A}_e)$, i=1, ... , n_{EAS} inside each element $\mathcal{A}_e$. These modes are multiplied by a coefficient α^i, which are the new internal variables of the element.

While the element membrane energy I^e_m part of the functional I_h (56) had the expression $I^e_m\left(\boldsymbol{u}_h\,,\varepsilon_{h\alpha\beta},\tilde{n}^{\alpha\beta}_h\right):\ \mathbb{P}^k(\mathcal{A}_e)\times\mathbb{P}^k(\mathcal{A}_e)\times\mathbb{P}^k(\mathcal{A}_e)\to\mathbb{R}$:

$$I^e_m\left(\boldsymbol{u}_h,\varepsilon_{h\alpha\beta},\tilde{n}^{\alpha\beta}_h\right)=\int_{\mathcal{A}_e}\frac{1}{2}\varepsilon_{h\alpha\beta}\mathcal{H}^{\alpha\beta\gamma\delta}_n\varepsilon_{h\gamma\delta}\bar{j}_0 d\mathcal{A}+$$
$$\int_{\mathcal{A}_e}\tilde{n}^{\alpha\beta}_h\left(\frac{1}{2}\boldsymbol{\varphi}_{0,\alpha}\cdot\boldsymbol{u}_{h,\beta}+\frac{1}{2}\boldsymbol{u}_{h,\alpha}\cdot\boldsymbol{\varphi}_{0,\beta}-\varepsilon_{h\alpha\beta}\right)\bar{j}_0 d\mathcal{A}\,, \tag{A.1}$$

the modified functional obtained by inserting the new internal modes, is $\tilde{I}^e_m\left(\boldsymbol{u}_h\,,\varepsilon_{h\alpha\beta},\tilde{n}^{\alpha\beta}_h,\tilde{\phi}^i\right):\ \mathbb{P}^k\left(\mathcal{A}_e\right)\times\mathbb{P}^k\left(\mathcal{A}_e\right)\times\mathbb{P}^k\left(\mathcal{A}_e\right)\times\mathbb{R}^{n_{\text{EAS}}}\rightarrow\mathbb{R}$:

$$\tilde{I}^e_m\left(\boldsymbol{u}_h,\varepsilon_{h\alpha\beta},\tilde{n}^{\alpha\beta}_h,\alpha^1,...,\alpha^N\right)=\int_{\mathcal{A}_e}\frac{1}{2}\varepsilon_{h\alpha\beta}\mathcal{H}^{\alpha\beta\gamma\delta}_n\varepsilon_{h\gamma\delta}\bar{j}_0 d\mathcal{A}+$$
$$\int_{\mathcal{A}_e}\tilde{n}^{\alpha\beta}_h\left(\frac{1}{2}\boldsymbol{\varphi}_{0,\alpha}\cdot\boldsymbol{u}_{h,\beta}+\frac{1}{2}\boldsymbol{u}_{h,\alpha}\cdot\boldsymbol{\varphi}_{0,\beta}+\alpha^i\tilde{\phi}^i_{\alpha\beta}-\varepsilon_{h\alpha\beta}\right)\bar{j}_0 d\mathcal{A}\,. \tag{A.2}$$

Minimizing this relation with respect to the resultant stress tensors leads to a new definition of the membrane strains,

$$\varepsilon_{\alpha\beta}=\frac{1}{2}\boldsymbol{\varphi}_{0,\alpha}\cdot\boldsymbol{u}_{,\beta}+\frac{1}{2}\boldsymbol{u}_{,\alpha}\cdot\boldsymbol{\varphi}_{0,\beta}+\alpha^i\tilde{\phi}^i_{\alpha\beta}\,, \tag{A.3}$$

which should be compared to the standard strains (36). Minimization with respect to the new strain tensor gives back relation (38), showing that the internal modes modify explicitly the strain tensor only, while the constitutive relation is still applied.

Using the finite element discretization (138) and (140) in combination with these two minimization equations, the element functional can be rewritten $\tilde{I}^e_m\left(\boldsymbol{u}^a\,,\tilde{\phi}^i\right):\ \mathbb{R}^{3n_{\text{nodes}}}\times\mathbb{R}^{n_{\text{EAS}}}\rightarrow\mathbb{R}$:

$$\tilde{I}^e_m\left(\boldsymbol{u}^a,\alpha^i\right)=$$
$$\int_{\mathcal{A}_e}\frac{1}{2}\left(\boldsymbol{B}_{n\alpha\beta}^{\ a}\cdot\boldsymbol{u}^a+\alpha^i\tilde{\phi}^i_{\alpha\beta}\right)\mathcal{H}^{\alpha\beta\gamma\delta}_n\left(\boldsymbol{B}_{n\gamma\delta}^{\ b}\cdot\boldsymbol{u}^b+\alpha^j\tilde{\phi}^j_{\gamma\delta}\right)\bar{j}_0 d\mathcal{A}\,, \tag{A.4}$$

where n_{nodes} is the element number of nodes. Minimization with respect to α^i leads to the orthogonality condition of the internal modes

$$0=\int_{\mathcal{A}_e}\tilde{\phi}^i_{\alpha\beta}\mathcal{H}^{\alpha\beta\gamma\delta}_n\left(\boldsymbol{B}_{n\gamma\delta}^{\ b}\cdot\boldsymbol{u}^b+\alpha^j\tilde{\phi}^j_{\gamma\delta}\right)\bar{j}_0 d\mathcal{A}\delta\alpha^i=R^i\delta\alpha^i\,, \tag{A.5}$$

while minimization with respect to the nodal displacements leads to a new expression of the internal membrane forces

$$\left(\tilde{\boldsymbol{F}}^e_n\right)^a\cdot\delta\boldsymbol{u}^a=\int_{\mathcal{A}_e}\boldsymbol{B}_{n\alpha\beta}^{\ a}\mathcal{H}^{\alpha\beta\gamma\delta}_n\left(\boldsymbol{B}_{n\gamma\delta}^{\ b}\cdot\boldsymbol{u}^b+\alpha^j\tilde{\phi}^j_{\gamma\delta}\right)\bar{j}_0 d\mathcal{A}\cdot\delta\boldsymbol{u}^a\,. \tag{A.6}$$

Linearization Eqs. of (A.5) and (A.6) leads to the definition of element Jacobians

$$\mathbf{K}^{e\ i\,a}_{\phi n}=\frac{\partial R^i}{\partial\boldsymbol{u}^b}=\int_{\mathcal{A}_e}\tilde{\phi}^i_{\alpha\beta}\mathcal{H}^{\alpha\beta\gamma\delta}_n\boldsymbol{B}_{n\gamma\delta}^{\ b}\bar{j}_0 d\mathcal{A}\,, \tag{A.7}$$

$$\mathbf{K}^{e\ i\,j}_{\phi\phi}=\frac{\partial R^i}{\partial\tilde{\phi}^j}=\int_{\mathcal{A}_e}\tilde{\phi}^i_{\alpha\beta}\mathcal{H}^{\alpha\beta\gamma\delta}_n\tilde{\phi}^j_{\gamma\delta}\bar{j}_0 d\mathcal{A}\,,\ \text{and} \tag{A.8}$$

$$\mathbf{K}^{e\ a\,i}_{n\phi}=\frac{\partial\left(\tilde{\boldsymbol{F}}^e_n\right)^a}{\partial\alpha^i}=\int_{\mathcal{A}_e}\boldsymbol{B}_{n\alpha\beta}^{\ a}\mathcal{H}^{\alpha\beta\gamma\delta}_n\tilde{\phi}^i_{\gamma\delta}\bar{j}_0 d\mathcal{A}\,. \tag{A.9}$$

Owing to these Jacobians, Eq. (A.5) is solved with Newton-Raphson iterations until $R^i = 0$ is satisfied, by computing

$$\Delta\alpha^i = -\left(\mathbf{K}^e_{\phi\phi}{}^{-1}\right)^{ij} R^j\left(\boldsymbol{u}^*, \alpha^*\right) , \tag{A.10}$$

where * values are guessed values. The element Jacobian matrix (143) has to be corrected in order to take into account the internal modes, leading to

$$\begin{aligned}\left(\tilde{\mathbf{K}}^e_n\right)^{ab} &= \frac{\partial\left(\tilde{\boldsymbol{F}}^e_n\right)^a}{\partial \boldsymbol{u}^b} + \frac{\partial\left(\tilde{\boldsymbol{F}}^e_n\right)^a}{\partial\alpha^i}\frac{\partial\alpha^i}{\partial \boldsymbol{u}^b} \\ &= \mathbf{K}^{e\,ab}_n - \mathbf{K}^e_{n\phi}{}^{ai}\left(\mathbf{K}^e_{\phi\phi}{}^{-1}\right)^{ij}\mathbf{K}^e_{\phi n}{}^{jb} .\end{aligned} \tag{A.11}$$

As it is shown, the resolution of the system is on the element level, and no new degrees of freedom are added to the global system.

What remains to be defined are the EAS linearly independent modes. For 9-node bi-quadratic quadrangular elements, Bischoff and Ramm [29] proposed expressions for the modes, which are orthogonal to the stress tensor. In the present work, these modes are completed by the 2 additional stretch modes not present for 8-node bi-quadratic quadrangular elements. The stretch modes are

$$\begin{aligned}
\tilde{\phi}^1 &= \begin{pmatrix} 1-3\left(\xi^1\right)^2 & 0 \\ 0 & 0 \end{pmatrix} , \quad \tilde{\phi}^2 = \begin{pmatrix} \xi^2 - 3\xi^2\left(\xi^1\right)^2 & 0 \\ 0 & 0 \end{pmatrix} , \\
\tilde{\phi}^3 &= \begin{pmatrix} \xi^1 - 3\xi^1\left(\xi^2\right)^2 & 0 \\ 0 & 0 \end{pmatrix} , \tilde{\phi}^4 = \begin{pmatrix} \left(\xi^2\right)^2 - 3\left(\xi^1\xi^2\right)^2 & 0 \\ 0 & 0 \end{pmatrix} , \\
\tilde{\phi}^5 &= \begin{pmatrix} 0 & 0 \\ 0 & 1-3\left(\xi^2\right)^2 \end{pmatrix} , \quad \tilde{\phi}^6 = \begin{pmatrix} 0 & 0 \\ 0 & \xi^2 - 3\xi^2\left(\xi^1\right)^2 \end{pmatrix} , \\
\tilde{\phi}^7 &= \begin{pmatrix} 0 & 0 \\ 0 & \xi^1 - 3\xi^1\left(\xi^2\right)^2 \end{pmatrix} , \tilde{\phi}^8 = \begin{pmatrix} 0 & 0 \\ 0 & \left(\xi^1\right)^2 - 3\left(\xi^1\xi^2\right)^2 \end{pmatrix} ,
\end{aligned} \tag{A.12}$$

while the shearing modes are

$$\tilde{\phi}^7 = \begin{pmatrix} 0 & 1-3\left(\xi^1\right)^2 \\ \text{SYM.} & 0 \end{pmatrix}, \tilde{\phi}^8 = \begin{pmatrix} 0 & 1-3\left(\xi^2\right)^2 \\ \text{SYM.} & 0 \end{pmatrix},$$
$$\tilde{\phi}^9 = \begin{pmatrix} 0 & \xi^2-3\xi^2\left(\xi^1\right)^2 \\ \text{SYM.} & 0 \end{pmatrix}, \tilde{\phi}^{10} = \begin{pmatrix} 0 & \xi^1-3\xi^1\left(\xi^2\right)^2 \\ \text{SYM.} & 0 \end{pmatrix},$$
$$\tilde{\phi}^{11} = \begin{pmatrix} 0 & 1-3\left[\left(\xi^1\right)^2+\left(\xi^2\right)^2\right]+9\left(\xi^1\xi^2\right)^2 \\ \text{SYM.} & 0 \end{pmatrix}. \tag{A.13}$$

In their paper [17], Simo *et al.* had to transform the EAS modes into the Cartesian coordinates, since their formulation is stated in the reference frame. In order to verify the patch tests, they had to apply the frame-transformation by taking the Jacobian matrix at the center of the element ($\xi^\alpha = 0$) for all of the Gauss points. In the current situation, we are working with the reduced coordinates, so this step is not necessary.

References

[1] A. Lew, P. Neff, D. Sulsky, M. Ortiz, Optimal BV estimates for a discontinuous Galerkin method for linear elasticity, Applied Mathematics Research eXpress 3 (2004) 73–106.

[2] A. Ten Eyck, A. Lew, Discontinuous Galerkin methods for non-linear elasticity, International Journal for Numerical Methods in Engineering 67 (2006) 1204–1243.

[3] L. Noels, R. Radovitzky, A general discontinuous Galerkin method for finite hyperelasticity. Formulation and numerical applications, International Journal for Numerical Methods in Engineering 68 (1) (2006) 64–97.

[4] L. Noels, R. Radovitzky, An explicit discontinuous Galerkin method for non-linear solid dynamics. Formulation, parallel implementation and scalability properties, International Journal for Numerical Methods in Engineering,In press.

[5] G. Engel, K. Garikipati, T. Hughes, M. Larson, L. Mazzei, R. Taylor, Continuous/discontinuous finite element approximations of fourth-order elliptic problems in structural and continuum mechanics with applications to thin beams and plates, Computer Methods in Applied Mechanics and Engineering 191 (2002) 3669–3750.

[6] P. Hansbo, M. Larson, A discontinuous Galerkin method for the plate equation, CALCOLO 39 (1986) 41–59.

[7] G. Wells, N. Dung, A C^0 discontinuous Galerkin formulation for Kirchhoff plates, Computer Methods in Applied Mechanics and Engineering 196 (2007) 3370–3380.

[8] G. Wells, K. Garikipati, L. Molari, A discontinuous Galerkin method for strain gradient-dependent damage, Computer Methods in Applied Mechanics and Engineering 193 (2004) 3633–3645.

[9] L. Molari, G. Wells, K. Garikipati, F. Ubertini, A discontinuous Galerkin method for strain gradient-dependent damage: Study of interpolations and convergence, Computer Methods in Applied Mechanics and Engineering 195 (2006) 1480–1498.

[10] F. Cirak, M. Ortiz, P. Schröder, Subdivision surfaces: a new paradigm for thin-shell finite-element analysis, International Journal for Numerical Methods in Engineering 47 (2000) 2039–2072.

[11] F. Cirak, M. Ortiz, Fully C^1-conforming subdivision elements for finite deformation thin-shell analysis, International Journal for Numerical Methods in Engineering 51 (2001) 813–833.

[12] T. Belytschko, I. Leviathan, Physical stabilization of the 4-node shell element with one point quadrature, Computer Methods in Applied Mechanics and Engineering 113 (1994) 321–350.

[13] Q. Zeng, A. Combescure, A new one-point quadrature, general non-linear quadrilateral shell element with physical stabilization, International Journal for Numerical Methods in Engineering 42 (1998) 1307–1338.

[14] K. Bathe, N. Dvorkin, A four-node plate bending element based on Mindlin/Reissner plate theory and a mixed interpolation, International Journal for Numerical Methods in Engineering 21 (1985) 367–383.

[15] K. Bathe, N. Dvorkin, A formulation of general shell elements - the use of mixed interpolation of tensorial components, International Journal for Numerical Methods in Engineering 22 (1986) 697–722.

[16] J. Simo, D. Fox, On a stress resultant geometrically exact shell model. Part I: formulation and optimal parametrization, Computer Methods in Applied Mechanics and Engineering 72 (1989) 267–304.

[17] J. Simo, D. Fox, M. Rifai, On a stress resultant geometrically exact shell model. Part II: the linear theory; computational aspects, Computer Methods in Applied Mechanics and Engineering 73 (1989) 53–92.

[18] D. Arnold, F. Brezzi, L. D. Marini, A family of discontinuous Galerkin finite elements for the Reissner-Mindlin plate, Journal of Scientific Computing 22-23 (2005) 25–45.

[19] F. Celiker, B. Cockburn, Element-by-Element post-processing of discontinuous Galerkin methods for Timoshenko beams, Journal of Scientific Computing 27 (1–3) (2007) 177–187.

[20] S. Güzey, H. Stolarski, B. Cockburn, K. Tamma, Design and development of a discontinuous Galerkin method for shells, Computer Methods in Applied Mechanics and Engineering 195 (2006) 3528–3548.

[21] S. Güzey, B. Cockburn, H. Stolarski, The embedded discontinuous Galerkin method: Application to linear shell problems, International Journal for Numerical Methods in Engineering.

[22] M. Ortiz, A. Pandolfi, Finite-deformation irreversible cohesive elements for three-dimensional crack-propagation analysis, International Journal for Numerical Methods in Engineering 44 (1999) 1267–1282.

[23] F. Brezzi, G. Manzini, D. Marini, P. Pietra, A. Russo, Discontinuous Galerkin approximations for elliptic problems, Numerical Methods for Partial Differential Equations 16 (4) (2000) 365–378.

[24] P. Hansbo, M. Larson, Discontinuous Galerkin methods for incompressible and nearly incompressible elasticity by Nitsche's method, Computer Methods in Applied Mechanics and Engineering 191 (2002) 1895–1908.

[25] J. Lions, E. Magenes, Problèmes aux limites non homogènes, Dunod, Paris, France, 1968.

[26] S. Timoshenko, S. Woinowsky-Kreiger, Theory of plates and shells, McGraw-Hill, 1959.

[27] R. MacNeal, R. Harder, A proposed standard set of problems to test finite element accuracy, Finite Elements in Analysis and Design 1 (1) (1985) 3–20.

[28] M. Bucalem, J. Bathe, Higher-order MITC general shell elements, International Journal for Numerical Methods in Engineering 36 (1993) 3729–3754.

[29] M. Bischoff, E. Ramm, Shear deformable shemm elements for large strains and rotations, International Journal of Plasticity 40 (1997) 4427–4449.